17-03-2015

Open Call Deliverable OCF-DS1.1 Coherent Optical system Field-trial For spectral Efficiency Enhancement (COFFEE)

Open Call Deliverable OCF-DS1.1

Grant Agreement No.:	605243
Activity:	NA1
Task Item:	10
Nature of Deliverable:	R (Report)
Dissemination Level:	PU (Public)
Lead Partner:	CNIT
Document Code:	GN3PLUS14-1288-43
Authors:	Luca Poti

The research leading to these results has received funding from the European Community's Seventh Framework Programme (FP7 2007–2013) under Grant Agreement No. 605243 (GN3plus).

Abstract
This document provides the detailed report on the scope, objectives and progress of the project "Coherent Optical system Field-trial For spectral Efficiency Enhancement (COFFEE)".

Table of Contents

Table of Figures

Table of Tables

Executive Summary

This document provides the detailed report on the scope, objectives and progress of the project ***"Coherent Optical system Field-trial For spectral Efficiency Enhancement (COFFEE)".*** The document begins with the introduction to the objectives, scope and project execution plan. The introduction section also describes the methodology the key tasks and milestones and their scientific impact. The rest of the document is divided into three main sections corresponding to each work package of the project work plan.

The second section describes the system design related activities carrier out during the project. The activities include technical analysis of the Milan- Finkenstein link for the interoperability with the CNIT Terabit coherent system. Then activities related to re-commissioning of Alcatel 1626LM DWDM system are described. The second portion of the section explains the channel model, candidate solutions for Tb transmission and numerical modelling of the link. A numerical tool has been developed for this purpose by CNIT labs.

The third section explains the innovative techniques to be introduces in the system design for spectral efficiency enhancement. The techniques include channel shortening, non-linear impairment mitigation and multiuser processing at the receiver. A novel nonlinear impairment mitigation technique named Enhanced Split Step Fourier Method (ESSFM) has been proposed and demonstrated. The mitigation of nonlinear impairment allows to launch additional power in the system improving the OSNR and hence the spectral efficiency. The multiuser processing processes multiple channels at the same time at the receiver and utilizes its information to cancel the inter-channel effects thus enabling further tight packing of channels.

The fourth section describes the activities related to actual lab demonstrations and field trials activities being carried out on the Milan-Finkenstein link. The key results are presented and challenges are also reported. In the field trial the performance of the link will be evaluated for single channel both in the linear and nonlinear regimes. The optimal network power profiles will be drawn for enhanced spectral efficiency. In the second set of experiments innovative multiuser techniques will also be tested on the real link and the resultant achievable gain in terms of spectral efficiency will be quantified. The set of new problems if any for future research will also be highlighted.

In the end the document concludes with the key achievements, issues and future recommendations.

1 Introduction

The **COFFEE** project demonstrates, through field trial experiments, the coherent optical data transmission of a single superchannel at the high capacity of 1Tbps using a reduced bandwidth (<200 GHz) over long-haul testbed routes. In order to fulfil such requirements, innovative techniques, already developed in laboratory, are introduced in a field trial environment. Time-Frequency Packing (TFP) is used to increase the spectral efficiency. With respect to other commonly used techniques like orthogonal frequency division multiplexing (OFDM) and M-ary quadrature amplitude modulation format (M-QAM), TFP can guarantee for **lower** transceiver **complexity** and bandwidth requirements, higher tolerance with respect to fibre propagation nonlinearities, **reduced power** consumption, and **larger flexibility**. The implementation of such advanced techniques represents a **strong innovation** in the area of telecommunications, and the use of GEANT infrastructures pushes the relevance of the **COFFEE** objectives also toward market visibility. GEANT installed links permitted the evaluation of the 1Tbps transceiver prototypes in a real network infrastructure. Due to the high level of adaptation and flexibility, intrinsically given by our novel technique, it was possible to transmit the Tb superchannel in the presence of other signals such as 10 Gbps on-off keying (OOK), 40-100 Gbps differential quadrature phase shift keying (DQPSK) or 16-QAM signals and together with independent on-going experiments. An example of a field trial configuration is shown in the figure below:

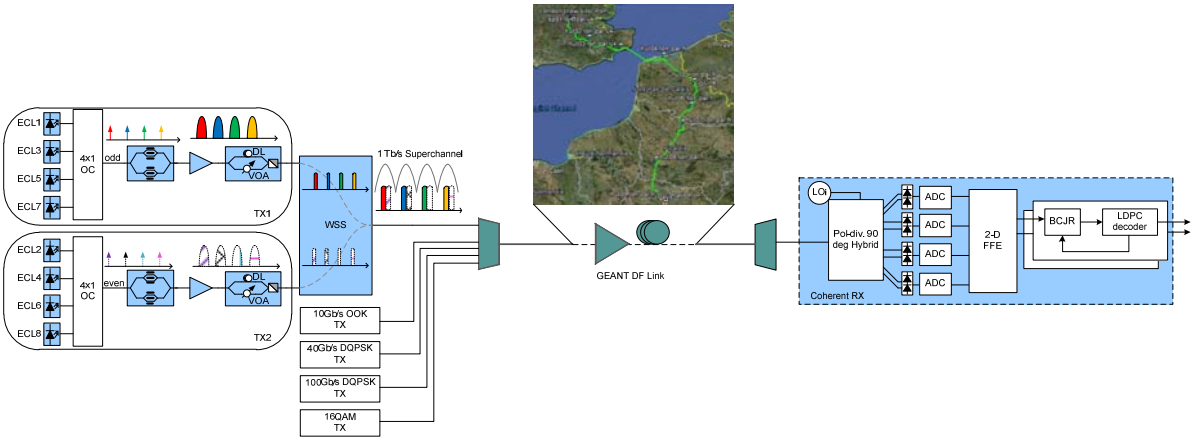

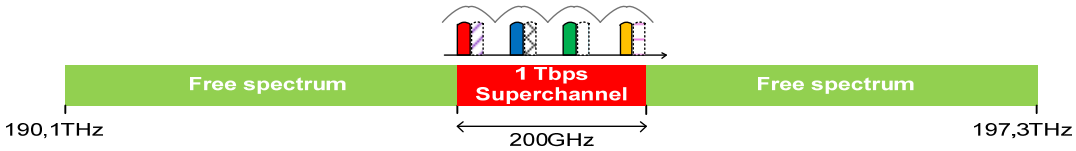

As a fundamental outcome within the GN3plus community the **COFFEE** project allows to build expertise on innovative transmission techniques for next generation optical networks and disseminate through scientific publications and reports within and outside the GN3plus consortium.

1.1 Methodology and associated Work Plan

The design and performance evaluation activity related to COFFEE project are organized in three Work Packages (WPs) concerning theaspects of system modeling and design, investigation of innovative techniques, andtransmission performance evaluation of a 1 Tbps prototype over a long-haul testbed. The transceiver prototype evolved along the project duration. At the beginning the system was adapted to the selected link in order to prove the benefit of our solution with respect to the others. At the same time, the innovative techniques have been developed and included in the model first, and consequently, in the system design in order to improve the overall performance thanks to the introduction of channel shortening, nonlinear impairment mitigation, and multiuser detection. This step-by-step approach garanteed a successful final field trial capable of discriminating the benefit of each new introduced techniques in order to provide appropriate guidelines for the scientific and industrial communities within and outside the GN3 plus consortium.

Work package no.	Work package title	Type of activity	Start month	End month
WP2	System design	RTD	1	16
WP3	Innovative techniques	RTD	1	15
WP4	Field-trial demonstration	DEM	3	18
	TOTAL			

Table 1.1: Work package list

The WP2 is related to the investigation on the architecture to be employed for the Tbps transmission trial. WP2 is composed by 6 milestones. The table below reports a brief description of the milestones which will be discussed more in detail in the next sections.

Milestone number	Milestone title / description	Month
M 2.1	Dark FiberTestBed: Technical description of the installed dark fibre links available for the Terabit transmission trial summarizing all technical specifications of the available test-bed in terms of fibre spans, amplifier spacing, OSNR evolution and nonlinearities.	M6
M.2.2	The operational status of Alcate.Lucent equipment for the candidate links will be assessed as well as the availability of software required for equipment control.	M6
M.2.3	Channel model Channel specifications will be used to derive a numerical model of the transmission channel, required for conducting numerical simulations of the transmission trial within T2.5.	M6
M.2.4	Candidate solutions for Tb transmission A set of possible solutions for the realization of 1 Tbps data transmission over fibre optic will be identified, comparing strength and weakness of each candidate architecture.	M14
M.2.5	Single-user system design and numerical simulations A tool for performing numerical simulations of the transmission system will be realized. Single user receiver including "channel shortening" functionality and mitigation of nonlinear impairments will be considered. Through simulations, all system parameters will be defined to achieve maximum performances and provide guidance to WP4 for tuning and upgrading the transmitter and receiver prototypes to be used in the experimental trial.	M16
M.2.6	Multi-user system design and numerical simulations System model including the multi-user receiver will be developed and numerical simulations will be carried out to evaluate performances and define all system parameters required to WP4 for experimental implementation.	M16

Table 1.2: Milestones for WP2

An exhaustive investigation of innovative techniques was carried out in WP3. This WP is divided in three milestones as shown in the table below.

Milestone number	Milestone title / description	Month
M.3.1	Channel shortening in single user optical coherent systems Algorithm for implementation of channel shortening techniques will be developed, capable to indentify a combination of linear filter and proper MAP coefficients based on estimation of the overall system response.	M3
M.3.2	Nonlinear impairment mitigation advanced techniques Algorithms for mitigation of nonlinear impairments due to fiber propagation will be produced as outcome, by applying novel approaches based on recent theoretical results about nonlinearity modeling and mitigation. A nonlinear equalizer based on a logarithmic perturbation model will replace the linear equalizer used in standard receivers, while modified detection metrics in the BCJR detector will account for the presence of nonlinear effects for TFP receiver. The outcomes will provide the necessary processing tools for WP2 and WP4.	M7
M.3.3	Multi-user receiver in optical time-frequency-packing Realization of novel multi-user algorithms to attain complexity-affordable solution to be provided to WP2 and WP4 and included in the receiver DSP in case of multi-user equalization and detection or at the transmitter side in case of precoding.	M14

Table 1.3: Milestones for WP3

The WP4 is concerning to the experimental demonstration of the 1 Tbps point-to-point coherent transmission on the selected testbed. The system parameters were optimized in order to obtain the best performance in terms of bit error rate and achievable spectral efficiency, considering both single-user and multi-user configuration.

Milestone number	Milestone title / description	Month
M.4.1.1	Single user system optimization and testing. Optimized system considering BER measurements and spectral efficiency in back to back and transmission configurations, for a single user approach.	M9
M4.2.1	Multi user system optimization and testing. Optimized system considering BER measurements and spectral efficiency in back to back and transmission configurations with a multi user approach.	M14
M.4.3.1	Field trial with receiver single user approach (linear regime). Network testbed characterization and system performance evaluation for different network power profile with a single user approach at the receiver.	M16
M.4.3.2	Field trial with receiver single user approach (nonlinear regime). Implementation of the novel electrical processing technique for the nonlinear impairments mitigation and system performance evaluation for different network power profile with a single user approach at the receiver. Comparison between stochastic technique and the new proposed algorithms.	M16
M.4.4.1	Optimum power profile evaluation with nonlinear impairments mitigation. Evaluation of the optimum network power profile considering a multi user approach at the receiver.	M17

Table 1.4: Milestones for WP4

The advanced technique for nonlinear impairments mitigation outputted in WP3 by the numerical simulations in WP2 has been evaluated for the system performance improvement. The most suitable candidate solution, identified in WP2 has been implemented and experimentally validated in the field trial demonstration for both single-user and multi-user configuration.

2 System Design

2.1 Dark Fibre Test Bed MS2.1

The fibre optic link chosen for the field trial connects Milan, Italy and Finkenstein, Austria over a length of 675km. The link consists of ten spans of ITU-T G.655 [1] fibre with lengths between 45 and 80km, with amplification provided by Erbium Doped Fibre amplifiers (EDFAs), and is shown in Fig 2.1.The installed fibre is Corning Leaf [2] on all spans, with a short length of 13km of G.652 [3] Corning fibre spliced into the last span within Milan.

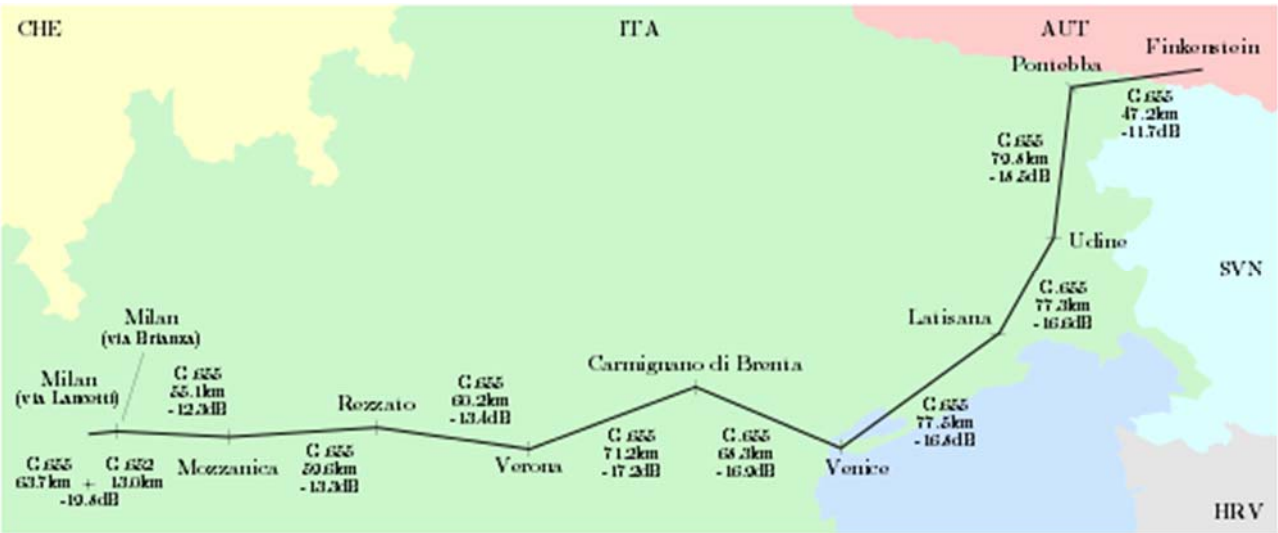

Figure 2.1: Link map, fibre types and loss values on the Milan-Finkenstein link.

The different loss figures in the spans are adjusted to an equal span loss of 20dB through the introduction of inline optical attenuators on all spans (with exception of the Pontebba-Finkenstein span which is levelled to a span loss of 18dB). Tab 2.1 gives an overview of the spans, fibre types, incurred losses and dispersion parameters, whereas Tab 2.2 details amplifier settings, inline attenuators and dispersion compensation modules (DCMs).

Amplifier specifications are taken from the Link Description Table (LDT) and correspond to EDFA modules as found in the Alcatel 1626LM. The LDT assumes utilization of the link with 40 channels and

specifies an optical signal to noise ratio (OSNR)coarse target of 13dB with a margin of 5dB. The specified N-parameter is 10. Although a low target of 13dB is specified, the described link should exhibit a much higher OSNR which may be approximated as:

$$OSNR = \frac{P_{in}}{N_{Amp} \cdot N_F \cdot G \cdot h \cdot \nu \cdot \Delta\nu}$$

Where P_{in} is the input power at each amplifier span, N_{Amp} the number of amplifiers, G the gain, h Planck's constant and ν and $\Delta\nu$ the frequency and regarded bandwidth respectively. With an assumed noise figure of 6dB this yields a theoretical OSNR of about 22dB.[1]

Chromatic dispersion is compensated through a number of DCMs inserted in the mid-stage access of the employed EDFAs as shown in 2. 2. Fig 2.2 shows the resulting dispersion maps of the link in both forward and backward directions. In both cases dispersion is overcompensated, with resulting residual dispersion values of -406ps/nm (Milan-Finkenstein) and -256ps/nm (Finkenstein Milan).

From	**To**	**Fibre Type**	**Length** (km)	**Loss** (dB)	**Dispersion Coefficients** **Chromatic**[2] (ps/nm/km)	**PMD**[3] (ps/√km)
Milan (GEANT)	Milan (Via Caldera)	G.652	13.0	0.0[4]	16.3	0.05
Milan (Via Caldera)	Milan (Via Brianza)	G.655	63.7	19.8	6.0	0.05
Milan (Via Brianza)	Mozzanica	G.655	55.1	12.3	6.0	0.05
Mozzanica	Rezzato	G.655	59.6	13.3	6.0	0.05
Rezzato	Verona	G.655	60.2	13.4	6.0	0.05
Verona	Carmignano	G.655	71.2	17.2	6.0	0.05
Carmignano	Venice	G.655	68.3	16.9	6.0	0.05
Venice	Latisana	G.655	77.5	16.8	6.0	0.05
Latisana	Udine	G.655	77.3	16.6	6.0	0.05
Udine	Pontebba	G.655	79.8	18.5	6.0	0.05
Pontebba	Finkenstein	G.655	47.2	11.7	6.0	0.05

Table 2.1: Spans and loss adjustments on the Milan-Finkenstein link

[1] Based on the full load amplifier output of 17dB with 40 channels (from Tab 2), a gain and span loss of 20dB and the noise bandwidth of 0.1nm typically regarded for OSNR measurements.

[2] No actual chromatic dispersion values are available. Values are estimates based on [1] (G.655) and [3] G.652.

[3] No actual PMD values are available. Values listed are estimates based on an average manufacturer specification including Corning, TrueWave and Alcatel. Values do not differ significantly between G.652 and G.655 fibres and thus a uniform value will be used. The current ITU-T specification is not used since it indicates a maximum PMD coefficient of 0.5ps/√km, which is 10 times worse than the expected performance.

[4] Loss of the G.652 fibre length between Milan (GEANT) and Milan (Via Caldera) is included in the loss of the span Milan (Via Caldera) to Milan (Via Brianza).

Site	Amp. Out[5] (dBm)	OP_ DIFF	K_ DIFF GO	K_ DIFF RET	DCM Type	-Length GO (km)	-Length RET (km)	Att. GO[6] (dB)	Att. RET (dB)
Finkenstein	17	5	0	0	G.655	75		4	
Pontebba	17	5	0	0	G.655	25	50	2	4
Udine	17	5	0	0	G.655	50	150	2	2
Latisana	17	5	0	0	G.655	50	150	2	2
Venice	17	5	0	0	G.655	50	50	3	2
Carmignano	17	5	0	0	G.655	50	50	3	3
Verona	17	5	0	0	G.655	125	25	5	3
Rezzato	17	5	0	0	G.655	125	25	5	5
Mozzanica	17	5	0	2	G.655	25	25	6	5
Milan (Via Brianza)	17	5	0	0	G.655		75	3	6
Milan (GEANT)	17	5	0	0	G.652	60	60		3

Table 2.2: Spans and loss adjustments on the Milan-Finkenstein link

Polarization Mode Dispersion (PMD) across the whole link is estimated to amount to a differential group delay (DGD) of 1.3ps.

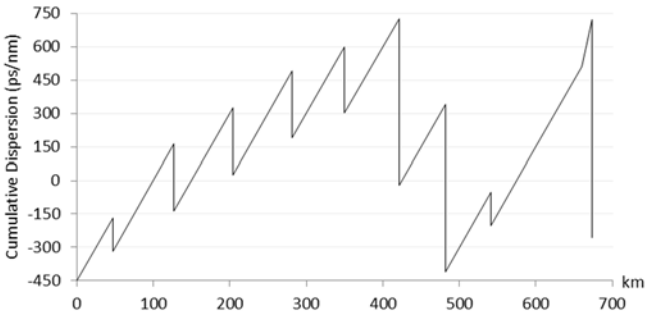

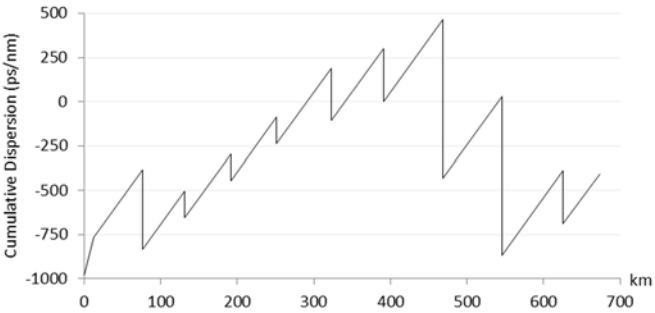

[5] Amplifier output power at full load.
[6] Go refers to the Finkenstein-Milan direction.

a) GO: Finkenstein-Milan b) RETURN: Milan-Finkenstein

Figure 2.2: Dispersion maps for the Milan-Finkenstein link.

2.2 Re-Commissioning of Alcatel Equipment MS2.2

2.2.1 Introduction

In order to establish a field trial on the fibre optic link connecting Milan, Italy and Finkenstein, Austria over a length of 675km as described in MS2.1, existing Alcatel telecommunications equipment must be re-commissioned and employed. To allow such re-commissioning a sample of the same Alcatel equipment was commissioned in the laboratory, tested for functionality and characterised for optical properties.

The equipment available for testing in the laboratory is the following:

- 3x Alcatel 1626LM Shelf
- 3x ESCT1000 Control Unit
- 4x FANS1000 Cooling Unit
- 8x PSUP1000 Power Supply Unit
- 4x RAIU1000 Rack Alarm Interface Unit
- 2x HSKU1000 Housekeeping Unit
- 4x OSCU1010 Optical Supervisory Channel Unit[7]
- 2x TRBD1111 Direct Tributary Unit @9.95320 Gb/s client data rate
- 1x TRBD1131 Direct Tributary Unit @10.31 Gb/s client data rate
- 2x CMDX1010 Channel Multiplex Unit (both Band 8)
- 2x BMDX1000 Band Multiplex Unit
- 3x ALCT1010 Automatic Laser Control Unit (all Band 5)
- 5x LOFA1110 Optical Fibre Amplifier, 22/9 EDFA
- 1x LOFA1120 Optical Fibre Amplifier, 28/9 EDFA

Out of this equipment the ESCT and OSCU boards are of special interest regarding the re-commissioning, control and supervision of the Alcatel equipment; their commissioning and configuration is thus described in section 2.2.2. The TRBD, LOFA and BMDX/CMDX boards are of special interest due to their implications on transmission performance and available contiguous bandwidth slices; their optical characteristics are therefore described in section 2.2.3. Section 2.2.4 concerns itself with creating a loop from the Milan-Finkenstein link, while finally section 5 describes link configurations tested in the laboratory.

[7] One of the four available OSCU1010 units was found to be at least partially faulty and was thus discounted from the testing.

2.2.2 Re-commissioning of Equipment and Equipment control

Commissioning and control of the 1626LM equipment may be performed either through a network management system (NMS) or a locally attached Craft Terminal (CT); since only the Alcatel 1320 CT software was available for testing, all of the following is only concerned with commissioning and management through the latte, although management through the former is assumed to be similar.
In order to manage a 1626LM shelf and the equipment contained therein the CT must be connected to a shelf configured to be 'Master', i.e. its ESCT board must be equipped with a flash card containing equipment control software (the version of which must correspond to that of the equipment management software embedded in the 1320CT software package used) and the management information database (MIB). A shelf configured as 'Slave' may only be managed through a 'Master' shelf which is directly connected to via a Local Area Network (LAN) connection (10BASE2 or 10BASE-T).
Management of remote nodes (that is: their 'Master' shelf and through the latter the attached 'Slave' shelves) is possible through the optical supervisory channel (OSC) provided by the OSCU board in the 'Master' shelves. This channel is terminated at the ingress of every node passed and re-inserted at the output. As such it forms a chain of loops between adjacent nodes, allowing remote control of all nodes on the link if properly configured. Adding and dropping of the channel is achieved through filters included in the LOFA boards and thus configuration of the OSCU channel requires association between the OSCU and LOFA board interfaces, prior to LAPD configuration of the OSC; in the LAPD configuration the two nodes partaking in any of the OSC loops must be configured to have the roles of 'User' and 'Network'.

2.2.3 Characterization of Optical Properties

2.2.3.1 *Description of TRBD11x1 boards*

The TRBD1111 and TRBD1131 boards allow translation of data received on a black and white (B&W) client interface to wavelength division multiplex (WDM) signals to be used for transmission. The WDM signal generated by the TRBD boards can be tuned to the channel frequencies defined by the ITU-T dense WDM grid [4] between 191.15 and 195.90 THz.
The TRBD boards provide 10Gb/s data transmission, with the TRBD1111 board allowing the translation between arbitrary client signals at a data rate of 9.95328 Gb/s (e.g. STM-64 SDH [5], OC-192 SONET [6] or 10GB Ethernet WAN (10BASE-W) [7]) into OTU2 [8] signals at a data rate of 10.709225 Gb/s, while the TRBD1131 allows the translation of 10GB Ethernet LAN (10BASE-R) [7] signals at 10.3125 Gb/s into OTU2e [9] signals at 11.096 Gb/s

2.2.3.2 *Characterization of LOFA1110 EDFA boards*

The LOFA1110 boards are EDFA amplifier boards allowing mid-stage access and having a variable optical attenuator (VOA) integrated on the board to allow tuning of the inter-stage loss. The LOFA1110 boards support three operating modes:

- 'Manual': Manual control of output power of both stages

- 'Power': Automatic control of the output power of the 1st stage, 2nd stage output power remains manually controlled; the OP_DIFF parameters allows indirect influence on the output power of the 1st stage, since: OP1 = OP2 – OP_DIFF + VOA [2, p. 36]
- 'Gain': Manual control of overall gain, with output powers automatically controlled

The integrated VOA may be controlled manually or automatically; automatic control allows influencing the flatness constant (i.e. total gain) which the amplifier works to, via the K_DIFF parameter as: K_FLAT = K_THEORIC + K_DIFF. K_THEORIC is factory determined and is close to 31 dB [2, p. 35], fitting the definition of the LOFA1110 being a 22/9 EDFA.

The EDFA modules contained in the LOFA1110 boards have been characterised for the noise figure of their two stages and their overall gain flatness in the different operating modes. Results for the noise figure measurements at frequencies of 191.5 and 195.0 THz are shown in Figure 2.3 and show a noise figure below 4.5 dB for the 1ststage, while the 2ndstage noise figure falls as gain increases, but is above 5 dB in any case.[8]

Gain flatness of the EDFA modules has been measured by using a broadband input source and measuring the output spectrum; the difference of input and output spectra gives the EDFA gain spectrum.[9] Such measurements are shown in Figures 2.4 a) and b) for 'Manual' and 'Power' mode, for input powers of -5.1 and -10.1 dB and an overall gain of 20.1 dB; it is immediately visible that automatic control of powers allows much better gain flatness in this case, which is further confirmed by all other measurements where 'Manual' and 'Power' settings result in similar working conditions for the amplifier.

Further gain flatness measurements were performed in order to compare gain flatness (in 'Power' mode) for different working conditions. Figures 2.5 a) shows the achieved gain flatness for different settings of OP_DIFF, while maintaining a constant input power of -5.1 dB and gain of 20.1 dB.**Error! Reference source not found.** shows the gain flatness for different gain values while maintaining a constant input power of -5.1 dB and OP_DIFF parameter of 4.5 dB.

These measurements show a slight gain tilt with lower gain at longer wavelengths, but maximum and minimum gain values are generally within 2 dB of each other. With an input power of -5.1 dB and gain values of up to 20.1 dB a gain flatness within 1 dB may be achieved, regardless of the chosen OP_DIFF parameter.

[8] The employed measurement setup is largely that detailed in [3, pp. 553-554], but under neglect of the effects of Source Spontaneous Emission and thus likely giving a slight overestimation of the noise figure.
Measurements were taken with an OSA resolution bandwidth of 0.1 nm, a sensitivity of -80 dBm and a span ranging from 1525 to 1585 nm with 1001 measurement points per span reported. OSA power levels were calibrated to absolute values through the use of a power meter.

[9] Measurements were taken with an OSA resolution bandwidth of 1 nm, a sensitivity of -65 dBm and a span ranging from 1510 to 1585 nm with 1001 measurement points per span reported.

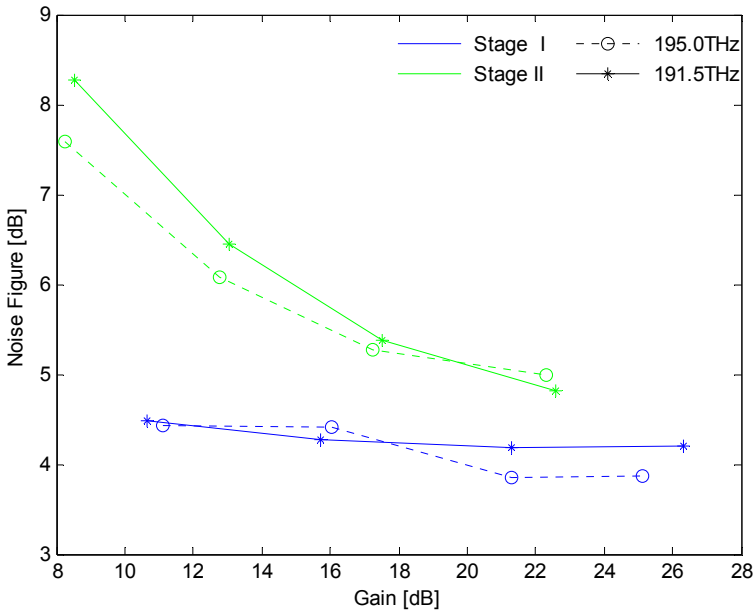

Figure 2.3: Amplifier noise figures for first and second stage amplifiers of LOFA1110.

BMDX1000		CMDX1010	
MUX	DEMUX	MUX	DEMUX
7.9 dB	7.0 dB	7.7 dB	7.0 dB

Table 2.3: Insertion losses for BMDX1000 and CMDX1010 boards

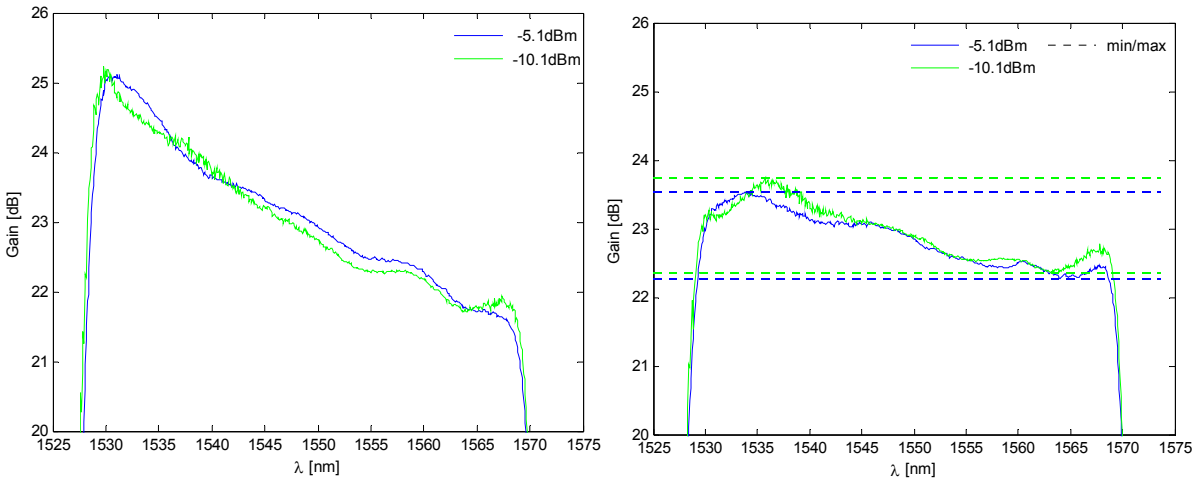

a) 'Manual' control

b) 'Power' control

Figure 2.4: Gain flatness for different input power and control modes at a gain of 20.1 dB.

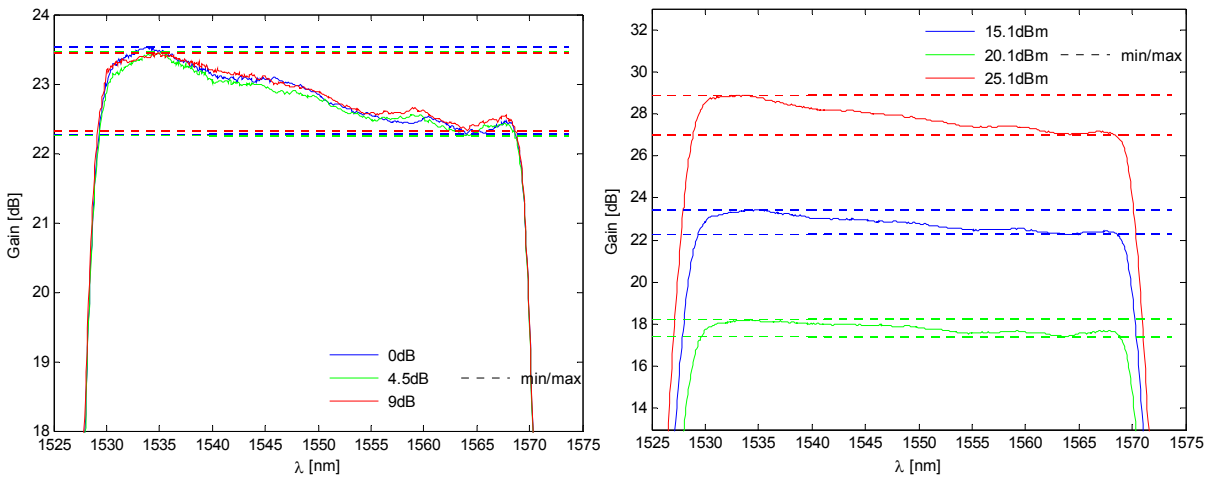

a) Gain flatness for different OP_DIFF values

b) Gain flatness at different Gain levels

Figure 2.5: Gain flatness for different OP_DIFF values and gain values.

2.2.3.3 *Characterisation of BMDX1000 and CMDX1010 multiplex boards*

Characterisation of BMDX and CMDX boards has been performed in terms of filter shapes and bandwidth as well as insertion loss. Insertion losses measured in single laser operation for both multiplex and demultiplex directions are shown in Table 2.3.

The shape and bandwidth of the filtering function performed by the BMDX and CMDX board was recorded by using a broadband source as input signal and recording the output signal; the difference between the input and output spectra gives the filter shape. Filter shapes for the BMDX1000 boards are shown in Figures 2.6 and are found to have bandwidth characteristics as shown in Table 2.4, whereas the measured and normative centre frequencies are shown in Table 2.5.[10]Frequencies are found to mostly be within the measurement tolerance from the nominal frequency, with the largest measured deviations being on the order of 75 GHz.

[10] Measurements were taken with an OSA resolution bandwidth of 0.06 nm, a sensitivity of -80 dBm and a span ranging from 1525 to 1575 nm with 1001 measurement points per span reported. This results in a measurement accuracy of ±20 GHz for bandwidth and frequency measurements.

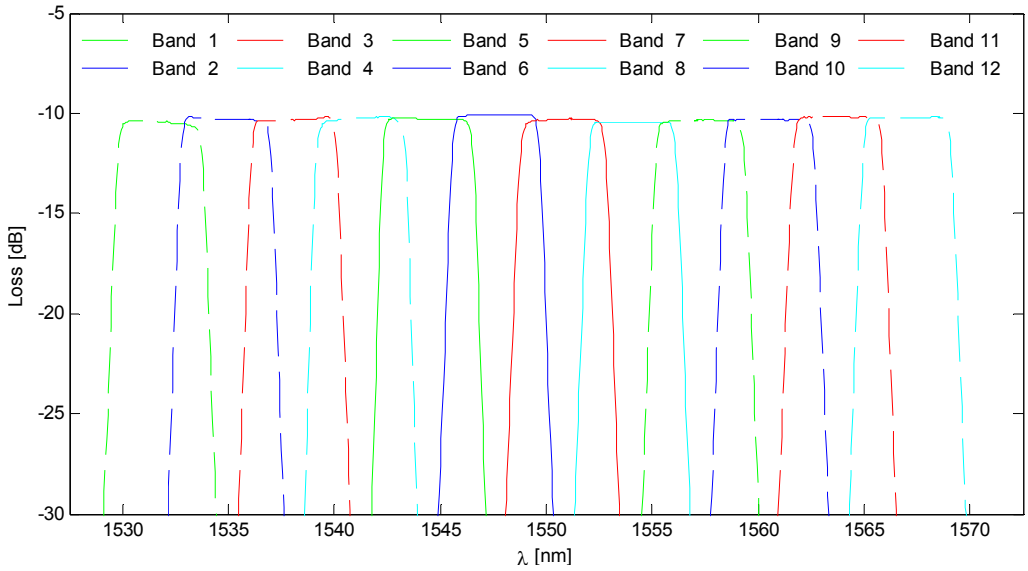

a) Multiplex

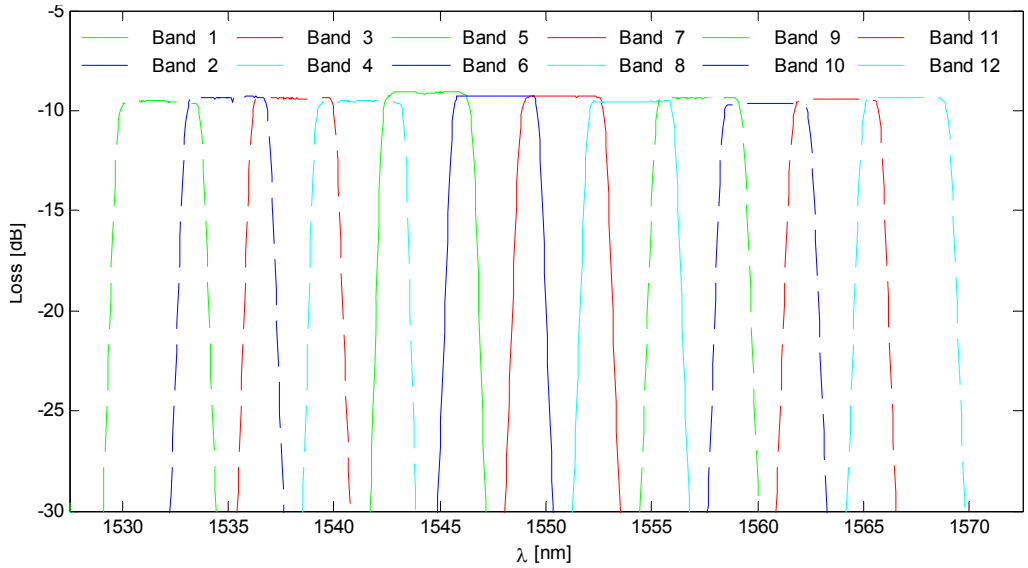

b) Demultiplex

Figure 2.6: Multiplex and demultiplex bands of the BMDX1000 board.

Similarly filter shapes for the CMDX1010 board are shown in Figure 2.7 with their bandwidth characteristics also shown in Figure 2.8 a) and b).4, while measured and normative centre frequencies are also shown in Table 2.5.[11] Frequencies show a general shift by about +5 GHz, but are otherwise within ±2 GHz of each other and thus within the measurement tolerance. Additionally the recorded bandwidth and central frequencies are overlaid in Figure 2.8, showing a slight left-shift of the actual

[11] Measurements were taken with an OSA resolution bandwidth of 0.06 nm, a sensitivity of -80 dBm and a span ranging from 1550 to 1558 nm with 1001 measurement points per span reported. This results in a measurement accuracy of ±2 GHz for bandwidth and frequency measurements.

channels within the band, with still all channels in the clear passband region of the band. The fit of a channel generated by the TRBD1111 board inside the multiplex and demultiplex channels of a CMDX1010 board is shown in Figure 2.8 and shows a good fit.[12]

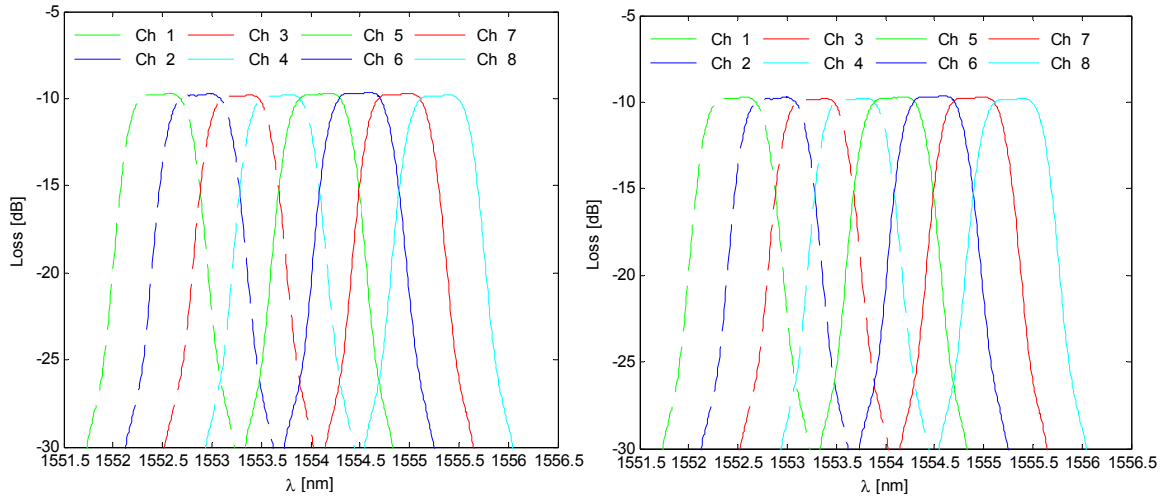

a) Multiplex b) Demultiplex

Figure 2.7: Multiplex and Demultiplex channels of the CMDX1010 board (Band 8).

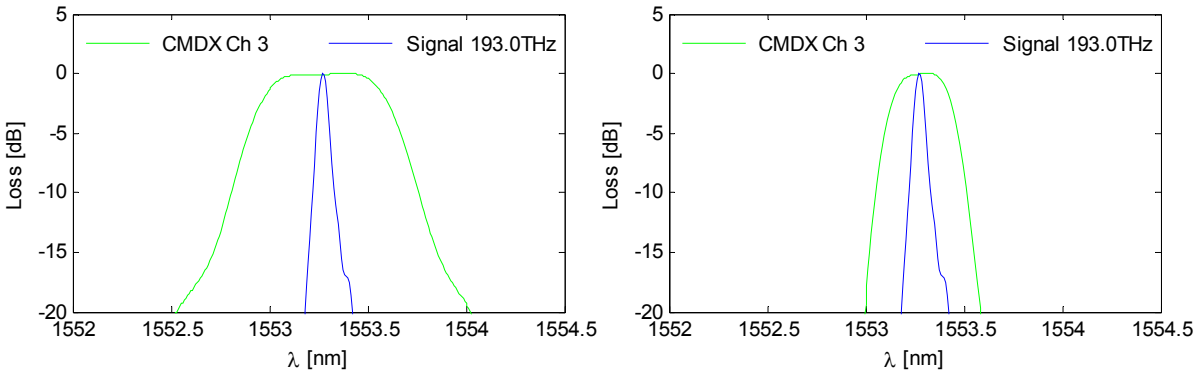

Figure 2.8: TRBD1111 signal inside CMDX1010 channel.

BMDX1000				CMDX1010			
MUX		DEMUX		MUX		DEMUX	
3dB BW (GHz)	10dB BW (GHz)	3dB BW (GHz)	10dB BW (GHz)	3dB BW (GHz)	10dB BW (GHz)	3dB BW (GHz)	10dB BW (GHz)
531	593	531	593	86.4	119.2	40.7	58.6

[12] Note that the recorded signal is as received with directly connecting the TRBD board to the respective input of the CMDX board for both multiplex and demultiplex direction.

Table 2.4: Measured filter bandwidth for BMDX1000 and CMDX1010 boards.

BMDX1000						CMDX1010		
mux (THz)	demux (THz)	nominal (THz)	mux (THz)	demux (THz)	nominal (THz)	mux (THz)	demux (THz)	nominal (THz)
195.7157	195.7189	195.7125	193.3147	193.3178	193.3125	193.106	193.106	193.100
195.3204	195.3109	195.3125	192.9073	192.9135	192.9125	193.057	193.056	193.050
194.9109	194.9141	194.9125	192.5140	192.5140	192.5125	193.006	193.006	193.000
194.5125	194.5189	194.5125	192.1100	192.1125	192.1125	192.956	192.956	192.950
194.1127	194.1158	194.1125	191.7138	191.7199	191.7125	192.906	192.905	192.900
193.7113	193.7113	193.7125	191.3131	191.3192	191.3125	192.856	192.856	192.850
						192.805	192.804	192.800
						192.756	192.755	192.750

Table 2.5: Measured and normative centerfrequencies for the BMDX1000 and CMDX1010 boards[13].

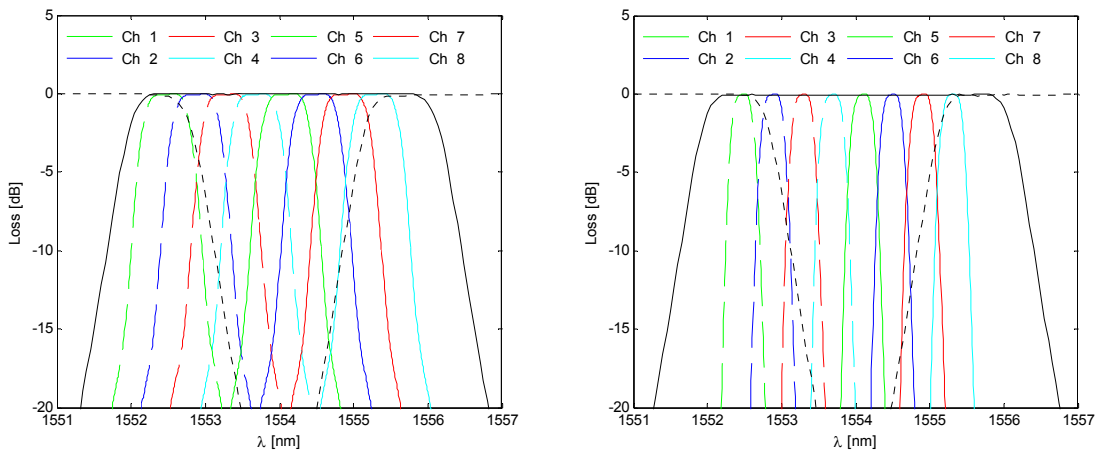

a) Multiplex

b) Demultiplex

Figure 2.9: Overlap graph for Band 8 of BMDX1000 and CMDX1010[14].

[13] Nominal values are according to [1, p. 224] for the BMDX1001 and according to [1, p. 130] for the CMDX1010.
[14] Curves have been normalized for the benefit of legibility.

2.2.4 Loopback Configuration Milan-Finkestein-Milan

The Milan-Finkenstein link is to be employed in a loopback configuration for the field trial, in order to increase transmission distance and facilitate testing with a single point of access. To achieve this, the site in Finkenstein must be reconfigured to loop received signals on the incoming fibre from Milan onto the outgoing fibre back to Milan. For such a loopback, a number of options have been identified and evaluated:

1. *Unamplified loopback*: It is possible to loop the received signal without amplification, creating a single long fibre span connecting Pontebba to itself, encountering losses of about 24 dB.

   This solution has been evaluated to likely show a very high OSNR degradation, although such span losses may be overcome by amplifier tuning.This option completely cuts the OSC between Finkenstein and Pontebba, rendering remote control of equipment in Finkenstein impossible.

2. *Fully Amplified loopback*: The incoming signal may be looped to become the outgoing signal from the output of the receiving amplifier to the input of the transmitting amplifier in Finkenstein. This is effectively equal to inserting an additional span between the two physical halves of the Milan-Finkenstein-Milan loop, requiring corresponding attenuation in the loop connection created in Finkenstein.

   This solution has been evaluated to likely outperform option 1, but may itself be outperformed by option 4 and 5. The OSC channel is not affected, maintaining full remote control over the Finkenstein node.

3. *Band loopback*: Contrary to all other options, option 3 considers looping bands separately using the BMDX1000 board in Finkenstein, while optionally allowing the standard 10 Gb/s transponders of the original system to work as 3R elements.

   This solution has been evaluated to be a possible option in order to guarantee functionality of the 10 Gb/s interfaces, but in terms of OSNR is likely outperformed by option 4 and 5. Again the OSC channel is not affected.

4. *Inter-stage loopback*: A loop connection between the output of the 1st stage of the receiving and the input of the 2nd stage of the transmitting amplifier in Finkenstein may render the two amplifiers effectively as one.

   This option is questionable in terms of gain flatness achievable when using stages to two independent amplifiers as a single amplifier and raises questions of operating modes concerning the automatic power shutdown (APSD) of the system. This option has been tested in the lab, with results described in section 4.2.

5. *Single-Amplifier loopback*: Improving on option 4, a scheme using both stages of a single amplifier in Finkenstein has been developed. As such, lab tests have shown that a configuration using only the receiving amplifier is possible, looping its output signal straight into the outgoing fibre.

   This option is found to most likely show the best OSNR performance of all evaluated options. It will require minor changes to OSC cabling, but critically does not require local OSC reconfiguration, thus maintaining full remote control over the Finkenstein node. Option 5 is shown in Figure 2.11.

2.2.5 Link Configurations Tested in the Laboratory

2.2.5.1 *Bidirectional Transmission Links*

In order to test setup of actual transmission links, a number of tests have been performed in the laboratory. First a simple back-to-back connection between two network nodes configured as line terminals with a single 'Master' and no slave shelves has been performed, including setup of the OSC channel and remote supervision of one of the nodes.

This setup was extended through transmission across an 80 km fibre span between the two line terminals and insertion of proper dispersion compensation modules (DCMs) in the receiving or transmitting amplifiers of the nodes, confirming both pre- and post-compensation to be functional options.

These tests allowed gaining insight into configuration of the equipment within a shelf especially in three distinct points:

- Configuring tributary and multiplex boards to form a tree of associations, being configured in top-down direction.
- Configuration of amplifiers as associated receiving and transmitting amplifiers and the resulting APSD behaviour.
- Configuration of the OSC channel and its association to amplifier interfaces.

All tests were performed with active performance monitoring, finding excellent post-FEC performance in all cases; an exemplary performance monitoring log is shown in Figure 2.10.

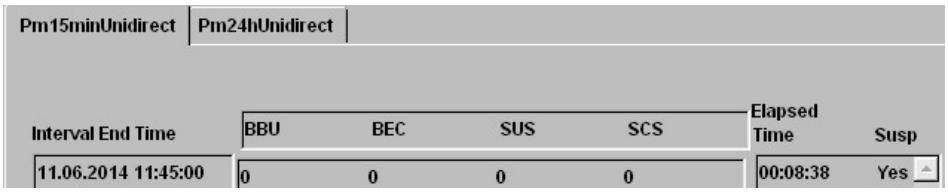

Figure 2.10: Error free performance monitoring log.

2.2.5.2 *Loopback Configurations*

Employing the Milan-Finkenstein link in loopback configuration as discussed in section 4 requires a number of tests in the laboratory to establish feasibility of the proposed solutions.

In relation to all discussed options, functionality of optically looped 10 Gb/s has been test and established, rendering the use of TRBD boards as 3R elements for the 10 Gb/s lines possible, but not necessary. Such 3R use of TRBD boards has been tested and is easily accomplished by configuring an internal electrical loopback on the OCH port of the TRBD board.

Using two stages of two amplifiers to effectively form a single amplifier – as proposed in option 4 – requires testing for both gain flatness and impact of APSD. The latter is designed to ensure no output power is given from the amplifiers in case a fibre might be disconnected to broken. As such output

power of amplifier stages depends on input power of other amplifier stages of the associated contro-directional pair. In the proposed configuration the 1st stage of the receiving amplifier is deactivated by having no input at the same amplifier's 2nd stage (thus assuming a fibre cut between first and second stage), requiring 'tricking' the APSD feature by giving an artificial input signal to the second stage of the receiving amplifier in Finkenstein.

In addition to the problems associated with APSD, option 4 depends on the achievable gain flatness with using two stages of two separate amplifiers – the performance observed effectively prohibits this approach, since gain flatness cannot be achieved to a reasonable level. In 'Power' configuration the two amplifiers effectively enter an oscillating pattern where gain tilt changes periodically as each amplifier reacts to automatic changes in the other amplifier's configuration. Configuration of the amplifiers in 'Manual' mode has been shown to perform badly in terms of gain flatness in section 3.2 and performs even worse across two stages of two separate amplifiers. This discards option 4, but lead to the development of option 5, which was successfully tested in the lab, requiring very little re-cabling on both the signal and OSC channels (avoiding reconfiguration of the OSC and thus avoiding needing local configuration access) and promising better OSNR performance than options 2 and 3 (for any custom transmissions and the standard 10 Gb/s signals, unless 3R regeneration on the 10 Gb/s TRBD boards is used). Option 5, incl. re-cabling of the OSC is shown in Figure 2.11.

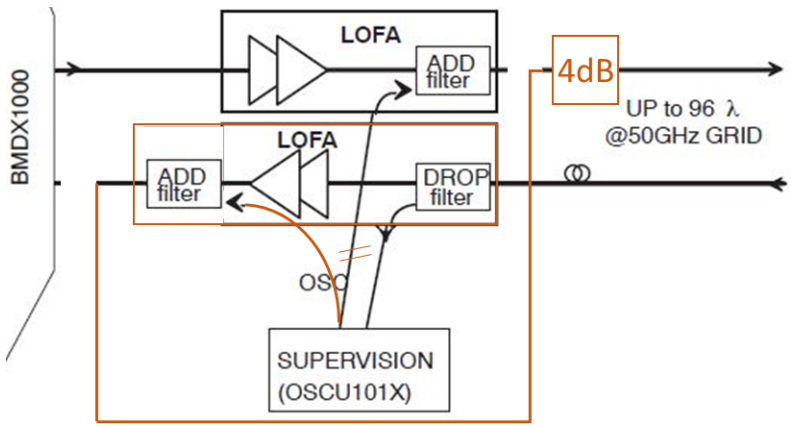

Figure 2.11: Single-Amplifier loopback configuration.

2.3 Channel model MS2.3

A discrete time model of the transmission channel has been derived to evaluate propagation over the link through simulations. The fibre optic link chosen for the field trial connects Milan, Italy and Finkenstein, Austria over a length of 675km and is described in MS2.1. In a first implementation, the model has included linear effects such as chromatic dispersion and polarization-mode dispersion, system filters, and laser phase noise. OSNR degradation along the link due to amplified spontaneous emission (ASE) of amplifiers has been estimated as well, considering reasonable values for EDFAs noise figures (5-7).

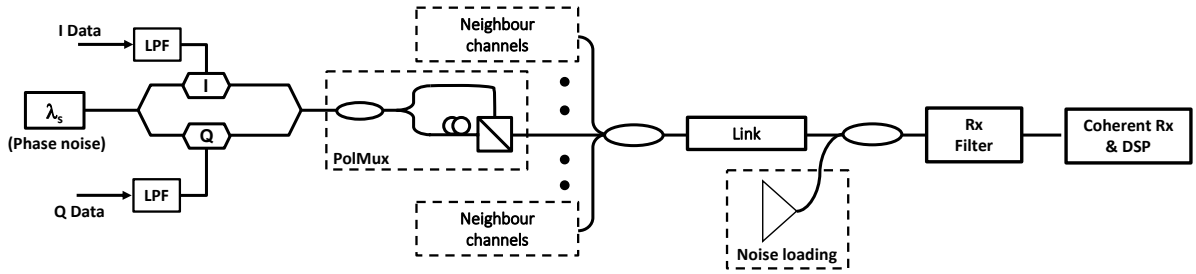

Figure 2.12: System setup considered for simulations, including transmitter, transmission link and receiver.

At transmitter, electrical filters are considered to apply the desired shape. At receiver, optical filtering is considered to extract each channel for coherent detection and offline processing (including BER measurements). As an example, Fig .2.13 shows three channels obtained through time-frequency packing (TFP) QPSK at 40GBaud and 21GHz channel spacing.

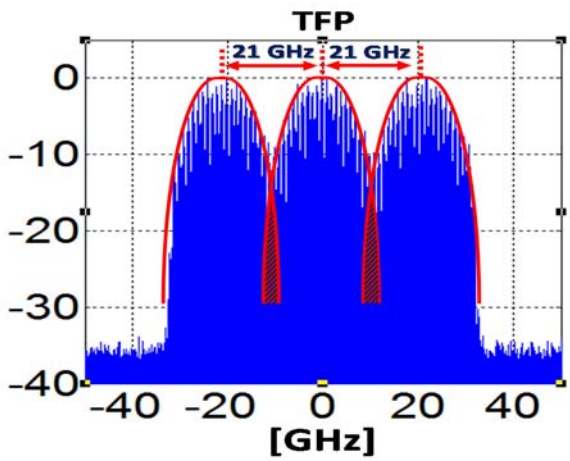

Figure 2.13: Simulation of three adjacent sub-channels employing TFP modulation format.

Following link specifications, the model includes all 11 spans covering the 675km from Milan to Finkenstein, with corresponding attenuation, GVD, PMD. EDFAs are considered to be set at 20dB gain to compensate for propagation loss, and ONSR degradation is estimated consequently. DCM are included in the model to partially compensate for GVD along the link.

In a second step, nonlinear effects based on Kerr effect have been included. Propagation of the optical signal along the fiber spans is simulated through the well-known split step Fourier method. The method consists in separating propagation into small steps (i.e. few hundred meters) and then computing linear and non-linear propagation separately. The effects of chromatic dispersion are computed and applied in the frequency domain, whereas the effects of Kerr-based nonlinearities (i.e. self-phase modulation, SPM, and cross phase modulation, XPM) are computed and applied in the time domain. The method allows to simulate accurately the interplay between linear impairments such as GVD and nonlinear effects such as SPM and XPM. At each step, signal power is reduce considering conventional propagation loss of 0.22 dB/km.

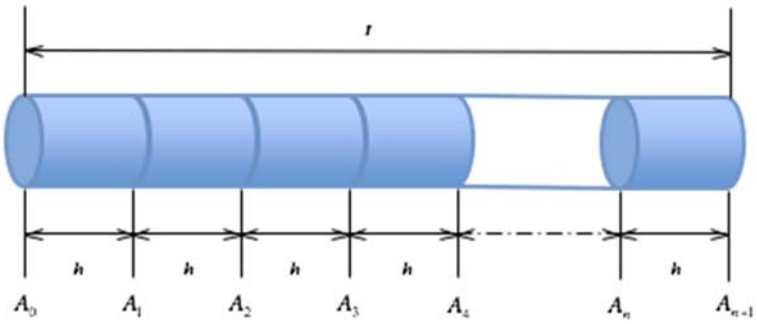

Figure 2.14: Split-step Fourier method. Fiber span is divided into short segments and impact GVD and kerr-based nonlinearities are simulated separately.

Fig. 2.15 shows a capture of the MATLAB software realized to import link specifications in the simulative tool, while in Fig. 2.16 an example of simulated propagation of three subchannels over the dark fiber link is reported.

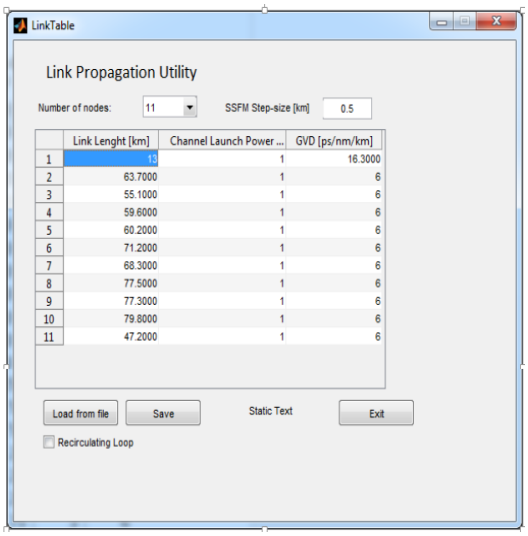

Figure 2.15: Link propagation utility.

```
----------------------------------------
Propagating on link 1 of 11: Milan (GEANT) - Milan (Via Caldera), 13 Km, 211.9 ps/nm (16.3 ps/nm/km)
Launch Power = 3.7768mW (5.7712 dBm)
Split Step Fourier Method: Step-size = 0.5 Km -> 26 steps
Link Progress: 26 steps (100.0%),  0 hrs 19 min 22 sec remaining ==============================
----------------------------------------
----------------------------------------
Propagating on link 2 of 11: Milan (Via Caldera) - Milan (Via Brianza), 63.7 Km, 382.2 ps/nm (6 ps/nm/km)
Launch Power = 3.7768mW (5.7712 dBm)
Split Step Fourier Method: Step-size = 0.5 Km -> 127 steps
Link Progress: 127 steps (100.0%),  0 hrs 16 min 22 sec remaining ==============================
----------------------------------------
----------------------------------------
Propagating on link 3 of 11: Milan (Via Brianza) - Mozzanica, 55.1 Km, 330.6 ps/nm (6 ps/nm/km)
Launch Power = 3.7768mW (5.7712 dBm)
Split Step Fourier Method: Step-size = 0.5 Km -> 110 steps
Link Progress: 110 steps (100.0%),  0 hrs 14 min 44 sec remaining ==============================
----------------------------------------
----------------------------------------
Propagating on link 4 of 11: Mozzanica - Rezzato, 59.6 Km, 357.6 ps/nm (6 ps/nm/km)
Launch Power = 3.7768mW (5.7712 dBm)
Split Step Fourier Method: Step-size = 0.5 Km -> 119 steps
Link Progress: 119 steps (100.0%),  0 hrs 13 min  3 sec remaining ==============================
----------------------------------------
----------------------------------------
Propagating on link 5 of 11: Rezzato - Verona, 60.2 Km, 361.2 ps/nm (6 ps/nm/km)
Launch Power = 3.7768mW (5.7712 dBm)
Split Step Fourier Method: Step-size = 0.5 Km -> 120 steps
Link Progress: 120 steps (100.0%),  0 hrs 11 min 23 sec remaining ==============================
----------------------------------------
----------------------------------------
Propagating on link 6 of 11: Verona - Carmignano, 71.2 Km, 427.2 ps/nm (6 ps/nm/km)
Launch Power = 3.7768mW (5.7712 dBm)
Split Step Fourier Method: Step-size = 0.5 Km -> 142 steps
Link Progress: 142 steps (100.0%),  0 hrs  9 min 26 sec remaining ==============================
----------------------------------------
----------------------------------------
Propagating on link 7 of 11: Carmignano - Venice, 68.3 Km, 409.8 ps/nm (6 ps/nm/km)
Launch Power = 3.7768mW (5.7712 dBm)
Split Step Fourier Method: Step-size = 0.5 Km -> 137 steps
Link Progress: 137 steps (100.0%),  0 hrs  7 min 35 sec remaining ==============================
----------------------------------------
----------------------------------------
Propagating on link 8 of 11: Venice - Latisana, 77.5 Km, 465 ps/nm (6 ps/nm/km)
Launch Power = 3.7768mW (5.7712 dBm)
Split Step Fourier Method: Step-size = 0.5 Km -> 155 steps
----------------------------------------
Propagating on link 9 of 11: Latisana - Udine, 77.3 Km, 463.8 ps/nm (6 ps/nm/km)
Launch Power = 3.7768mW (5.7712 dBm)
Split Step Fourier Method: Step-size = 0.5 Km -> 155 steps
Link Progress: 155 steps (100.0%),  0 hrs  3 min 25 sec remaining ==============================
----------------------------------------
----------------------------------------
Propagating on link 10 of 11: Udine - Pontebba, 79.8 Km, 478.8 ps/nm (6 ps/nm/km)
Launch Power = 3.7768mW (5.7712 dBm)
Split Step Fourier Method: Step-size = 0.5 Km -> 160 steps
Link Progress: 160 steps (100.0%),  0 hrs  1 min 16 sec remaining ==============================
----------------------------------------
----------------------------------------
Propagating on link 11 of 11: Pontebba - Finkenstein, 47.2 Km, 283.2 ps/nm (6 ps/nm/km)
Launch Power = 3.7768mW (5.7712 dBm)
Split Step Fourier Method: Step-size = 0.5 Km -> 94 steps
Link Progress: 94 steps (100.0%),  0 hrs  0 min  0 sec remaining ==============================
----------------------------------------
```

Figure 2.16: Screenshot of simulated propagation through Split-step Fourier method.

2.4 Candidate solutions for Tb transmission MS2.4

2.4.1 System Design

The TFP approach allows to introduce an arbitrary constraint on the detector complexity, and provides the optimum in terms of SE for that detector complexity. To this aim—limiting the analysis to single-user detectors and focusing, without loss of generality, on the 0-th carrier, such that the others are considered only as a source of ICI and are, therefore, a part of the "real" channel depicted in Fig. 2.17—a slightly different (and more practical, as shown later) definition of SE is adopted by replacing the mutual information rate $I(\mathbf{X};\mathbf{Y})$ in with the achievable information rate(AIR) for a mismatched decoder.

$$\hat{I}(\mathbf{X}^{(0)};\mathbf{Y}^{(0)}) \triangleq \lim_{K\to\infty} \frac{1}{K} E\left\{ \log \frac{q(\mathbf{y}^{(0)}|\mathbf{x}^{(0)})}{q(\mathbf{y}^{(0)})} \right\} \leq I(\mathbf{X};\mathbf{Y}) \qquad (1)$$

The design of a multicarrier fiber-optic system by employing the TFP approach is presented. The ideal low-pass equivalent scheme reported in Fig. 2.17, is, under some assumptions, a reasonable representation of the fiber-optic channel. A sequence of i.i.d. symbols $\{x_k\}$, drawn from a DP-QPSK alphabet, modulates the selected carrier (ℓ= 0, in the scheme) at rate $1/T$ with a real shaping pulse $p(t)$. All the modulated carriers are then combined and transmitted through an AWGN channel with noise $\boldsymbol{n}(t)$.

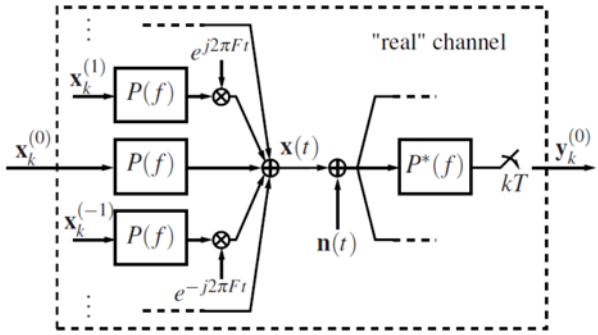

Figure 2.17: Low-pass equivalent model employed to design the TFP system.

At receiver side, the selected carrier is demodulated by a matched filter and a symbol-time sampler. Received samples $\{y_k\}$ are finally sent to a MAP symbol detector that operates on the output of the matched filter [3], [4] and is implemented through the algorithm by Bahl, Cocke, Jelinek, and Raviv (BCJR) [5]. The MAP symbol detector is matched to an auxiliary channel, whose selection determines the distributions $q\left(y^{(0)}\middle|x^{(0)}\right)$ and $q(y^{(0)})$ .In particular, as an auxiliary channel we take an approximation of the real channel, obtained from the latter by neglecting ICI, truncating ISI to the first $L_T \leq L$ pre- and post-cursor symbols (afterthe matched filter)—where $2L\ +1$ is the actual memory of the channel and L_T is a design parameter strictly related to detector complexity—and increasing the noise variance $\sigma_{n'}^2 > \sigma_n^2$(up to a numerically optimized value) to account for the neglected ICI and ISI. This choice provides a reasonable trade-off between performance (how tight is the bound of AIR) and complexity (of the matched BCJR detector). Moreover, as the DP-QPSK modulation can be seen as the combination of four orthogonal BPSK modulations (one per each quadrature component of each state of polarization of the signal),four independent and identical BCJR detectors with 2^{L_T} states are used to separately detect the fourBPSK components.Although also the pulse shape $p(t)$ can be optimized to maximize the SE [6], in this work we consider only the pulse shape obtained by employing a ninth-order type I Chebyshev filter (selected among the electrical low-pass filters available in our laboratory) with 3 dB bandwidth B. For the given shape, (1) is evaluated through numerical simulations

as explained in [1] on a grid of values of the normalized time and frequency spacing TB and F/B, seeking the maximum SE(2) and the corresponding optimum spacings.

$$\hat{\eta}_{\max} = \max_{F,T>0} \frac{\hat{I}(\mathbf{X}^{(0)};\mathbf{Y}^{(0)})}{FT} \leq \eta \qquad (2)$$

To account for unsynchronized channels and unlocked lasers, each modulated carrier is also subject to a random phase and time shift and polarization rotation. The optimizations performed considering a truncated channel memory L_T=3 (8-state MAP symbol detectors)and two different values of the SNR per bit (defined as the ratio E_b/N_0between the mean energy perbit and the noise power spectral density and related to the OSNR through $OSNR = R_b E_b/(2N_0 B_{ref})$,where R_b is the total net bit rate and $B_{ref} \cong 12.5$ GHz the conventional reference bandwidth) of 7.5and 22.5 dB. The corresponding contour plots of the achievable SE are reported in Fig. 2.18(a) and (b).In principle, the TFP optimization procedure described here can be applied also to a realistic fiber-optic channel, as the AIR definition (1), its properties, and the simulation-based method for its computation [1] are valid for any channel. The only requirement is that of computing the output sequence $\{y_k\}$ for the desired real channel (e.g., through the split-step Fourier method). This, however, significantly increases the computation time required to estimate a single AIR value and makes the optimization procedure cumbersome. For this reason, we decided to optimize the system in the absence of nonlinear effects, and then tested the obtained suboptimum configuration (the one in Fig. 2.18)over a realistic link.

The achievable SE obtained with this design procedure can be practically approached by employing properly designed codes. When the TFP technique is adopted, and thus ISI is intentionally introduced, codes designed for the AWGN channel no longer perform satisfactorily. So a redesign is required. We designed proper LDPC codes specifically tailored for the ISI channels resulting from the adoption of the TFP technique. The adopted procedure is based on two steps. The heuristic technique for the optimization of the degree distributions of the LDPC variable and check nodes proposed in [7] is first adopted. This technique consists of a curve fitting on extrinsic information transfer (EXIT) charts, is based on a Gaussian assumption on all messages involved in the iterative process, and is much simpler than other optimization techniques, such as density evolution, which require intensive computational efforts. The parameters of the designed codes are reported in Table 2.6 where *r* denotes the rate of the code and the degree distributions of variable and check nodes are provide by using the notation in [8]. In any case, the codeword length is *N* = 64800.Once the degree distributions of the LDPC variable and check nodes have been designed, the parity check matrix of an LDPC code with those degree distributions is built through the very effective PEG algorithm [9], [10], which allow to design an LDPC code whose underlying Tanner graph hasa large girth. The BER curves for uncoded QPSK transmission and for the designed LDPC codes(independent encoding of the in-phase and quadrature components of each polarization) obtained through numerical simulations for the back-to-back system with the TFP configuration adopted inthe experimental setup (constrained optimum at 40 GBd) are reported in Fig. 2.19. With this TFP configuration, the 8/9 LDPC code requires $E_b/N_0 \cong 9.3$dB and provides an

SE of about 7.1 bit/s/Hz. Thus, we can compare it with Fig. 2.18(a), which shows that approximately the same SE (7.2 bit/s/Hz)is theoretically achievable at E_b/N_0 = 7.5dB. This means that the designed code over the (back-to-back)TFP channel has a penalty of less than 2 dB with respect to the theoretical limit provided by the AIR in (2). In our simulations, we transmitted up to 10000 codewords without observing any floor, meaning that error floors, if present, are probably located at a BER lower than10^{-8}. In any case, outer hard-decision external codes withvery low overhead can be employed to correct the residual errors and remove the floor. For instance, inthe DVB-S2 standard, where LDPC codes with same length and rates as in Tab. 2.6 are adopted, outer BCH codes with less than 0.4% overhead are used to correct from 8 to 12 residual errors (depending on the rate) per codeword [11].

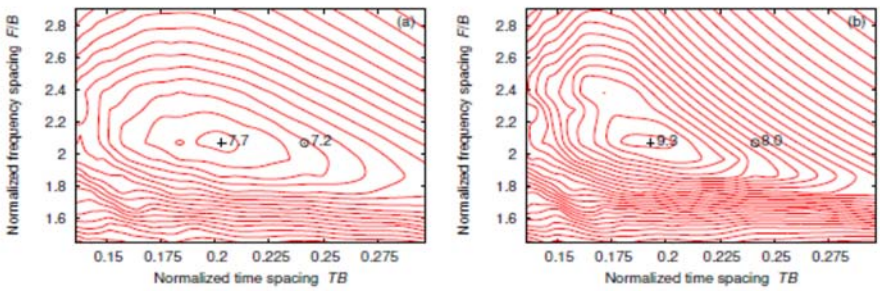

Figure 2.18: Contour plots of the achievable SE (obtained by numerical simulations and shown with increments of 0.2) as a function of the normalized time and frequency spacing for DP-QPSK modulation on the AWGN channel for: (a) E_b/N_0 = 7:5dB; (b) E_b/N_0=22:5dB. The maximum value (+) and the value obtained with one of the configurations adopted in the experimental setup (o) are also reported at the corresponding coordinates.

r	variable node distribution	check node distribution
2/3	$0.333318x+0.6x^2+0.0666821x^{12}$	$0.000277778x^8+0.998935x^9+0.000787037x^{10}$
3/4	$0.249985x+0.666682x^2+0.0833333x^{11}$	$0.000679012x^{12}+0.99858x^{13}+0.000740741x^{14}$
4/5	$0.2x+0.699985x^2+0.100015x^{10}$	$0.999383x^{17}+0.000617284x^{18}$
5/6	$1.54321\cdot10^{-5}+0.166651x+0.75x^2+0.0833333x^{12}$	$9.25926\cdot10^{-5}x^{20}+0.999907x^{21}$
8/9	$0.111096x+0.777793x^2+0.111111x^3$	$0.999861x^{26}+0.000138889x^{27}$

Table 2.6: Code rates and degree distributions of the designed LDPC codes.

2.4.2 System Implementation

A fiber-optic system based on the TFP approach can be implemented by using the same hardware configuration typically used for WDM systems based on coherent detection [12]. A significant difference is in the DSP algorithms actually required at the receiver. Moreover, some care should be taken to ensure that the transmitted signal is linearly modulated. In this section, we will refer to the transmitter and receiver implementation schemes shown in Fig. 2.20, focusing on those element

switch are peculiar to the TFP implementation. Practical details about the experimental setup actually employed in the experimental demonstration will be given in Section 3.Since the system employs single-user detectors, an independent transmitter and receiver pair is used per each optical carrier. Each optical carrier is thus generated at the desired wavelength (e.g., by an external-cavity laser (ECL)), modulated, optically multiplexed with the other modulated carriers, transmitted through the optical link, extracted by an optical de-multiplexer, and independently detected. In each transmitter, the in-phase and quadrature components of two orthogonal states of polarization are independently and linearly modulated by a pair of nested Mach-Zehnder modulators (MZMs). In principle, the desired pulse shape $p(t)$ can be obtained either operating on the electricalsignals that drive the modulator (through a low-pass filter (LPF), as actually shown in the scheme of Fig. 2.20) or on the optical signal after the modulator (through an optical band-pass filter), provided that the overall equivalent low-pass impulse response of the transmitter (driver, modulator, electrical filter and/or optical filter) is $p(t)$ and that linearity of the modulator is preserved by employing a drivingvoltage significantly lower than the modulator V_π. A comparison of the performance obtained by optical or electrical filtering when employing different driving voltages is presented in [13]. An alternative modulation scheme, where linear modulation is obtained by operating the MZM at its maximum driving voltage (to reduce its insertion loss), may also be devised. For instance, by using an additional MZM as a pulse carver and employing optical filtering to obtain the desired pulse shape $p(t)$ and BT product [2], [14], the nonlinearity of the MZM affects only (and slightly) the overall pulse shape $p(t)$, but does not introduce nonlinear ISI. In this scheme, however, the insertion loss saved by increasing the MZM driving voltage is replaced by the additional loss introduced by the pulse carver and optical filter. Finally, a possible implementation based on an arrayed waveguide grating device that filters and multiplexes all the frequency sub-channels in the optical domain has been proposed in [15].Here, we considered a modulation scheme based on a single MZM (driven at low voltage) and analogue electrical filtering which, at the present, seems to be the most practical choice in terms of cost and complexity. Moreover, as discussed in Section 1, the choice of $p(t)$ is not critical and a reasonably good performance can be obtained by employing available analogue low-pass filters, as shown in Fig. 2.18. At the receiver side, each optical carrier is demodulated by employing a phase- and polarization diversity coherent detection scheme. After optical de-multiplexing, each carrier is split into two orthogonal states of polarizations, which are then separately combined with the optical field of a local oscillator (LO) laser in a 2 x4 90° optical hybrid and detected with two pairs of balanced photodetectors. The four resulting electrical signals (the in-phase and quadrature components of each state of polarization) are then sampled by an analog-to-digital converter (ADC) with a bandwidth at least equal to the total bandwidth of the shaping pulse $p(t)$ and

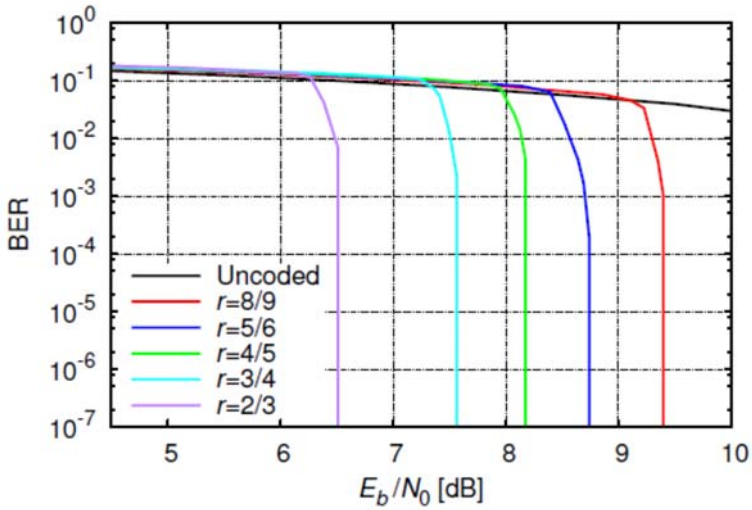

Figure 2.19: Back-to-back BER for uncoded transmission and for the designed LDPC codes, obtained through numerical simulations with the TFP configuration adopted in the experimental setup (40 GBd configuration).

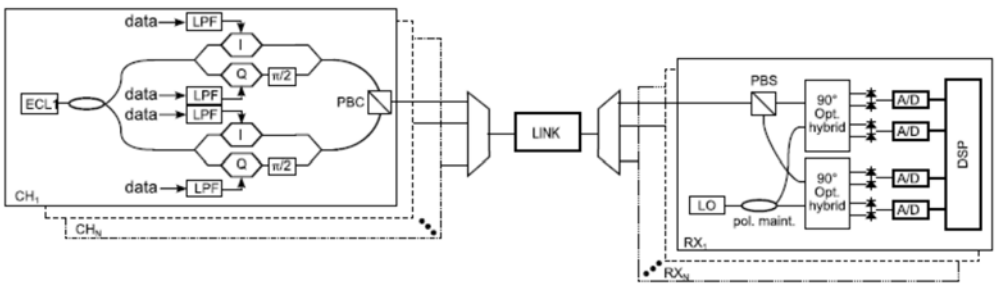

Figure 2.20: Transmitter and receiver schemes of a TFP system employing DP-QPSK modulation.

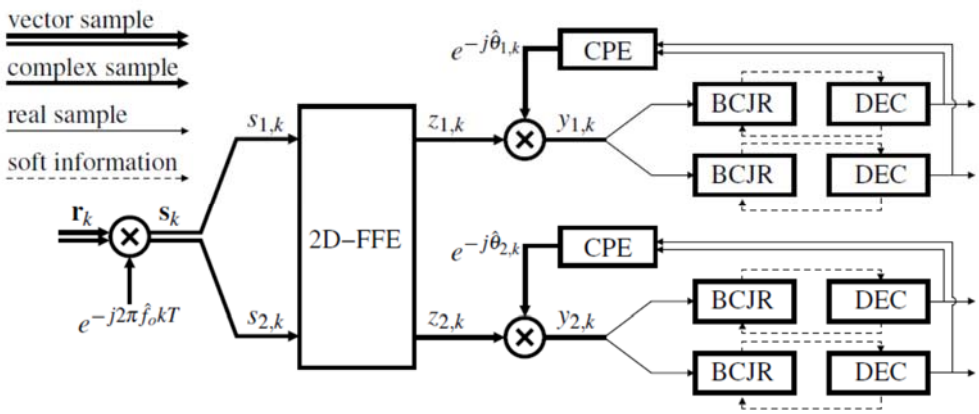

Figure 2.21: Digital signal processing scheme.

twice the sampling rate. The remaining part of receiver processing is digitally implemented according to the scheme depicted in Fig. 2.21, assuming a sampling rate of 1/*T*. Note that, since TFP is employed, the required bandwidth and sampling rate are typically lower than 1/(2*T*) and 1/*T*, respectively, and digital up-sampling can be employed to achieve the 1/*T* rate required for symbol-time processing, without any performance degradation. The *k*-th received column vector of samples $r_k = (r_{1,k}, r_{2,k})^T$(one complex sample per state of polarization)is first processed to compensate for the presence of any large and slowly varying frequency offset $f_0$between the transmit and receive lasers. The estimate $\hat{f}_0$is obtained during the training phase (on a known training sequence) by employing the frequency estimation algorithm describedin [16], and then slowly updated based on decisions. Compensated samples $s_k = r_k e^{-j2\pi\hat{f}_0 kT}$are thenprocessed by an adaptive 2-D N_c-tap synchronous feed-forward equalizer (FFE) that compensates forlinear propagation impairments, such as group-velocity dispersion (GVD), polarization rotations, andpolarization-mode dispersion (PMD), and completes (as explained later) the implementation of the matched filter. At the output of the equalizer, the components $z_{1,k}$ and $z_{2,k}$ of the equalized samples z_k are then separated and independently processed. For each component, decision-directed carrier phaseestimation (CPE) based on the Tikhonov parameterization algorithm [17] and taking into account ISI is employed to cope with the laser phase noise. Finally, the in-phase and quadrature components of the compensated samples $y_{1,k} = z_{1,k} e^{-j\theta_{1,k}}$and $y_{2,k} = z_{2,k} e^{-j\theta_{2,k}}$are separated and sent to four parallel 2^{L_T}-state BCJR detectors [5], followed by four LDPC decoders. The BCJR detectors and LDPC decoders iteratively exchange information to achieve MAP detection according to the turbo principle [18]. At each iteration, as new (more accurate) preliminary decisions are available from the decoders, the CPEs update the phase estimates $\theta_{1,k}$and $\theta_{2,k}$and a new set of compensated samples $y_{1,k}$and $y_{2,k}$isfed to the BCJR detectors. At the first iteration, as preliminary decisions are not available, the CPE exploit pilot symbols (evenly inserted in the transmitted sequence at rater_p) to provide a rough initialestimate of the phase and make the iterative process bootstrap.The equalizer should be configured to make the low-pass equivalent model of the system as close as possible to the ideal scheme considered in Fig. 2.17. Considering that the amplified-spontaneous-emission (ASE) noise accumulated during propagation can be modeled as independent AWGN on each polarization at the input (or, equivalently, at the output) of the fiber, and that the transfer matrix of the fiber $\boldsymbol{H}_f\ (f)$ (in the linear regime) is unitary, i.e, $\boldsymbol{H}_f(f)^{-1} = \boldsymbol{H}_f(f)^{+}$ the required transfer matrixof the 2D-FFE equalizer should be $\boldsymbol{H}_{eq}(f) =$

$$\boldsymbol{H}_f(f)^{+} P(f)^{*} / H_{fe}(f) \qquad (3)$$

where $H_{fe}(f)$is the low-pass equivalent transfer function of the optoelectronic front-end (optical filter, photodetector, and ADC). In this case, the corresponding overall channel transfer matrix would be$\boldsymbol{H}_f(f) = |P(f)|^2 \boldsymbol{I}$, that is independent of the actual transfer matrix of the fiber. The evaluation of (3)for the system at hand requires an accurate characterization of transmitter and receiver front-end, and an adaptive estimate of the fiber transfer matrix $\boldsymbol{H}_f(f)$. Here, instead, taking inspiration from [3],an algorithm has been devised that configures the equalizer according to (3), without requiring a

separate knowledge of $\boldsymbol{H}_f(f), P(f$, and$H_{fe}(f)$. Denoting by $\boldsymbol{C}i$ the 2x2 matrix of coefficients of the *i*-th tap of the equalizer, the equalized samples are:

$$\mathbf{z}_k = \sum_{i=0}^{N_c-1} \mathbf{C}_i \mathbf{s}_{k-i} \qquad (4)$$

Denoting by $x_k$the *k*-th column vector of transmitted symbols, by $h_i$the column vector of the two*i*-th coefficients of the desired (but unknown) overall impulse responses at the output of the matched filter (one per polarization), and by $g_k = (e^{j\hat{\theta}_{1,k}}, e^{j\hat{\theta}_{2,k}})^T$the column vector of the phase estimates forthe *k*-th samples on the two polarizations, the error with respect to the desired channel response is

$$e_k = g_k^{*\circ} z_k - \sum_{i=-L}^{L} h_i \,^\circ x_{k-i} \qquad (5)$$

where ° denotes the Hadamard (entrywise) product. As shown in [3], the variance of each element of(7) is minimum when the matched filter condition is met, i.e., when $\boldsymbol{H}_f(f) H_{fe}(f) \boldsymbol{H}_{eq}(f) = P(f)^* \boldsymbol{I}$.Given the unitarity of $\boldsymbol{H}_f(f)$, this is equivalent to (3) and provides the desired overall response$\boldsymbol{H}_f(f) = |P(f)|^2 \boldsymbol{I}$. Thus, both the required equalizer coefficients and the desired channel coefficientsof the Ungerboeck observation model can be simultaneously estimated by an iterative data-aidedstochastic-gradient algorithm that minimizes the variance of (5). By holding h_0 constant (to anarbitrary value) and forcing the symmetry condition$h_{-i} = h_i^*$, the update law for the equalizer coefficients and the estimated channel coefficients are, respectively

$$\mathbf{C}_i^{(k+1)} = \mathbf{C}_i^{(k)} - \alpha_c (\mathbf{g}_k \circ \mathbf{e}_k) \mathbf{s}_{k-i}^{\dagger}, \qquad 0 \le i \le N_c - 1 \qquad (6)$$

$$\mathbf{h}_i^{(k+1)} = \mathbf{h}_i^{(k)} + \alpha_g (\mathbf{e}_k \circ \mathbf{x}_{k-i}^* + \mathbf{e}_k^* \circ \mathbf{x}_{k+i}), \quad 1 \le i \le L_T \qquad (7)$$

where $\alpha_c$and $\alpha_h$are the step-size gains. Updates (6) and (7) require knowledge of the transmitted symbols. While the equalizer coefficients need to be continuously updated to track variations of the fiber-optic channel, coefficients $\{h_i\}$of the overall channel response do not change with time and can be estimated only once when setting up the link. The initial convergence of the algorithm can be guaranteed by the use of a known training sequence, while a slow tracking of the fiber channel can be achieved by updating only the equalizer coefficients according to (6), possibly at a much lower rate than $1/T$and with a significant delay. This allows to use pilot symbols and/or to replace transmitted symbols with final decisions (after successful decoding of the whole codeword), with a negligible

impact on information rate and performance. The computation of the channel metric for the BCJR algorithm requires knowledge of the channel coefficients$\{h_i\}$ and of the noise variance. Thus, once estimated by (7), channel coefficients are passed to the BCJR processing blocks together with an estimate of the variance of (5).

2.4.3 Experimental Demonstration

Fig. 2.22 shows the experimental setup employed for the practical implementation of the TFP system and for the transmission experiments. Five external-cavity lasers (ECL) are grouped into two sets(odd and even channels), which are separately modulated by means of two integrated nested Mach-Zehnder modulators (IQ-MZM). Bandwidth, rate, and spacing of the five TFP channels are optimized(under some constraints posed by the available hardware) according to the design procedure described in Section 1 to maximize the achievable SE with the desired detector complexity. In particular, the optical carrier spacing is set to *F* = 20GHz and the binary electrical signals that drive the in-phase (I)and quadrature (Q) port of each IQ-MZM are modulated at a rate $R = 1/T = 40GBd$ and filtered by aninth-order Chebyshev low-pass filter (LPF) with a bandwidth $B = 10GHz$ (cut-off frequency). The peak-to-peak modulation voltage is set to $Vpp = 1.5V$, while the half-wave voltage of each MZM is$V_\pi = 2.8\,V$. For the same fixed bandwidth and spacing, lower transmission rates of 35 and 30 GBd are also considered. Polarization multiplexing is emulated by means of a 50/50 beam splitter, an optical delay line, and a polarization beam combiner (PBC). Each I and Q component is modulated by a sequence of random information bits, which are independently encoded according to one of the LDPC codes reported in Tab. 2.6. Odd and even channels are then combined by means of a 2x1 optical coupler (OC). The optical spectrum of the transmitted TFP superchannel (at the input of the recirculating loop) is depicted in Fig. 2.23.At the receiver side, one of the five TFP channels is detected by employing coherent phase- and polarization-diversity detection and setting the local oscillator (LO) at the nominal wavelength of the selected channel. The received optical signal is mixed with the LO through a polarization-diversity90° hybrid optical coupler, whose outputs are sent to four couples of balanced photodiodes. The four photodetected signals are sampled and

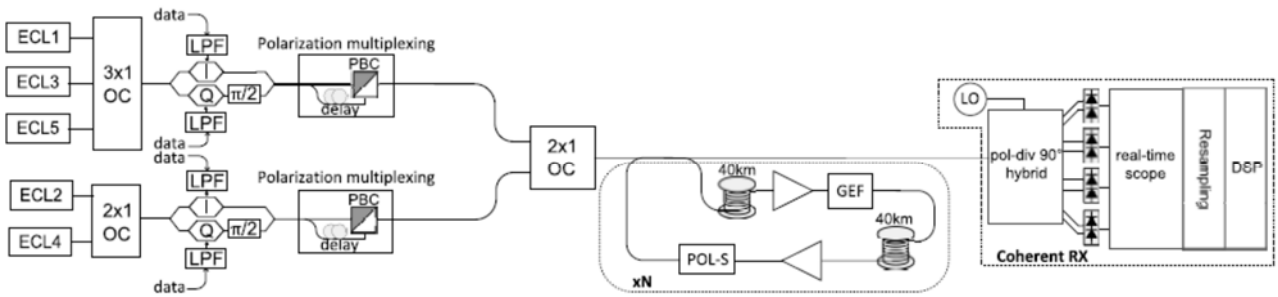

Figure 2.22: Experimental setup.

digitized through a 20 GHz 50 GSa/s real-time oscilloscope in separate blocks of one million samples at a time, corresponding to about 12 codewords (at 40 GBd)per each quadrature component. After

digital re-sampling at rate $1/T$ (one sample per symbol), each block is processed off-line according to the scheme of Fig. 2.21, with N_c= 23 equalizer taps and $L_{T=}3$ truncated channel memory (8-state BCJR detector). The first received codeword of each block (on each quadrature component) is used as a training sequence for the convergence of the DSP algorithms(initial estimate of the frequency offset$\hat{f}_0$, equalizer coefficients $\boldsymbol{C}i$, and channel coefficients $\boldsymbol{h}i$),while the others are effectively employed to measure system performance. This is not consideredin the computation of the SE as, in a real system, the training sequence would be transmitted only once. After decoding of each codeword, the equalizer coefficients are then slowly updated (one update each 500 decoded symbols) according to (6) by employing decisions. Pilot symbols at rate $r_p = 1/400$ are finally employed (and accounted for in the SE computation) to make the iterative decoding process (CPE, BCJR detection, and LDPC decoding) bootstrap. A maximum of 20 turbo iterations is considered.

Bit-error rate (BER) measurements are performed off-line by averaging over a total of about 500randomly selected codewords (of length 64800). This sets a limit for the minimum measurable BER at about 10^{-7}, and for reliable BER measurements at about 10^{-6}. Transmission is considered to beerror-free when all the information bits are correctly decoded at the receiver, which means, in fact, BER < 10^{-6} with high probability. The detection of the adopted LDPC code is characterized by the presence of possible error floors at BER $<10^{-8}$ (which where, therefore,never observed neither experimentally nor in simulation), which can be practically removed by concatenating outer hard-decision BCH codes with small additional overhead (<0.4%), complexity, and latency [11]. We account for this fact by virtually including a BCH code with rate $r_{BCH} = 0.996$ (0.4%redundancy) in the computation of the experimentally achieved SE, which is therefore defined as the actual amount of information that is reliably transmitted (error-free within measurement accuracy)per unit time and bandwidth once the overhead due to the LDPC code, outer BCH code (virtually present), and pilot symbols is removed

$$\tilde{\eta} \triangleq \frac{4 r_{\mathrm{LDPC}} r_{\mathrm{BCH}} (1 - r_p)}{FT} \leq \hat{\eta}_{\max} \qquad (8)$$

Depending on the available $Eb/N0$ and on the presence of uncompensated transmission impairments, different code rates r_{LDPC} are required to obtain reliable transmission. The transmission system can thus be adapted to finely adjust the information rate to the channel conditions (accumulated noise and propagation penalties) by changing r_{LDPC} (selected among the values available in Tab. 2.6) while keeping the transmission rate $1/T$ and channel spacing F constant. A wider tuning of the SE is finally obtained by changing also the transmission rate. In particular, rates of 40, 35, and 30 GBd are considered. The difference between the experimentally achieved SE (8) and the theoretically achievable SE (1) depends on the performance (and available rate granularity) of the designed LDPC codes and on the presence of any additional impairment unaccounted for in this design procedure (e.g., modulator imperfections, nonlinearity, etc.).Long-distance transmission is emulated by using a re-circulating loop, composed of two 40 km long spans of standard single mode fiber, two optical amplifiers, a polarization scrambler (POL-S),and a gain equalizer filter (GEF). The total dispersion accumulated during propagation through there-circulating loop is compensated by a static frequency-

domain equalizer, placed in front of the 2DFFEequalizer and configured according to the selected link length

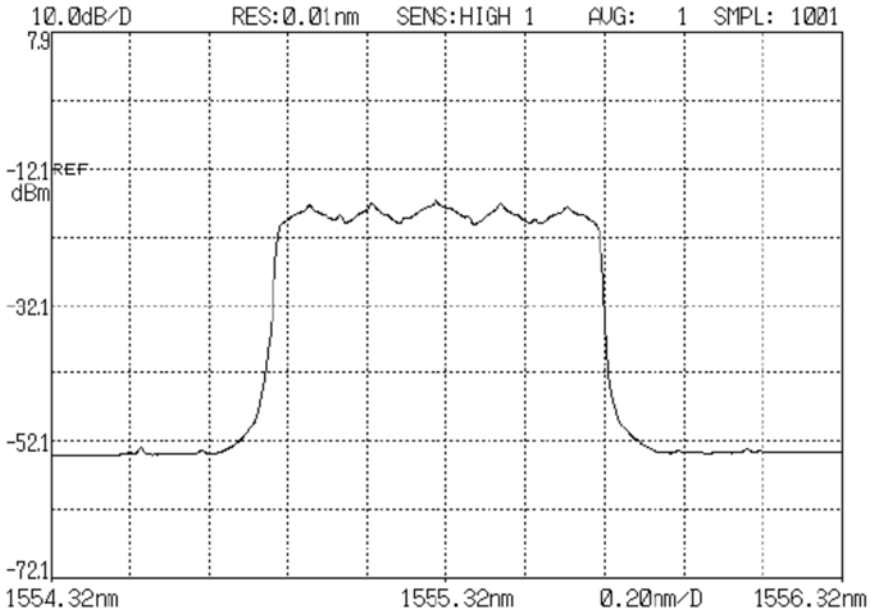

Fig. 4.7: Optical spectrum of the TFP superchannel at the input of the recirculating loop.

Figure 2.23: Optical spectrum of the TFP superchannel at the input of the recirculating loop.

2.4.4 Back to back measurements

The back-to-back performance of the system is investigated by bypassing the recirculating loop and measuring only the BER of the central channel. In order to experimentally verify the TFP optimization performed numerically in Section 1, signals at different baud rates are generated and coded with different code rates. Fig. 2.24(a) shows the measured BER values as a function of E_b/N_0(obtained by measuringthe OSNR through an optical spectrum analyzer and using the relation $E_b/N_0 = 2BrefOSNR/Rb$)for a 40 GBd transmission and some of the LDPC codes reported in Tab. 2.6. Compared to simulation results in Fig. 2.19, the experimental penalty is about 2 dB for the 3/4 LDPC code and increases up to more than 3 dB for the 8/9 code. This can be explained by considering that the measuredE_b/N_0ratio reported on the x-axis accounts only for optical noise. Thus, we expect an experimental penalty due to electrical noise (and other receiver imperfections) that becomes more relevant as the measuredE_b/N_0increases (i.e., the amount of optical noise decreases). Fig. 2.24(b) shows the achieved SE, defined according to (8), for 30, 35, and 40GBd transmission. In practice, Fig. 8(b) reports, for each code rate and baud rate, the achieved SE and the corresponding minimum required E_b/N_0ratio to obtainreliable transmission (where the BER curves in Fig. 2.24(a)suddenly drop to zero). As predicted by Fig. 2.18, the highest SE is achieved at 40 GBd transmission (and could be possibly increased by further increasing the transmission rate up to 50 GBd, tough we could not verify

it due to limitations of the available hardware). However, for low SNRs, a slightly better efficiency can be obtained at35 GBd.

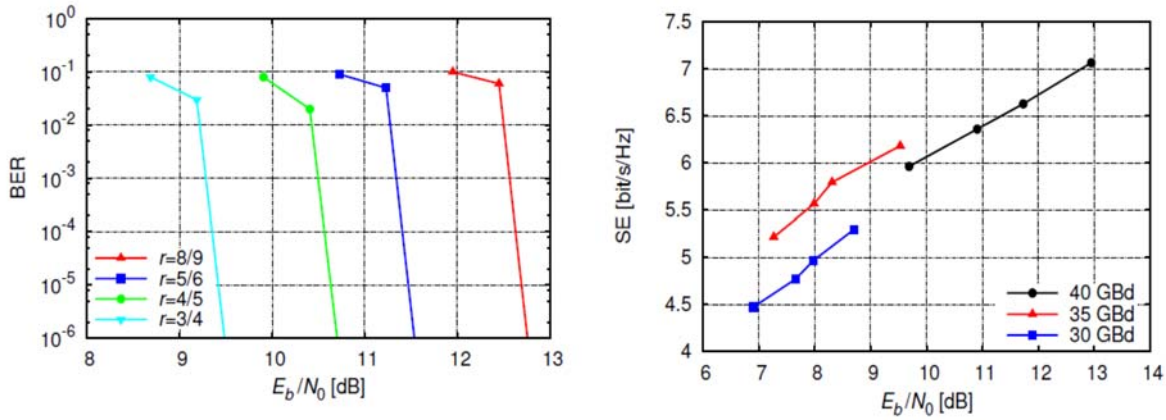

Figure 2.24: (a) Experimental back-to-back performance of the TFP system (only central channel): BER with the 40 GBd DP-QPSK configuration and different code rates.(b) Experimental back-to-back performance of the TFP system (only central channel): achieved SE with the 40 GBd, 35 GBd, and 30 GBd DP-QPSK configuration.

2.4.5 Transmission experiments

Transmission experiments are performed by properly setting the number of rounds that the signal travels through the recirculating loop in Fig. 2.22. The launch power is optimized to obtain the best trade-off between noise and nonlinear propagation effects. For the sake of simplicity, it is assumed that the optimal launch power is independent of the transmission distance and code rate. The optimizations performed by setting the same power for the five channels and measuring the performance of the third (central) one, which is the most affected by inter-channel nonlinearity. Fig. 2.25(a)shows the maximum achievable transmission distance as a function of the launch power, for either 30 or 40 GBd transmission and a fixed SE $\tilde{\eta} \cong 5.3$ bit/s/Hz (obtained with code rates of 8/9 and 2/3, respectively). A slightly different result is obtained for 30 GBd and 40 GBd transmission, the optimum launch power being -5 and -6 dBm per channel, respectively. However, in the following measures, the same launch power of -5 dBm per channel is used for any transmission rate. Once the launch power has been set, the maximum achieved SE $\tilde{\eta}$—defined in (8) and obtained by selecting the highest code rate(among the available ones reported in Tab. 2.6) guaranteeing error-free transmission—is measured as a function of the transmission distance for a transmission rate of 30, 35, and 40 GBd. Fig. 2.25(b) shows the results for each of the five TFP channels (symbols) as well as for the whole super-channel(lines, corresponding to the worst-performing channel). In the same figure, the code rates employed to achieve the measured SEs are also indicated. Due to inter-channel nonlinearity (as $F = 2B$, linear crosstalk among channels is practically negligible), the central channel is typically the worst performing, while the outer channels are the best performing. This is more evident at higher transmission rates. At short distances, i.e. at high OSNRs, the

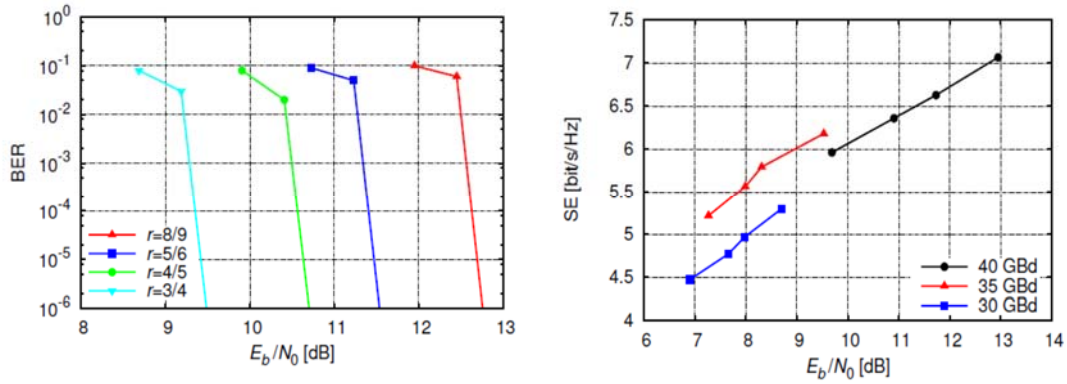

Figure 2.25: Optimization of the launch power: reached distance vs launch power at a fixed SE 5.3bit/s/Hz. (b): Experimentally achieved SE (all the TFP channels) vs reached distance with the 40 GBd 35 GBd, and 30 GBd DP-QPSK configuration.

achieved SE is much higher (about 7.1 bit/s/Hz at400 km) than the theoretical limit of 4 bit/s/Hz achievable by Nyquist-WDM transmission with same DP-QPSK modulation format, and remains higher up to almost 6000 km. Moreover, the SE can be adapted to the propagation conditions by simply changing the code rate or, for significant OSNR variations, the amount of packing (i.e., the baud rate $1/T$ or, equivalently, the bandwidth B and the frequency spacing F), without changing the modulation format.

2.4.6 Conclusions

We have investigated application of the TFP approach to fiber-optic systems. The main challenges pertain to the peculiar nature of the channel (the optical fiber, impaired by linear and nonlinear propagation effects) and to the high data rates involved. We have thus discussed the implementation schemes, focusing on the main differences with respect to a conventional coherent WDM system. The only relevant difference is a modification of the DSP algorithms employed for detection. In the proposed scheme, a butterfly equalizer adaptively addresses propagation impairments and performs matched filtering, while intentional ISI due to TFP filtering is accounted for by a BCJR detector. To ensure a proper distribution of tasks between the equalizer and BCJR detector, an algorithm has been proposed that adaptively controls the equalizer and provide channel metrics to the BCJR detector. This makes the receiver fully adaptive, without requiring a priori knowledge of the adopted TFP configuration. Soft-decoding forward-error correction is finally employed. In particular, irregular LDPC codes with various code rates (in the range 2/3–8/9) and specifically optimized for the TFP channel have been designed to operate at low error rates. They approach (within about 3 dB) the SE limits achievable by the proposed techniques at different SNRs. The performance of the proposed system has been tested both experimentally and by simulations, demonstrating technical feasibility and good performance. Five closely-packed DP-QPSK channels were transmitted through a re-circulating loop, keeping the net SE beyond the theoretical limit of Nyquist-WDM (4 bit/s/Hz) up to 6000 km. The channel bandwidth and spacing was held fixed to20 GHz, while the transmission rate and code rate

were adapted, depending on the transmission distance, to the available OSNR. At 400 km, a net SE of more than 7 bit/s/Hz was achieved by setting the transmission rate at 40 GBd (twice faster than the Nyquist limit) and the code rate to 8/9. The transmission distance was then gradually increased up to 6000 km, with a net SE which gradually decreased to about 4 bit/s/Hz (achieved with a 30 GBd transmission rate and a 2/3 code rate). Both the LDPC encoder and decoder were actually included in the experimental setup, as it is advisable in the presence of soft decoding, for which the use of a numerically evaluated "pre-FEC BER threshold" may be unreliable.

In conclusion, we have demonstrated that TFP with low-level modulation (e.g., DP-QPSK) can be considered as a practical and viable alternative to high-level modulations to achieve high SE over long-haul fiber-optic links, providing good performance and high flexibility (reach adaptation and filter configuration) with simpler transponder architectures (single modulation format, relaxed constraints on pulse shape, no DSP and digital-to-analog conversion at the transmitter). In the second place, a significant improvement can be obtained at the expense of an additional DSP complexity. For instance, by modifying the detection strategy to account for a longer ISI (e.g, increasing the number of trellis states or considering channel shortening techniques, as demonstrated in MS3.1) and/or also for ICI (multi-user detection), pulses can be more densely packed, achieving a higher SE. Finally, the DSP implemented in the experimental setup does not include any nonlinearity mitigation strategy, which could be adopted to improve the overall performance as already demonstrated in MS3.2.

2.5 Single-user system design and numerical simulations MS2.5

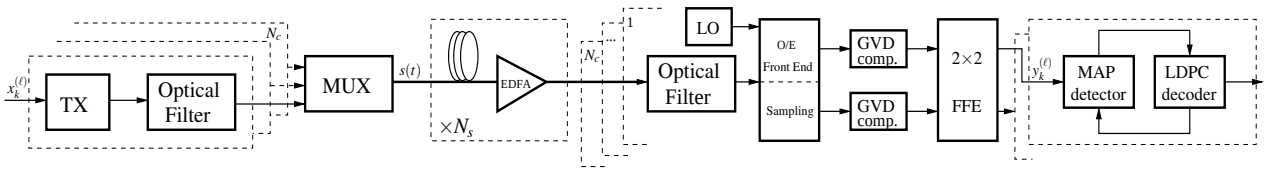

Figure 2.26: Schematic of the designed system.

The proposed system for time-frequency packing (TFP) is showed in Fig.2.26. N_c independent channels are generated and transmitted over the channel, each carrying a polarization-multiplexed (PM) quadrature phase shift keying (QPSK) signal, encoded with a low-density parity-check (LDPC) code. At the receive side each channel is separately detected by a specific opto-electronic front-end, followed by proper electrical processing designed to implement the TFP principle. After chromatic dispersion compensation, performed by fixed-tap filtering, and frame and frequency synchronization, the signal is processed by a 2x2 fractionally spaced adaptive equalizer that implements polarization multiplexing, decimates the samples, and compensates for possible residual chromatic dispersion and polarization dispersion; then, after phase noise compensation, signal samples are passed to the detector, that iteratively exchanges information with the LDPC decoder, in order to take reliable decisions on the transmitted symbols. Details on the implemented system can be found in [1], [2].

The experimental set-up clearly envisages a combination of real devices that often present unknown or poorly defined bandwidths and transfer function shapes. Through several measures of the impulse response of our system in back-to-back configuration, we were able to take into account the behavior of these devices, including specific filters in the simulated system. We developed a raw simulation tool, programmed in Fortran, in order to exploit a huge library of preexisting signal processing subroutines at our disposal, and because of its efficiency and simplicity. We used this tool to perform preliminary and indicative simulations, with the aim of defining specific system parameters. At the same time, we also developed a more elaborated processing tool, based on Matlab, with a complete graphical user interface, which performs the off-line software processing of the experimentally acquired signal on field. Besides the iterative detection/decoding stage used to take decisions on the transmitted symbols, we also implemented the method described in [3], which represent a very powerful and useful tool to predict system performance, without resorting to time-consuming simulations over wide sets of possible codes and extremely long bit sequences. In fact, the computation of the lower bounds on the system information rate, once that the receiver complexity has been chosen and defined, enables fast comparisons among different system parameters, so that an accurate optimization is possible (see [1] for details).

In order to improve the system spectral efficiency (SE), we also implemented a channel shortening (CS) technique, that is an effective processing which improves the performance of an ISI impaired system (details will be given in section 3.1). Nevertheless, its effectiveness depends on the kind of channel impulse response of the system, and on the capability to perform accurate and reliable processing at the receiver side. In time-frequency packing (TFP) systems, we must be able to design proper transmit and receive filters in order to maximize both the packing, and to improve the effectiveness of the channel shortener (i.e., a linear filter in addition to proper detector metrics) in compressing the intersymbol interference in a few taps. This task is obviously quite hard to be accomplished, since many system devices present imperfections that cannot be controlled, and they also have bandwidths and transfer function shapes that do not match the desired constraints. At the transmit side we process the electrical modulating signal with a 9th-order Chebyshev filter of the first type, with 5 GHz bandwidth. Such filter provides a good impulse response for a TFP system with 24 Gbaud transmitted signal, and, as shown in Fig. 2.27, simulation results on the system spectral efficiency with and without channel shortening, in this ideal single-channel system, highlight the benefit of the proposed technique. It must be noticed that these results can be reached with perfect synchronization and timing, in an ideal back-to-back system which envisages only the presence of transmit and receive side filters. Moreover, it should not surprise that the detector with L=3 has a worse performance than with L=2, since it is known that truncating the detector memory with certain impulse responses may entail benefits due to an effect of average interference cancellation. In the presented simulation results we also included a 1st-order Gaussian optical filter with 6 GHz bandwidth that fits the unknown impulse response of other transmit side devices. In Fig.2.28, we reported the impulse response at the output of the receive side matched filter (synthesized through by properly adapting the equalizer) of a high-power (HP) channel in presence of low-power (LP) interfering channels, for the experimental and the simulated system. The almost perfect agreement of two pulses allows to reliably simulate the system behavior in order to find the optimal frequency spacing and power ratio between odd and even channels. However, the experimental system, and consequently

its simulative counterpart that we set up accordingly, do envisage several impairments and imperfections that prevent the correct working of the channel shortening technique, which requires, on the contrary, an accurate control of the signal at the input of the detector. In fact, residual uncompensated frequency offsets, phase noise imperfect estimation, transmitter IQ unbalance, unavoidable slightly noisy equalization (which means imperfect matched filtering), influence the performance of the shortening technique. Fig. 2.29 shows the simulation results on the spectral efficiency in a back-to-back *actual* system, including all the mentioned impairments that we were able to estimate in the experimental set-up.

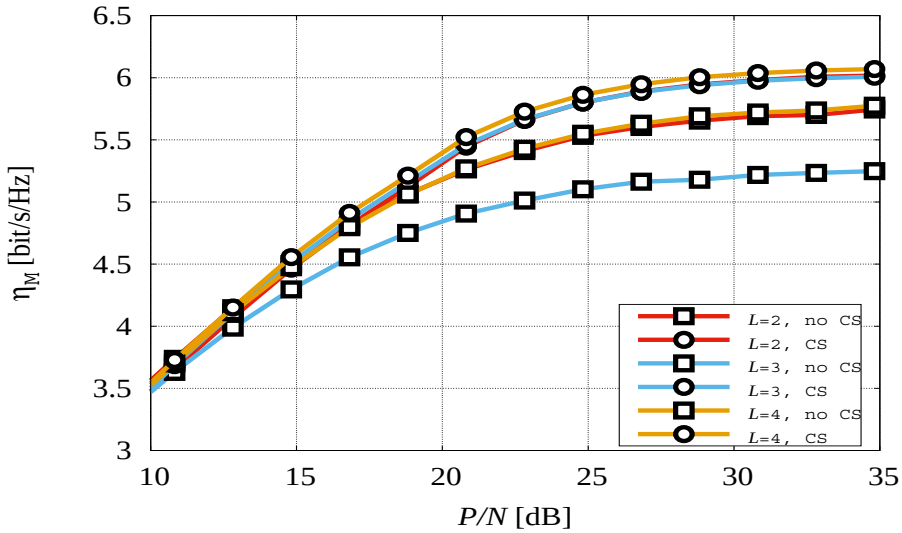

Figure 2.27: Schematic efficiency of back-to-back TFP in presence of a transmit side electrical 9th-order Chebyshev filter with 5 GHz bandwidth, and a 1st-order optical Gaussian filter with 6 GHz bandwidth.

The received side filter is matched to the transmit side impulse response. Results are plotted for increasing detector complexity, i.e., number of states (S), which is determined by the channel memory length ($S=2^L$), with and without channel shortening.

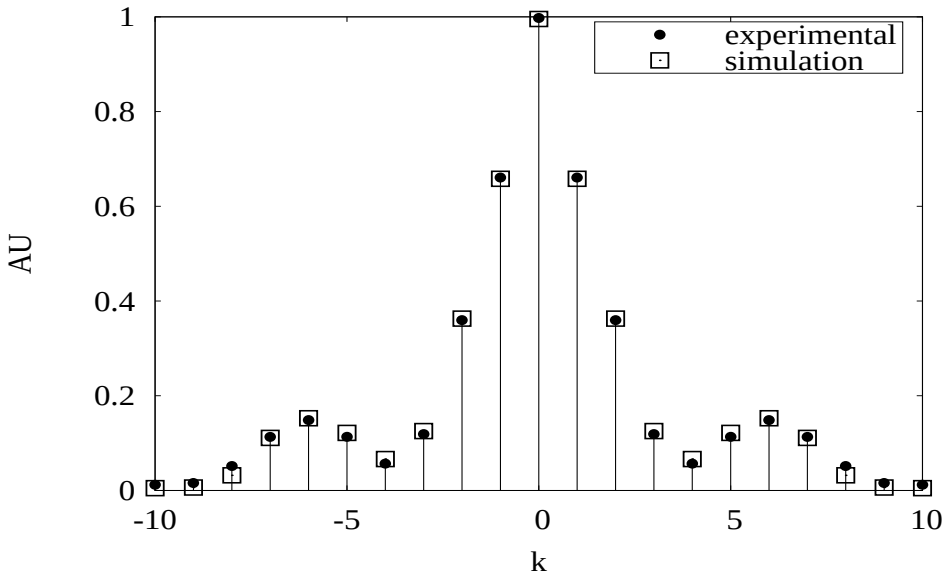

Figure 2.28: Impulse response at the output of the matched filter in the experimental and the simulated systems.

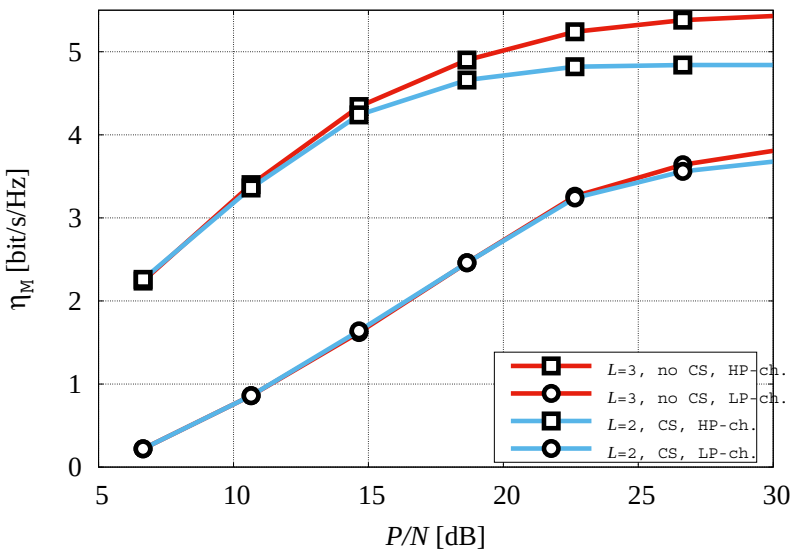

Figure 2.29: Spectral efficiency of the simulated actual systems, including frequency offset, phase noise, equalization-based matched filter, for L=2 and channel shortening and L=3 without channel shortening, and for the high-power (HP) channels and low-power (LP) channels.

It can be noticed that, even if Fig.2.27 predicted a benefit from the employment of *L*=2 with CS with respect to *L*=3, the performance gain is lost due to non-ideal matching of the expected system impulse response with the one obtained in actual conditions at the input of the detector. Thus, in order to obtain the best possible performance, we chose not to include the CS in the receiver set-up, for the

time being. Indeed, since through a proper optimization of each receiver side processing parameter it may be possible to, at least, obtain the same results by employing a 4-state detector with CS, in this way reducing the overall complexity, we consider to include this technique once the field-trial set-up will be completely defined.

2.6 Multi-user system design and numerical simulations MS2.6

The multi-user processing that we implemented is based on the double signaling technique. The choice was motivated by the fact that the alternative processing based on classical multi-user detection, though representing a more strict technique for simultaneous detection of parallel channels, entails two main drawback, especially in the case of high-speed optical communications. First, it is necessary to synchronize all channels that have to be processed simultaneously, and this a real hard task in optical systems, where locking signal paths and modulators may turn out to be almost impossible; second, the detector complexity grows exponentially with the number of users, thus it becomes unfeasible even for a few users. On the other hand, the processing that we implemented, namely double signaling, allows to increase the system spectral efficiency just by removing the signal of the detected channels from the overall received signal, through cancelling algorithms, enabling a reduced spacing between channels, whereas the receiver complexity does not increase (except for the processing due to cancellation), as we are still dealing with single-user detectors. In this case, we have two minor drawbacks: channels have to be split in two sets, a first set at a higher transmitted power, to be detected in the first place, and a second set at a lower power, that can be detected once the first set has been cancelled (notice, that, therefore, the relative power of the transmitted channels must be accurately controlled, and different codes must be used, as the low power channels are more impaired); then, an intrinsic, obvious, latency must be taken into account.

The cancellation of the received high-power (HP) channels is performed through two main algorithms, namely a discrete-time channel coefficient estimation and a time-varying phase noise estimation. We recall the transmitted signal model, as also reported in section 3.1, that is

$$s(t) = \sqrt{1-\beta^2}\sum_{k,\ell} x_k^{(\ell)} p(t-kT-\tau^{(\ell)}) e^{j(2\pi\ell Ft+\theta^{(\ell)})} + \beta \sum_{k,\ell} y_k^{(\ell)} p(t-kT-\tau^{(\ell)}) e^{j(2\pi(\ell+1/2)Ft+\theta^{(\ell)})} \quad (1)$$

where $\beta \in [0,1]$ is the power allocation factor, T is the symbol interval, $x_k^{(\ell)}$, $y_k^{(\ell)}$ the symbols transmitted over the ℓth and (ℓ+1/2)th carrier during the kth symbol interval, $\tau^{(\ell)}$ and $\Theta^{(\ell)}$ the delay and the initial phase of the carriers, respectively, and F the frequency spacing between two even or odd adjacent carriers (thus, the spacing between an odd and an even channel is $F/2$). Clearly, eq. (1)

refers to one polarization transmission only; when dealing with polarization multiplexing, we must take into account the 2x2 channel transfer function, and the transmission of the signal over two orthogonal polarizations, and thus the expression of the received signal that we need to cancel is

$$\mathbf{r}(t) = \beta[r_1(t), r_2(t)]^T = \beta \sum_k \mathbf{x}_k \mathbf{Q}(t-kT) e^{j(2\pi F t+\theta)} + \mathbf{w}(t) \quad (2)$$

where we indicated vectors with bold fonts, and matrices with capital bold font, in fact, we have **w**(t)= $[w_1(t), w_2(t)]^T$, the noise over the two orthogonal polarizations, $\mathbf{x}_{\boldsymbol{k}} = [x_{1,k}, x_{2,k}]^T$ the transmitted symbols belonging to the QPSK complex alphabet, and $\mathbf{Q}(\mathrm{t}) = \mathbf{H}(\mathrm{t}) \otimes \mathbf{P}(\mathrm{t})$ the 2x2 matrix that includes the well-known linear effects of the channel $\mathbf{H}(\mathrm{t})$**,** and of the supporting pulse $\mathbf{P}(\mathrm{t}) = p(t)\mathbf{I}$, being $\mathbf{I}$ the identity matrix. Notice that the effects of group velocity dispersion (GVD) are already compensated for by a fixed-tap electrical filter that equalize the overall signal, so only the impairments given by polarization rotation, possible residual GVD, polarization mode dispersion (PMD), timing jitter, etc., must be accounted for, so that a few tens taps are sufficient to estimate the channel response. The cancellation algorithm is thus designed to estimate the samples of $\mathbf{Q}_{\boldsymbol{k}} = \mathbf{Q}(t)|_{\boldsymbol{t}=\boldsymbol{t}_{\boldsymbol{k}}}$ and the possibly time-varying value of $\theta = \theta_k$. The estimation of the channel impulse response taps is performed through a decision-directed minimum mean square error (MMSE) algorithm (see [1]), namely

$$\begin{aligned} \hat{r}_{1,k} &= \sum_i \left(\hat{\mathrm{x}}_{1,\boldsymbol{k}-\boldsymbol{i}} \hat{q}_i^{11} + \hat{\mathrm{x}}_{\mathbf{2},\boldsymbol{k}-\boldsymbol{i}} \hat{q}_i^{12}\right) \\ \hat{r}_{2,k} &= \sum_i \left(\hat{\mathrm{x}}_{1,\boldsymbol{k}-\boldsymbol{i}} \hat{q}_i^{21} + \hat{\mathrm{x}}_{\mathbf{2},\boldsymbol{k}-\boldsymbol{i}} \hat{q}_i^{22}\right) \end{aligned}, \quad (3)$$

where the *hat* specifies estimated variables, and it must be noticed that the received samples have undergone frequency compensation. The update of the channel taps from instant *k* to instant *k+1* (the update interval length can be tuned according to complexity reduction constraints, but it is mandatory to periodically update the coefficients throughout the received signal extension) is then performed as

$$\hat{q}_i^{ml,(k+1)} = \hat{q}_i^{ml,(k)} + \alpha \cdot (\hat{r}_{m,k} - r_{m,k}) \hat{\mathrm{x}}_{l,k-i}^*, \quad m, l = 1,2. \quad (4)$$

The estimate of the phase term is instead obtained through a sliding window average of proper length, exploiting the received samples and the detected symbols filtered by the estimated channel taps, namely

$$\hat{\theta}^{(k+1)} = \tan^{-1}\left(\sum_\ell r_{m,k-\ell}^f \hat{r}_{m,k-\ell}^* e^{j2\pi k \hat{F}}\right), \quad (5)$$

where, in this case, the received samples do not undergo frequency compensation, so that this estimate is also useful to recover the phase error due to imperfect frequency offset compensation.

Clearly, there is no need of a further estimate of the frequency offset since it is already available from the detection processing.

As a result, it is possible to cancel the signal of the HP detected channel from the overall received signal, as shown in Fig. 2.30.

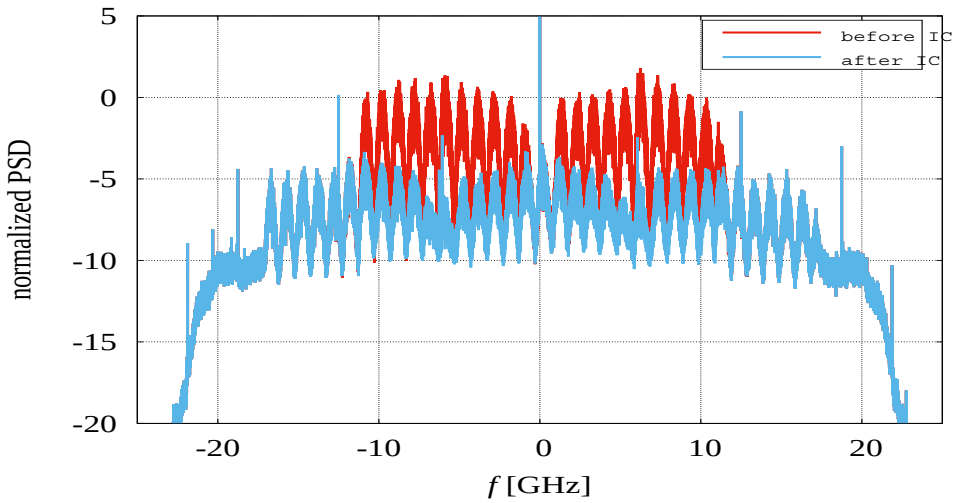

Figure 2.30: PSD of the overall received signal before processing, and after two HP channels were detected and cancelled (interference cancellation, IC).

It can be noticed that after cancellation of the two side HP channels, the three remaining LP channels are clearly distinguishable and can be detected in turn. The reported power spectral densities (PSD) refer to an experimental back-to-back measure, where the cancellation processing lowers the HP channel power by more than 10 dB.

The optimal spacing and interference power ratio has been found by computing lower bounds on the information rate, as explained in section 2.5; the overall transmitted signal in back-to-back configuration (i.e., we simulated the asymptotic values of the information rate curves, for very high signal-to-noise ratios) was simulated and processed by a properly designed receiver. Results are shown in Fig. 2.31, where contour plots are drawn as a function of channel frequency spacing *F* and power unbalancing between channels *C/I,* for 24 Gbaud signals. As a consequence, we chose 6 GHz spacing and we had a quite accurate hint about the power unbalance between channels, as we could later verify with experimental results.

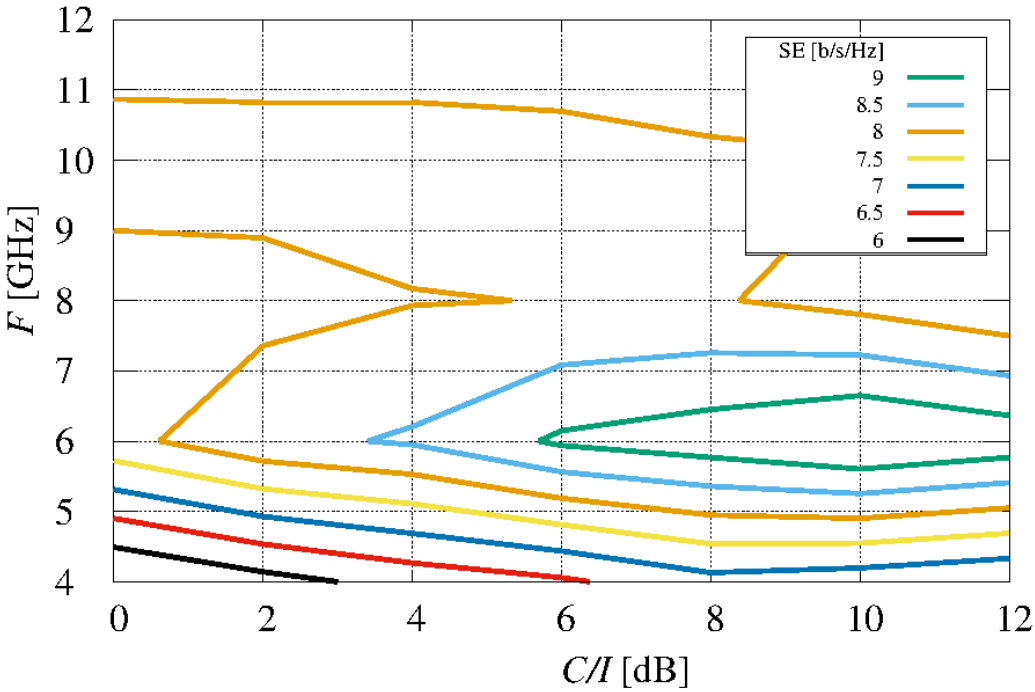

Figure 2.31: Contour plots of the spectral efficiency in back-to-back as a function of channel frequency spacing *F* and power unbalance between channels *C/I*.

In order to enhance the spectral efficiency of the time-frequency packing (TFP) system with multiuser processing, we also designed new low-density parity-check (LDPC) codes, to fit the particular channel response determined by tight filtering, i.e., heavily impaired by intersymbol interference (ISI). We first adopted codes derived from the European Space Agency (ESA) digital video broadcasting DVB-S2 standard [2], but it is known that such codes are designed for fast convergence in additive white Gaussian noise (AWGN) channels, in absence of ISI, which is quite far from our scenario. Thus, we exploited the progressive-edge-growth (PEG) algorithm described in [3] and the extrinsic information transfer (EXIT) charts analysis described in [4], to design new codes with proper characteristics and rates for our purposes. The EXIT charts provide useful information about the behavior or the designed code, given its rate, check and variable node degrees, and degree distributions. In Fig. 2.32 the EXIT curves are shown, i.e., the mutual information at the output of the decoder $\boldsymbol{I}_{out}$ as a function of the input mutual information $\boldsymbol{I}_{in}$, of a rate ½ ESA code compared to a new self-designed code with the same rate.

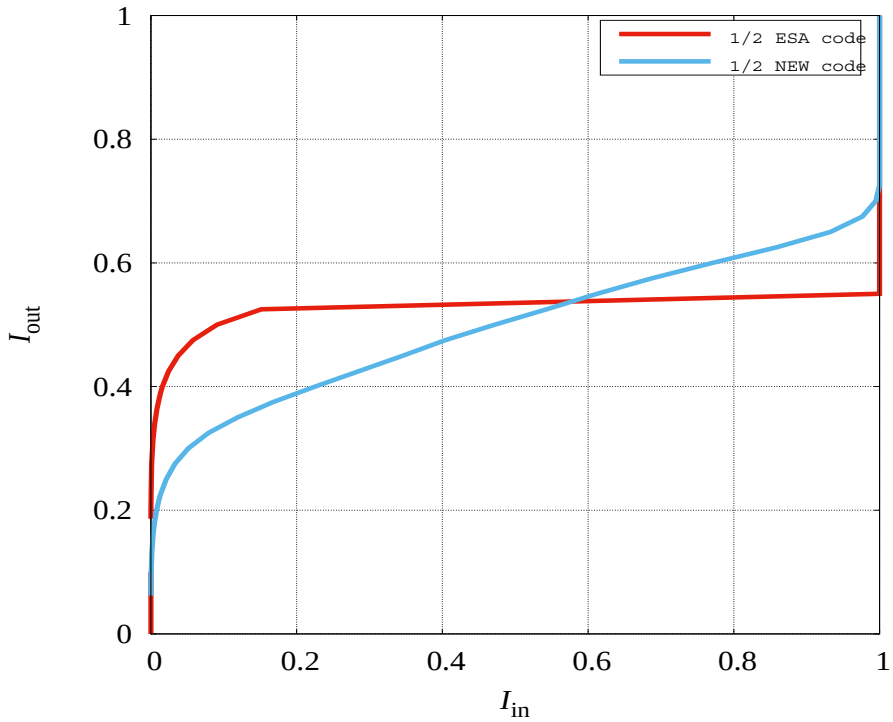

Figure 2.32: EXIT charts of the rate-1/2 ESA DVB-S2 LDPC code and of a self-designed rate-1/2 LDPC code.

The almost flat with quite high $I_{out}(0)$ value EXIT chart of the ESA code entails a fast convergence, which means that few iterations are needed to decode the codeword, but it also means that good starting conditions are required, that is the detector must provide a sufficiently low bit error rate (BER) already at first iteration. Since our scenario is characterized by strong ISI, this condition is hardly reached at low signal-to-noise ratios (SNR). Thus, we designed codes that present a lower $I_{out}(0)$ value, at the price of a more pronounced slope, in this way attaining a code that starts iterating at a higher BER but with slower convergence (i.e., more iterations). We designed several codes with different rates suitable for a wide range of operative conditions.

3 Innovation Techniques

3.1 Channel shortening in a single user optical coherent system MS3.1

The time-frequency packing (TFP) technique intentionally introduces intersymbol interference (ISI) and intercarrier interference (ICI) with the aim of improving the spectral efficiency. This is done by reducing the symbol time (the time spacing) and/or the frequency spacing among adjacent carriers. Time and frequency spacing can be reduced much more (and thus the spectral efficiency further increased) if a proper receiver able to cope with the intentionally introduced interference is adopted. Alternatively, a less complex detector can be used without affecting the target spectral efficiency. In order to take into account ICI at the receiver, multi-user detection should be considered, but, on the other hand, ICI can be decreased at the expense of introducing more ISI, which in TFP systems can be very large, i.e., a large channel memory is present as a result of the introduction of time packing. This would require a trellis-based detector with a very large complexity. This complexity can be reduced by properly "compressing" the equivalent channel response (in the linear regime) through the adoption of a proper channel shortening (CS) technique [1].
Let us consider the generic subcarrier of the transmitted signal model

Error! (1)

where T is the symbol interval, $x^{(\ell);k}$ the symbol transmitted over the ℓth carrier during the nth symbol interval, $\tau^{(\ell)}$ and $\Theta^{(\ell)}$ the delay and the initial phase of the ℓth carrier, respectively, and F the frequency spacing between two adjacent carriers. Assume a channel which simply introduces additive white Gaussian noise (AWGN). The received signal reads

Error! (2)

A sufficient statistics for detection is represented by the Ungerboeck observation model [2]. It is obtained by using a filter matched to $p(t)$, whose output is sampled with rate $1/T$. The sequence at the output of the matched filter reads

Error! (3)

where $\{g_i\}^{L_H;i=-L_H}$ are the ISI samples, and n_k is a discrete-time Gaussian process with $E\{n_{k+m}n^{*;m}\}=2N_0g_k$, where $N_0/2$ is the two-sided power spectral density of the amplified spontaneous emission (ASE) noise per polarization. It is useful to gather all samples in a matrix notation as

$$\mathbf{y}=\mathbf{G}\mathbf{x}+\mathbf{n} \quad (4)$$

where **G** is a properly defined Toeplitz matrix. Optimal MAP symbol detection for this channel can be performed by using a Bahl-Cocke-Jelinek-Raviv algorithm [3, 4]. However the complexity of the optimal detector increases as M^{L_H}, where M is the cardinality of the employed constellation, which makes the algorithm unmanageable for constellations with high cardinality or when the channel memory L_H is large.

To reduce the detector complexity, there are two main directions: (1) to process the original trellis, but with reduced complexity so that only a fraction of the trellis is explored (e.g., [5]), or (2) to construct a reduced trellis which is then processed with full complexity (e.g., [6]). The *channel shortening* technique belongs to this second class. In other words, the second class of algorithms performs detection by considering a memory $L<L_H$, properly filtering (with the so called *channel shortener*) the received signal in order to obtain a properly designed *target response* $\boldsymbol{g}_r$ shorter than the actual ISI **g**. The technique described in [1] designs the channel shortener to maximize the achievable information rate.

Going into mathematical details, the actual channel law reads

$$\textbf{Error!} \qquad (5)$$

whereas the detector, due to the constraints on the complexity, considers a mismatched channel law

$$\tilde{p}(\mathbf{y}|\mathbf{x}) \propto \exp\left\{2\Re(\mathbf{x}^{\dagger}\mathbf{H}_r\mathbf{y}) - \mathbf{x}^{\dagger}\mathbf{G}_r\mathbf{x}\right\} \qquad (6)$$

where $\mathbf{H}_r$ is a proper filtering (the *channel shortener*), and without loss of generality the noise variance is absorbed into $\mathbf{H}_r$ and $\mathbf{G}_r$.

The achievable information rate I_{AIR} is defined as

$$\textbf{Error!} \qquad (7)$$

where the average is with respect the actual densities $p(\mathbf{y}|\mathbf{x})$ and $p(\mathbf{y})$. The rate I_{AIR} is directly impacted by the choices of $\mathbf{H}_r$ and $\mathbf{G}_r$. The optimization problem reads

$$I_{OPT} = \max_{\substack{\mathbf{G}_r \\ \mathbf{H}_r}} I_{AIR}, \qquad (8)$$

under the constraint

$$(\mathbf{G}_r)_{ij} = 0 \,|i-j| \geq L. \qquad (9)$$

This optimization problem for a discrete alphabet is a hard task. On the other hand, it can be solved in closed form under the assumption that transmitted symbols are independent Gaussian random variables [2]. Although the channel shortener has been designed under the hypothesis of Gaussian symbols, the achieved performance is still excellent even when low-order constellations are employed.

In the case of Gaussian inputs, closed-form expressions for $\mathbf{H}_r$ and $\mathbf{G}_r$ can be found with the following algorithm:

- Compute the sequence $\{b_k\}^{L;\,;k=-L}$ as

Error!

- Compute the real-valued scalar $c=b_0-\mathbf{b}\mathbf{B}^{-1}\mathbf{b}^{\dagger}$, where $\mathbf{b}=[b_1,b_2,...,b_L]$, and $\mathbf{B}$ is $L\times L$ Toeplitz with entries $B_{ij}=b_{i-j}$.
- Define the vector **Error!** and find the optimal target response as

$$G_r(\omega)=|U(\omega)|^2-1.$$

- Finally, the optimal channel shortener is found as

Error!

For a proof see [1].

This channel shortener has been designed under with reference to the main transmit pulses that can be used in optical long-haul systems (depending on the adopted pulses before the Mach-Zehnder modulator, the transmit optical filter, etc.) under linear regime and the corresponding performance in terms of achievable spectrally efficiency properly evaluated.

In order to show some results, we indicate **Error!** [b/s/Hz] as the system spectral efficiency, and a proper signal to noise ratio (SNR)

Error! (10)

where P_c is the power for each carrier, B is the transmit side filter bandwidth, K the number of carriers.

Figure 3.1 shows the computed spectral efficiency in a simulated scenario corresponding to a plausible back-to-back experimental setup (five carriers each carrying 160 Gbit/s polarization multiplexed QPSK), with different receiver complexities (i.e., BCJR number of states), and with or without channel shortener. The performance is clearly improved by the employment of the CS technique; conversely, it can be possible to achieve the same performance of the traditional receiver, but with lower complexity (not in this case as the traditional receiver performance is only slightly influenced by its complexity). Notice that in Fig. 3.1the performance of the receiver without CS is better for L=3, than for L=4, which could be quite surprising, but, however, it can happen, as the effect of some ISI coefficient can be even beneficial on average. This does not happen with CS, as it represent the optimal processing for reduced-state receivers, in a spectral efficiency perspective, so the performance increases with the number of trellis states. The channel impulse response which was simulated can be seen in Fig. 3.2.

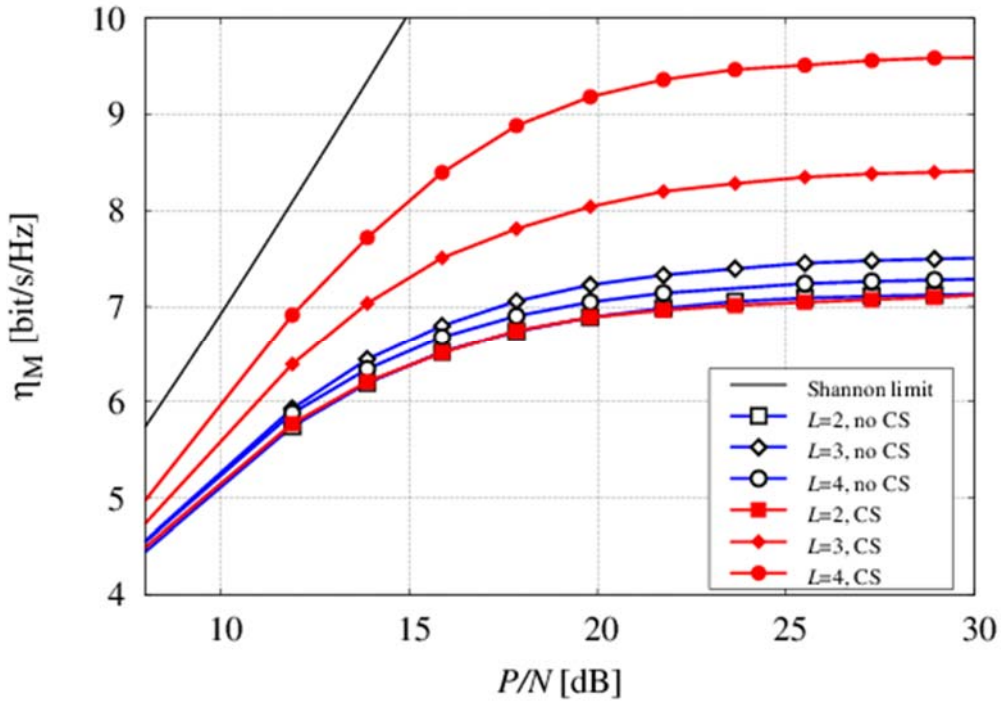

Figure 3.1: Spectral efficiencies computed through simulation for a back-to-back experimental setup, for different receiver complexities.

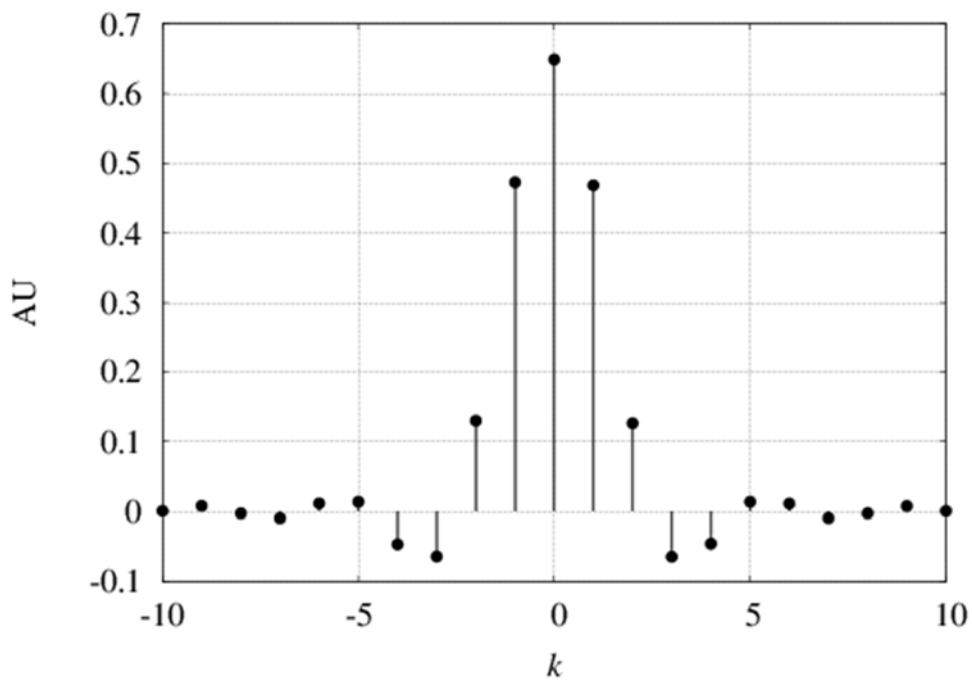

Figure 3.2: Overall channel impulse response.

3.2 Nonlinear impairment mitigation advanced techniques MS3.2

3.2.1 Introduction

In high-speed long-haul optical communication systems, Kerr nonlinearity is one of the major limiting factors. Digital backpropagation (BP) is one of the most studied strategies to counteract nonlinearities by channel inversion[1]. Due to both technological and practical reasons, BP is typically used only to compensate for intra-channel nonlinearity. In particular, while BP is most effective for combating nonlinear signal-signal interactions, its effectiveness against signal-noise interactions is limited [2]. In practice, BP is implemented through the split-step Fourier method (SSFM), probably the most efficient method known [3]. The SSFM allows for complexity vs accuracy trade-off by adjusting the number of steps N_s. The complexity per processed sample scales as $N_s \log M$, where M is the overall channel memory (number of samples) determined by chromatic dispersion.

In this work, a variation of the SSFM able to increase accuracy without requiring a significant increase in complexity is proposed. The complexity per processed sample still scales as $N_s \log M$, but a given accuracy can be obtained through a significantly lower number of steps N_s. This means that, at equal performance, digital BP can be implemented in the receiver with reduced complexity, latency and energy consumption with respect to standard SSFM.

3.2.2 Enhanced Split-Step Fourier Method

The propagation of an optical signal through a fiber-optic link is governed by the nonlinear Schrödinger equation (NLSE) and can be efficiently performed by employing the SSFM. Processing involves the computation of the fast Fourier transform (FFT) of the signal samples and is therefore limited to a finite number of samples (time-limited signal). In order to process an unlimited number of samples (as an example, performance evaluation requires transmitting and processing billions of samples), the overlap-and-save technique is typically employed. According to this technique, the input sequence of samples is divided into overlapping blocks which are separately processed, and the output sequence is then reconstructed by discarding the overlapping samples. For successful operation, the number of overlapping samples should be chosen to be not less than the overall memory M of the fiber-optic channel. Of course, the block length is $N>M$ and, for a given M, N can be optimized to minimize the computational cost per propagated sample. Typically, the optimum is in the range $4M<N<8M$.

In order to better understand the enhanced split-step Fourier method (ESSFM), let us briefly review the SSFM. According to the SSFM, the fiber link is divided into N_s small segments (steps). Each step is further divided into two substeps: a linear substep, accounting for dispersion, and a nonlinear substep, accounting for Kerr nonlinearity. Thus, the propagation of a block of N samples $\{x_k\}^{N;k=1}$ through a generic piece of fiber of length Δz, with dispersion coefficient β_2, nonlinear coefficient γ, and

attenuation coefficient α, entails performing the following four operations: *(i)* computation of the frequency components $\{X_k\}^{N;k=1}$ through the FFT algorithm; *(ii)* computation of the linear substep

$$Y_k = X_k e^{-j2\pi^2 \beta_2 f^{2;k} \Delta z}, \quad k=1,\ldots,N \qquad (1)$$

where f_k is the frequency of the k-th component; *(iii)* computation of the time components $\{y_k\}^{N;k=1}$ through inverse FFT; *(iv)* computation of the nonlinear substep

$$z_k = y_k e^{-j\gamma |y_k|^2 \Delta z_{eff}}, \quad k=1,\ldots,N \qquad (2)$$

$\Delta z_{eff}=(1-e^{-\alpha\Delta z})/\alpha$ being the effective length. The output sequence $\{z_k\}^{N;k=1}$ becomes, in turn, the input to the next fiber segment and so on, until the end of the link is reached. In the symmetric implementation of the method, the nonlinear substep is performed in the middle of the fiber segment rather than at the end. This increases the accuracy of the method without substantially modifying its complexity (the second half substep of each fiber segment combines with the first half substep of the next segment to give a single substep like (1), leaving the algorithm unchanged but for the first and last steps).

For any finite step size Δz, nonlinearity and dispersion cannot be exactly separated as in (1) and (2), but the overall error can be reduced by decreasing Δz (i.e., by increasing N_s). Given the low computational cost of (1) and (2), the complexity of the method is dominated by the couple of FFTs performed at each step, such that the required total number of operations per propagated sample scales as $N_s \log_2 N$ (or, equivalently, as $N_s \log_2 M$, being N proportional to M). A convenient trade-off between accuracy and complexity is typically obtained by properly selecting N_s.

The main idea behind the ESSFM proposed in this work is that of replacing the term (2) with another one that accounts also for the interaction between dispersion and nonlinearity along Δz. In this way, Δz can be increased (and, consequently, N_s decreased) without affecting accuracy overall (of course, the overall complexity is reduced only if the new term is less costly than the spared FFTs). An expression for the nonlinear substep more accurate than (2) is provided by the logarithmic perturbation method [4], which can be further simplified by retaining only the most relevant terms. In particular, it can be shown that in the nonlinear step the signal undergoes a nonlinear phase rotation that depends on a quadratic form of the signal samples [5]. Considering only the diagonal terms of the quadratic form, and limiting the memory to N_c future and past samples, results in the following modified nonlinear substep

Error! (3)

where $\{c_i\}^{N_c;i=0}$ are N_c+1 real coefficients to be determined, and the time-reversal symmetry of the NLSE has been exploited. Thus, each step of the ESSFM requires the same four operations required by the SSFM, but with (3) replacing (2). Such a modification can be applied to any implementation of the SSFM (symmetric or non-symmetric; with fixed, variable, or adaptive step-size [6]). With respect to the original substep (2), the modified nonlinear substep (3) additionally requires only N_c real

multiplications and $2N_c$ real additions per processed sample, as the exponential and all the squared modulus terms in (3) are evaluated also in (2). The number of additional operations is therefore independent of N and typically negligible (for reasonable values of N_c) compared to the number of operations required by the FFTs, the complex exponential, and the other complex multiplications in (1) and (2). Thus, the overall complexity per sample of the enhanced method still scales as $N_s \log_2 M$ and is only marginally increased with respect to the SSFM. The accuracy, on the other hand, is significantly increased, as shown in the next section (equivalently, the same accuracy can be achieved with a lower number of steps, i.e., with a lower complexity).

An analytical expression for the coefficients $c_0,\ldots,c_{N_c}$ could be derived by employing perturbation methods [4, 5]. This approach, however, requires an accurate knowledge of the system characteristics. An alternative and practical approach, adopted in the next section, is that of resorting to a numerical optimization of the coefficients by minimizing a suitable cost function, such as the mean square error (MSE) between the output samples and the desired output. For a given system, optimization is done only once. Thus, it does not affect the algorithm complexity in terms of real-time processing.

3.2.3 Numerical Results

In this section, the SSFM and ESSFM are compared in terms of accuracy and complexity. As a first comparison, the forward propagation of a modulated optical signal through an optical fiber is taken into account. For simplicity, a single span of lossless standard fiber of length L=[1000]km, with β_2=[−21.7]ps^2/km and γ=[1.27]$W^{-1}km^{-1}$ is considered. Using (frequency domain) root-raised cosine pulses with roll-off 0.2, a 32 Gbaud signal is modulated by a quaternary de Bruijn sequence of quadrature phase-shift keying (QPSK) symbols of length 4^7. The signal, with a launch power of [−3]dBm, is then propagated through the fiber using either the symmetric SSFM or ESSFM with two samples per symbol, considering a constant step size $\Delta z = L/N_s$ and a variable number of steps N_s. The accuracy of the methods is measured in terms of MSE between the output signal and the "exact solution", obtained by using the SSFM with N_s=10000. The coefficients $c_0,\ldots,c_{N_c}$ of the ESSFM are the same in each span and are numerically optimized by minimizing the MSE. Fig. 3.3 shows the MSE (normalized to the signal power) as a function of N_s for the two methods. Different number of coefficients N_c are considered.

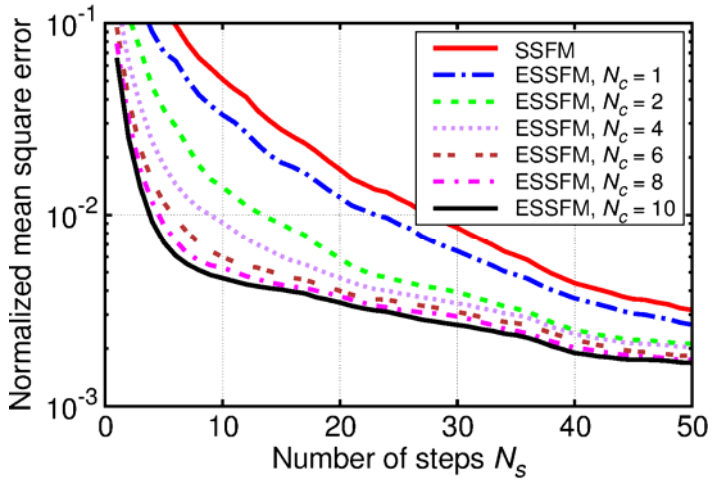

Figure 3.3: Accuracy of the SSFM and ESSFM in performing the forward propagation along 1000 km of lossless fiber.

It is apparent that, for a given number of steps, the ESSFM is significantly more accurate than the SSFM. The difference is more relevant when the number of steps is small (i.e., for large step sizes, when the memory of the nonlinear substep is relevant), the gain in terms of MSE being more than one order of magnitude, and decreases for increasing number of steps. The gain can also be read in terms of complexity. For instance, if a normalized MSE of 10^{-2} is desired (i.e., a signal-to-error ratio of 20 dB), the number of steps required by the ESSFM is up to seven times smaller than that required by the SSFM. We remark that the complexity of the ESSFM is only slightly higher than that of the SSFM, such that a saving in terms of number of steps N_s directly translates into a saving in terms of complexity. Similar results (not reported here) have been obtained by considering multispan links with attenuation and periodic amplification, different modulation formats, and different sampling rates.

As a second test, the two methods are compared for the mitigation of nonlinear impairments through digital BP at the receiver. In this case, transmission through a more realistic dispersion-unmanaged multispan fiber-optic link with attenuation and periodic amplification is considered. The link consists of 40 spans of standard single-mode fiber of length 120 km, with same β_2 and γ as in Fig. 3.3 and an attenuation of 0.2 dB/km. Attenuation is periodically compensated by in-line amplifiers with a noise figure of 6 dB. A QPSK modulated signal with same baud rate and pulse shape as in Fig 3.3 is transmitted. At the receiver side, the signal is sampled at two samples per symbol, backpropagated by using either the symmetric SSFM or ESSFM, filtered by the matched filter, downsampled at one sample per symbol, phase rotated to compensate for the average value of the nonlinear phase noise induced by signal-noise interaction, and finally sent to a standard symbol-by-symbol detector. The coefficients of the ESSFM are the same in each span and are numerically optimized by minimizing the MSE between the compensated samples (before detection) and the transmitted symbols. Optimization is performed by employing a quaternary de Bruijn sequence of QPSK symbols of length 4^5 as a training sequence. The optimized coefficients are then held fixed and the bit error rate (BER) is estimated by transmitting a random sequence of 2^{22} QPSK symbols. The overall length of 4800 km

corresponds to a memory $M \simeq 1500$samples (at two samples per symbol), for which a good block length is N=8192. Fig. 3.4 shows the BER as a function of the launch power, considering the receiver without BP (replaced by an ideal compensation of chromatic dispersion) and the receivers with BP implemented through the SSFM or ESSFM and different choices of $N_s$andN_c.

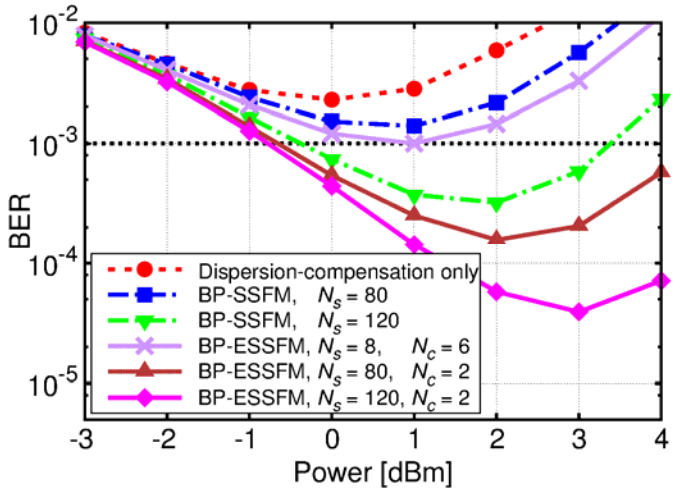

Figure 3.4: BER obtained when using the SSFM and ESSFM to mitigate nonlinear impairments through digital BP in a 40×120 km dispersion-unmanaged link

In order to reduce the system BER below a typical threshold of 10-3 (for coded transmission), digital BP is required. However, while two steps per span (N_S=80) are not enough with the SSFM implementation, and three steps per span (N_S=120) are required to achieve the BER threshold, the ESSFM implementation requires only one step each five spans (N_S=8) to achieve the threshold, with more than one order of magnitude of complexity reduction. Conversely, if the ESSFM is implemented with two (N_S=80) or three (N_S=120) steps per span as required by the SSFM, it provides a significant gain in terms of performance.

3.2.4 Conclusions

An enhanced version of the SSFM has been introduced, providing a significant gain over the classical SSFM in terms of accuracy vs complexity behavior. An efficient implementation of digital BP, based on the proposed method, has been tested by means of numerical simulations, obtaining a complexity reduction of up to one order of magnitude with respect to the classical SSFM.

3.3 Multi-user receiver in time-frequency packing coherent optical systems MS3.3

One possible solution for further increasing the spectral efficiency in the proposed time-frequency packing systems, is represented by the adoption of multi-user techniques at the receive side. Basically, such techniques are based on the processing of more than one channel at the same time, and the kind of processing is commonly designed as a trade-off between complexity and performance. There exist several multi-user techniques, with different implications; our choice was driven by the need for a substantial performance increase, at the expense of detection latency. Straightforward classical multi-user detection strategies [1], where multiple channels are received and processed simultaneously, entail a relevant complexity increase, even if considering reduced complexity receivers as in [2], but with a little performance gain, as can be seen in Fig.3.5, where a single-user detector (U=1) is compared to a multi-user detector (U=2) with and without memory L, in an AWGN channel with frequency packing F=0.8.In this case, it is possible to see how multi-user processing takes advantage from a detector with memory, as interchannel interference induces intersymbol intereference on each channel.

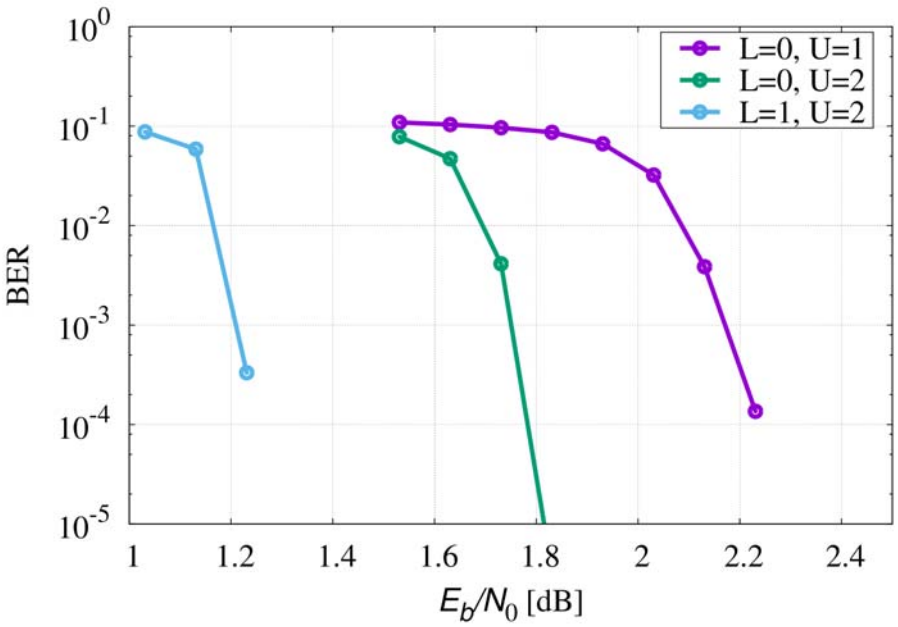

Figure 3.5 Bit error rate of single-user detector (U=1) and multi-user detector (U=2), with memory (L=1) and without memory (L=0) in an AWGN scenario and time-frequency packing.

Instead, we decided to rely upon the more effective technique of double signalling (DS) with interference cancellation [3], which exploits the previously adopted single-user detector for a first set of high-power channels; the detected channels are subsequently cancelled from the received signal, so that a second set of low-power channels can be detected. At the transmit side, the frequency spacing between channels can thus be further reduced with respect to single-user processing,

unbalancing even and odd channels power. In this way, the channels belonging to the two sets are impaired by different interchannel interference, being the low-power channels obviously more disadvantaged. Clearly, different code rates must be used for the two channel sets. Thus, the transmitted signal expression reads

$$s(t) = \sqrt{1-\beta^2}\sum_{k,\ell} x_k^{(\ell)} p(t-kT-\tau^{(\ell)}) e^{j(2\pi\ell Ft+\theta^{(\ell)})} + \beta \sum_{k,\ell} y_k^{(\ell)} p(t-kT-\tau^{(\ell)}) e^{j(2\pi(\ell+1/2)Ft+\theta^{(\ell)})} \quad (1)$$

Where βϵ [0,1] is the power allocation factor, where *T* is the symbol interval, $x_k^{(\ell)}$, $y_k^{(\ell)}$ the symbols transmitted over the ℓthand (ℓ+1/2)thcarrier during the *k*th symbol interval, $\tau^{(\ell)}$ and $\Theta^{(\ell)}$ the delay and the initial phase of the carriers, respectively, and *F* the frequency spacing between two even or odd adjacent carriers, whereas the spacing between two adjacent even and odd channels is reduced to *F* /2.

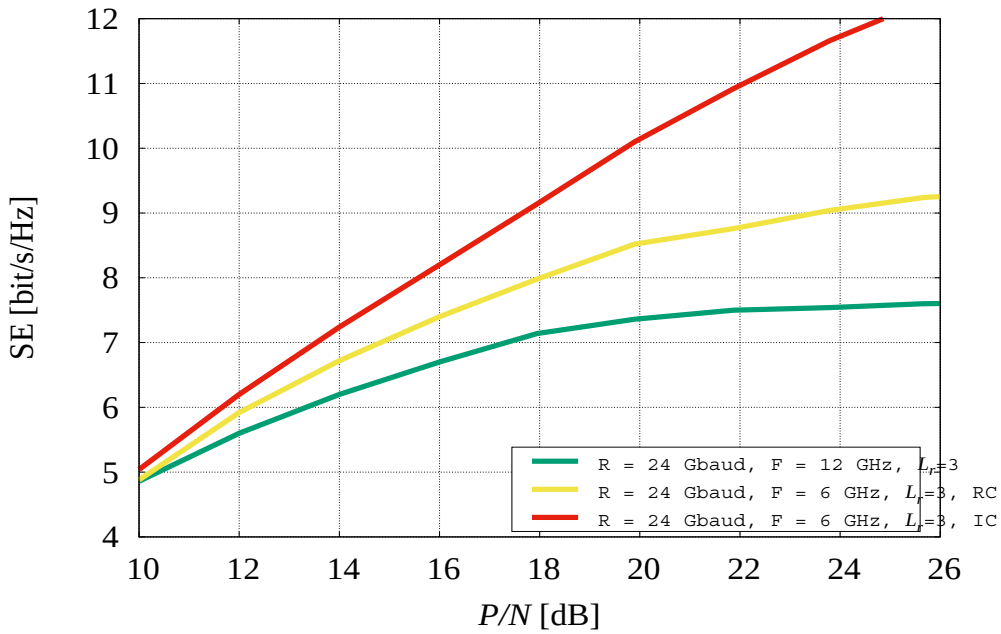

Figure 3.6 :Spectral efficiency (SE) of single-user detector in a back-to-back TFP scenario with frequency spacing F=12 GHz and symbol rate R=24 Gbaud, 5 channels, 9th-order Chebyshev transmit filter with bandwidth 5 GHz, detector memory L_r=3, and double signalling in the same scenario with F=6 GHz, power unbalance between odd and even channel equal to 11 dB, with ideal, or perfect, cancellation (IC), and with our estimation algorithms for the realistic cancellation (RC).

Through a careful optimization of the power unbalance, the frequency spacing and the code rates, it is possible to obtain a substantial increase of the system spectral efficiency, up to a theoretical 50 % (considering perfect cancellation), as can be seen in Fig. 3.6, where the abscissa reads $\frac{P}{N} = P_c/(2N_0F)$, with P_c the power per channel, and $N_0/2$ the two-sided power spectral density of AWGN (see [4]).

Comparing to single-user processing, this technique requires that each channel of the first set $x_k^{(\ell)}$ must be cancelled from (1) after detection, thus implying a latency for the detection of the second set $y_k^{(\ell)}$. From an implementation point of view, it is mandatory to design a proper cancellation algorithm, and to adapt the LDPC codes to a more impaired scenario. This task was carried out by using standard techniques based on the EXtrinsic Information Transfer (EXIT) charts [5], and, once the code degree distributions have been optimized, the algorithm in [6] was used for the generation of the code parity check matrix. Novel codes were designed, based on the EXIT charts computed at different link distance and considering the chosen system set-up, including tight filtering and interchannel interference. These codes are less performing in the AWGN scenario, but are much more effective in presence of strong intersymbol interference, at the expense of a slower convergence, i.e., more iterations between detector and decoder are required.

Ad-hoc data-aided algorithms were employed for the estimation of signal parameters used for cancellation, i.e. possibly time-varying intersymbol interference taps, phase noise, frequency offset, polarization rotation. The theoretical spectral efficiency gain that was observed over experimental measures by using the method descripted in [4] was 30%.

4 Field Trial Demonstration

4.1 Single User System Optimization and Testing MS4.1.1

4.1.1 Introduction

The system performance in a single user scenario has been tested and optimised by emulating the Milan–Finkenstein fibre optic link selected for the COFFEE project (see MS2.1) with a recirculating loop. The experimental setup is described in section 2. Section 3 gives transmission performance results in back-to-back configuration (3.1) and after transmission through the loop with lump dispersion compensation only (3.2) as well as when employing digital backpropagation (3.3).

4.1.2 System Setup

The system setup includes a transmitter and coherent receiver setup similar to that described in [1] and a recirculating loop composed of the optical components of the Alcatel 1626LM system (see MS2.2).

The transmitter generates a polarisation diversity multiplexed (PDM) signal employing time frequency packing (TFP) [2] and is shown in Figure 4.1. Odd and even channels are separately modulated by two double nested Mach Zehnder modulators (IQ-MZM) allowing modulation of both in phase and quadrature components by application of two data signals on the respective ports. The data streams applied were coded with a low density parity check (LDPC) code with code rate $9/10$ at a gross data rate of 32Gb/s – resulting in a symbol rate of 32GBd and a gross channel bit rate of 128Gb/s – and electrically low pass filtered to a bandwidth of 10GHz[15].

[15] Filtering was done using a 9th order Chebychev filter of type 1.

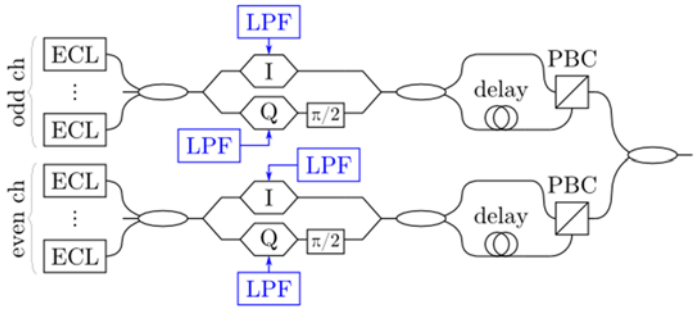

Figure 4.1 : Transmitter Setup

The receiver is a typical PDM intradyne coherent receiver and is shown in Figure 4.2. It employs coherent detection to retrieve full information on the optical complex amplitude, i.e. the amplitude and phase, in both polarisations. Analogue to digital conversion is performed by a Tektronix real time oscilloscope sampling at 50GSample/s, thus giving an oversampling of 1.5625Sample/Symbol. The digital signal processing consists of (optional) digital backpropagation, (optional) lump dispersion compensation and resampling to 2Sample/Symbol followed by a two dimensional adaptive feed forward equalizer (FFE) and a maximum a-posteriori symbol detector comprised of a Bahl-Cocke-Jelinek-Raviv (BCJR) detector [3] iteratively exchanging information with a low-density-parity-check (LDPC) [4] decoder following the turbo principle [5].

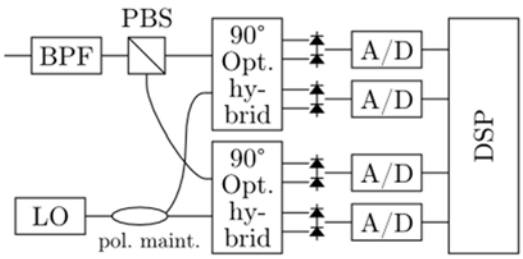

Figure 4.2 : Coherent Receiver Setup

The recirculating loop is designed to resemble the actual Milan–Finkenstein link in terms of spans (and thus number of amplifiers encountered). In order to achieve this, a loop with three spans has been designed using three lengths of non-zero dispersion shifted fibre (NZDSF) such as found in the actual link; this is shown in Figure 4.3. The fibre lengths provide a loss slightly below that of the actual link, allowing the addition of a variable optical attenuator at the input to each of the fibre lengths, also allowing for adjustment of input power to the fibre.

The amplifiers used in the setup are LOFA1110 amplifier boards from the Alcatel 1626LM system as described in MS2.2. Similar to the actual link setup a dispersion compensation module (DCM) may be added at the mid stage access of the amplifiers. Contrary to the link actual though this is performed at maximum one of the amplifiers since no DCM modules for NZDSF fibre were available and one for standard single mode fibre (SMF28) had to be used. Compensating for 80km of G.652 fibre a single such module overcompensates for the dispersion encountered in the three spans. A gain-flattening

filter (GFF) allows flattening of amplifier gain if necessary and a polarisation scrambler is used to emulate random polarisation variation.
The recirculating loop is managed by three acousto-optic modulators (AOMs): the first allows population of the loop with packages of a specified length, the second erases the loop after a given number of, while the third allows selection of packages to be received. Selecting to receive packages that have traversed the loop seven
times allows a good emulation of the link, with a total of 21 (actual link: 20, incl. loopback) spans of fibre and 22 (actual link: 21[16]) amplifiers encountered on the transmission path.

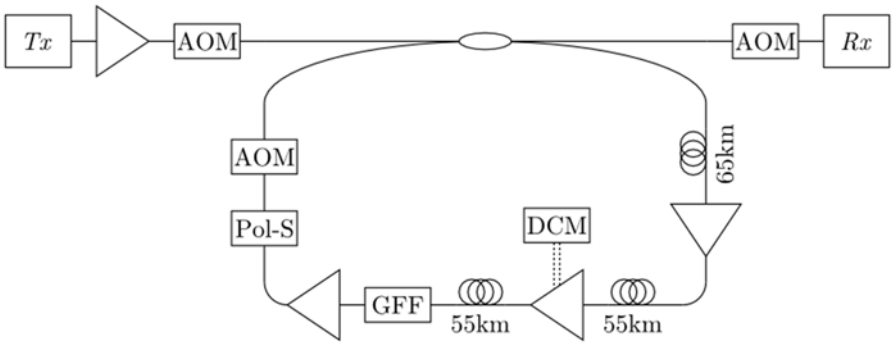

Figure 4.3 : Recirculating Loop Setup

4.1.3 Transmission Performance Measurement

4.1.3.1 *Back-to-Back*

Back-to-back measurements were taken with the transmitter and receiver described in section 2 (Figure 2.24), but at symbol rated of 30GBd and 35GBd. System performance was investigated in terms of required optical signal to noise ratio (OSNR), finding minimum OSNR values for error free[17] operation of 15.0 and 16.5dB respectively; results are shown in Figure 4.4.

[16] The number of amplifiers traversed in the actual link depends on the loopback option chosen; actual numbers of amplifiers for the different options are: 20 for option 1, 22 for options 2 & 3, 21 for options 4 & 5. See MS2.2 for discussion of the loopback options.
[17] "Error free" refers to the case with BER = 10^{-7}, i.e. equal to the error floor of the LDPC code.

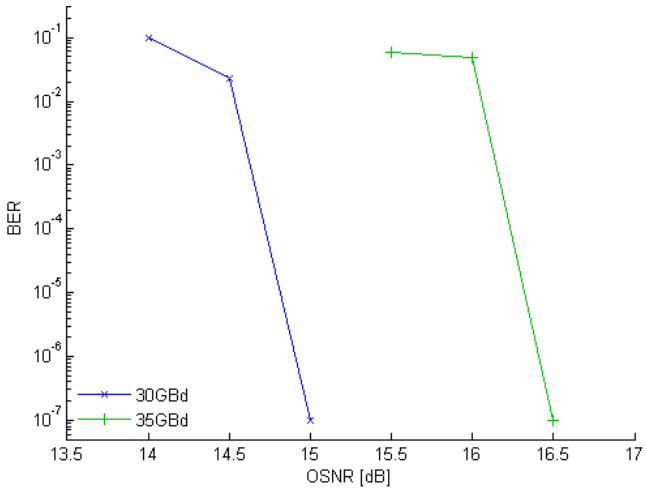

Figure 4.4 : Back-to-Back Measurement Results

4.1.3.2 *After 7x Rounds of the Recirculating Loop with Dispersion Compensation Only*

Allowing a package to traverse the recirculating loop 7 times constitutes a good emulation Milan–Finkenstein fibre optic link with similar numbers of amplifiers and fibre spans traversed. The chromatic dispersion encountered per round of the recirculating loop has been estimated to be 1047ps/nm (assuming a fibre dispersion value of 6ps/nm/km as suggested by [6] and using fibre lengths of 65.3km and 2·54.6km as measured through OTDR). The lump dispersion compensation in the DSP is thus set to compensate for a total dispersion of 7329ps/nm when no DCM module is present.

With the DCM module present, the chromatic dispersion encountered per loop is estimated to be -313ps/nm. A typical dispersion of 17ps/nm/km of G.652 fibre is assumed and DCM for 80km is used, yielding a DCM dispersion of -1360ps/nm that – together with the estimated 1047ps/nm dispersion of the fibre spans – gives a residual dispersion of -313ps/nm per round of the loop. The lump dispersion compensation in the DSP is thus set to compensate for a total dispersion of -2191ps/nm in the presence of the DCM module.
With chromatic dispersion compensated, system performance will depend on OSNR and nonlinear impairments mainly. Measurements have been taken at different launch powers per channel and for signals consisting of a single channel or three closely spaced (20GHz) time frequency packed channels at a symbol rate of 32GBd respectively. A rough estimation of OSNR was taken from a measurement of the received spectrum[18] and is shown in Table 4.1 alongside the channel launch powers for which measurements were taken; launch power into the DCM was set to be constant at -3dBm regardless of the number of channels.

no DCM with DCM no DCM with DCM

[18] OSNR estimation was achieved by deducting measured noise power (with an OSA resolution of 0.1nm) from the measured channel power; in the case of three channels, total power of the three channels was measured, divided by three and then the measured noise levels deducted.

P_{Ch}	OSNR	P_{Ch}	OSNR
0	20.0	-1	16.6
1	20.8	0	18.3
2	21.4	1	19.5
3	22.6	2	20.8
5	24.4	3	22.0

a) 1 channel

P_{Ch}	OSNR	P_{Ch}	OSNR
-2	18.0	-5	14.7
-1	19.5	-4	16.3
0	21.0	-3	17.7
1	22.0	-2	18.6
		-1	19.4
		0	19.9

b) 3 channels

Table 4.1: Channel Launch Powers and Observed OSNR

Decoding results with only lump dispersion compensation are shown in Figure 4.5 a) in terms of post LDPC BER and clearly show a maximum launch power limit for error free[19] decoding in all traces. This limit is found to be +2dBm for a single channel without the DCM module and reduces to +1dBm when the DCM module is included. In the case of three channels the limits are -1dBm and -2dBm for transmission without and with DCM respectively. The case of 3 channels including the DCM module also shows the existence of a minimum OSNR for error free detection which is not met for a channel launch power of -5dBm while being met with a launch power of -4dBm; the estimated minimum OSNR is thus roughly 16dB, suggesting a 0.5dB penalty in minimum OSNR compared to the back-to-back case. In order to differentiate the cases of error free decoding, the necessary number of turbo iterations may be compared, as is shown in Figure 4.5 b). This shows that while error free decoding is possible, the computational cost may vary as different impairments on the signal become relevant. This shows both the observed increase in computational cost due to the addition of more channels and the resulting inter symbol interference (ISI), as well as due to increased nonlinearities when including the DCM module.

[19] "Error free" refers to the case with BER = 10^{-7}, i.e. equal to the error floor of the LDPC code.

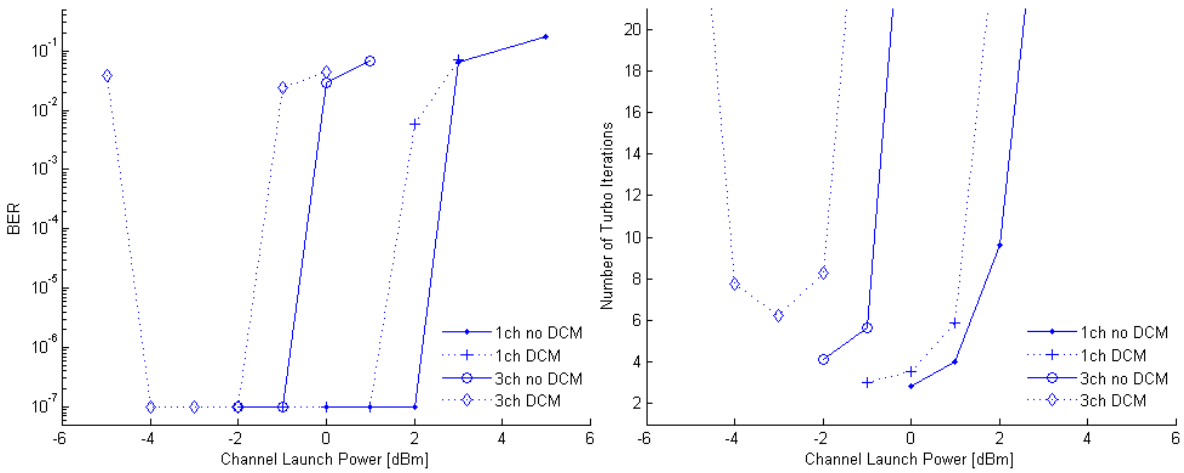

a) BER over P_{ch} b) Number of Turbo Iterations over P_{ch}

Figure 4.5: Performance with Dispersion Compensation

4.1.3.3 *After 7x Rounds of the Re-circulating Loop with Digital Back-propagation*

In order to negate or reduce the signal degradation caused by nonlinear effects – and thus to allow channel launch powers above the limits found in section 3.2 – digital backpropagation may be employed. This was done by replacing the lump dispersion compensation with split-step Fourier method based backpropagation, achieving both dispersion compensation and mitigation of nonlinear effects.

Backpropagation was performed with ten steps per fibre span and fibre parameters as given in Table 4.2. The channel launch power taken into account during backpropagation was optimised and the optimum found to be between 1.5 and 2dB below the actual measured channel launch power.[20]

Fibre Type	Length[21] [km]	Attenuation [dB/km]	Chr. Disp.[22] [ps/mn/km]	Nonlin. Coeff.[23] [1/W/km]
NZDSF	65.3 / 54.6	0.193	6	1.46
DCF	12.7	0.378	-107	5.43

Table 4.2: Fibre Parameters for Digital Backpropagation

[20] This is true with two exceptions: In the case of one channel and no DCM, the considered power for backpropagation had to be reduced to -5dBm in order to allow error free decoding. In the case of 3 channels with no DCM, considered power had to be stepped up by 1 and 3dB for traces at launch powers of 0 and -1dB respectively.

[21] Fibre length and attenuation measured through OTDR. Lengths are 65.3km for the 1st span, 54.6 for the 2nd and 3rd span.

[22] Dispersion of NZDSF according to [6], for DCF calculated with the assumption of compensation for 80km of G.652 fibre, i.e. 80km * 17ps/nm/km = 1360ps/nm, thus for 12.7km of DCM: D = -1360ps/nm / 12.7km = -107ps/nm/km.

[23] Nonlinear coefficients of NZDSF calculated from measured n_2 given by [7] and A_{eff} according to [6]. Nonlinear coefficient of DCF according to A_{eff}/n_2 values given in [8].

Figure 4.6 a) shows decoding results with backpropagation and compares them to the results with dispersion compensation only. It is immediately visible that while backpropagation has no impact on the minimum OSNR, it achieves error free decoding in all recorded cases. Performance within the error free range may be distinguished in terms of number of turbo iterations required as seen in Figure 4.6 b). This shows that backpropagation not only allows error free decoding for higher powers, but also reduces computational cost in all cases.

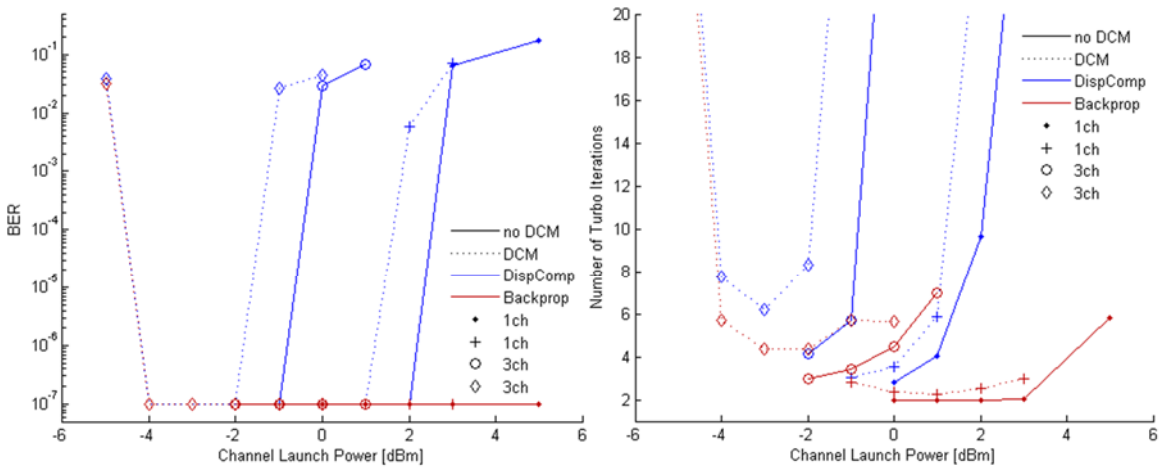

a) BER over P_{ch} b) Number of Turbo Iterations over P_{ch}

Figure 4.6: Performance with Digital Backpropagation

4.2 Multi User System Optimization and Testing

4.2.1 Introduction

The system performance in a multi user scenario has been tested and optimised in back to back conditions and by emulating the Milan–Finkenstein fibre optic link selected for the COFFEE project (see MS2.1) with a recirculating loop. The experimental setup is described in section 2. Section 3 gives transmission performance results in back-to-back configuration (3.1) and after transmission through the loop with lump dispersion compensation only (3.2).

4.2.2 System Setup

The system setup includes a transmitter and coherent receiver setup similar to that described in [1] and a recirculating loop composed of the optical components of the Alcatel 1626LM system (see MS2.2).

The transmitter generates a polarisation diversity multiplexed (PDM) signal employing time frequency packing (TFP) [2] and is shown in Figure 4.7. In a multi user detection all the channel are received by the same receiver. This impose a limitation on the number of channels and on the spectrum occupation, due by the receiver analog bandwidth. In order to avoid this limitation, alternative schemes can be adopted In particular, more receivers, opportunely "interleaved" and synchronized, can be considered. This way it could be possible to slice the spectrum of the received signal and detect each slice with a single receiver. At the end with the exchange of information between all the receivers it could be possible to receive a superchannel with an arbitrary spectrum occupation (i.e. arbitrary number of subchannels), considering a multi user detection. Note that the number of the required receivers depend on the single receiver analog bandwidth and the total superchannel spectrum occupation. In order to demonstrate the multi user detection, considering the limited number of coherent receivers available in our laboratory, a superchannel composed by five subchannels is considered. Odd and even channels are separately modulated by two double nested Mach Zehnder modulators (IQ-MZM) allowing modulation of both in phase and quadrature components by application of two data signals on the respective ports. The data streams applied were coded with different low density parity check (LDPC) codes for the odd and the even channels. The baud rate of the electrical data to be encoded was set to 24 Gbaud, giving a gross data rate of 96 Gb/s for each subchannel. The data are then encoded and electrically low pass filtered to a bandwidth of 5 GHz[24]. A preliminary study, considering also numerical analysis of the transmission system, was done in order to find the optimum value for the subchannels frequency spacing and the code rates for the odd and the even subchannels. The optimization of such a parameters was done considering the target of the spectral efficiency maximization. The employed code rates are R1=$11/20$ (from encoder 1 in 4.6) and R2=31/40 (from encoder 2 in 4.6), for the odd and the even subchannels respectively. This way, a more robust code was used for the odd subchannels while less redundancy was introduced for the even subchannels. In order to maximize the achievable SE, the odd and even subchannels also had a different optical power. In particular the odd subchannel were transmitted with a higher power with respect to the even ones.

A ratio defined as $C/I = P_{odd}/P_{even}$ was defined and considered as variable for the system optimization. An optimum subchannel frequency spacing of 9 GHz and a C/I of 8 dB was found. This way the superchannel total spectrum occupation was 45 GHz. With this configuration, only three subchannel (i.e. with a total pass band bandwidth of 27 GHz) can be simultaneously detected by a single coherent receiver with a base band bandwidth of about 20GHz.

[24] Filtering was done using a 9th order Chebychev filter of type 1.

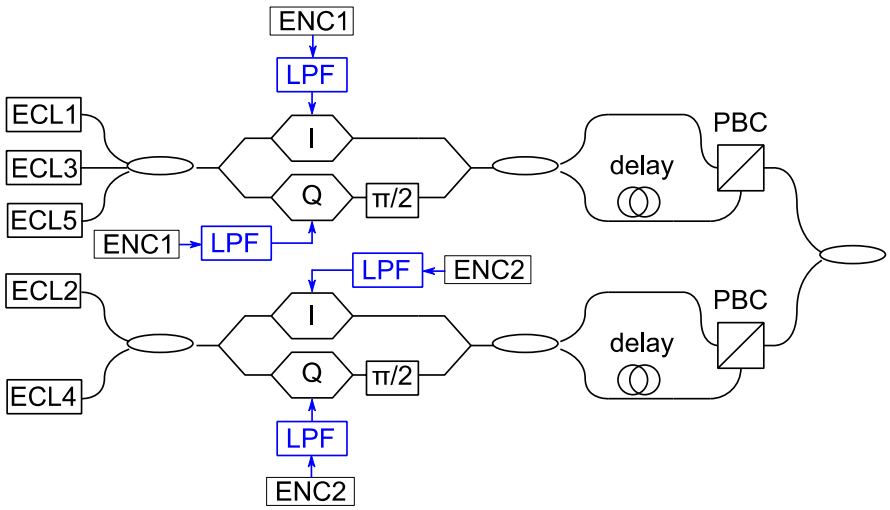

Figure 4.7 : Transmitter Setup

The receiver is a typical PDM intradyne coherent receiver and is shown in Figure 4.8. It employs coherent detection to retrieve full information on the optical complex amplitude, i.e. the amplitude and phase, in both polarisations. In order to correctly receive the channels exploiting multi user detection with a single coherent receiver, the local oscillator (LO) was centered on the third subchannel (i.e. the central subchannel). This way the 2nd, the 3rd and the 4th subchannels can be simultaneously received within the receiver bandwidth. The 1st and the 5th subchannels are included in the measurements in order to have the same cross talk issues for all the received subchannels. Analogue to digital conversion is performed by a Tektronix real time oscilloscope sampling at 50GSample/s. The digital signal processing consists of (optional) lump dispersion compensation and resampling/downsampling to 2 Sample/Symbol followed by a two dimensional adaptive feed forward equaliser (FFE) and a maximum a-posteriori symbol detector comprised of a Bahl-Cocke-Jelinek-Raviv (BCJR) detector [3] iteratively exchanging information with a low-density-parity-check (LDPC) [4] decoder following the turbo principle [5].

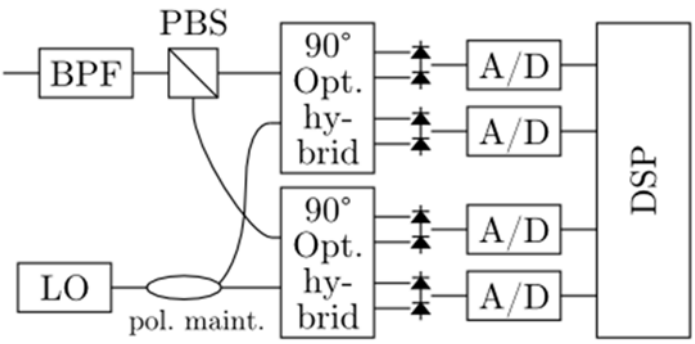

Figure 4.8 : Coherent Receiver Setup

The recirculating loop is designed to resemble the actual Milan–Finkenstein link in terms of spans (and thus number of amplifiers encountered). In order to achieve this, a loop with three spans has been designed using three lengths of non-zero dispersion shifted fibre (NZDSF) such as found in the actual link; this is shown in Figure 4.9. The fibre lengths provide a loss slightly below that of the actual link, allowing the addition of a variable optical attenuator at the input to each of the fibre lengths, also allowing for adjustment of input power to the fibre.

The amplifiers used in the setup are LOFA1110 amplifier boards from the Alcatel 1626LM system as described in MS2.2. Similar to the actual link setup a dispersion compensation module (DCM) may be added at the mid stage access of the amplifiers. Contrary to the link actual though this is performed at maximum one of the amplifiers since no DCM modules for NZDSF fibre were available and one for standard single mode fibre (SMF28) had to be used. Compensating for 80km of G.652 fibre a single such module overcompensates for the dispersion encountered in the three spans. A gain-flattening filter (GFF) allows flattening of amplifier gain if necessary and a polarisation scrambler is used to emulate random polarisation variation.

The recirculating loop is managed by three acousto-optic modulators (AOMs): the first allows population of the loop with packages of a specified length, the second erases the loop after a given number of, while the third allows selection of packages to be received.

Selecting to receive packages that have traversed the loop seven times allows a good emulation of the link, with a total of 21 (actual link: 20, incl. loopback) spans of fibre and 22 (actual link: 21[25]) amplifiers encountered on the transmission path.

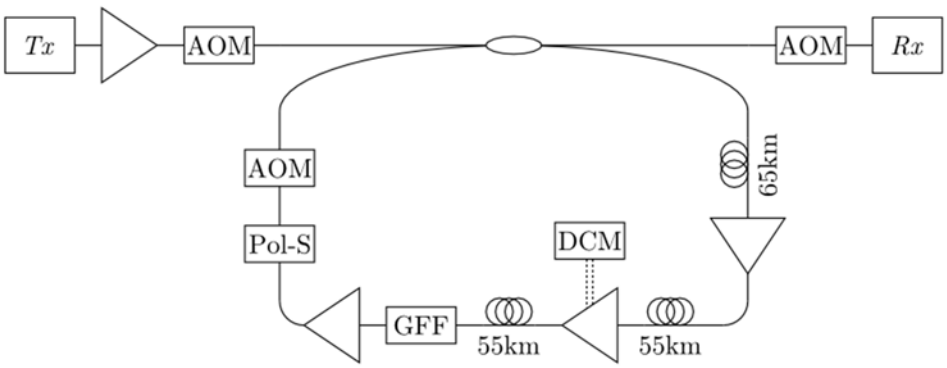

Figure 4.9 : Recirculating Loop Setup

4.2.3 Operation principle

In order to correctly receive the three central subchannels (i.e. ch2, ch3 and ch4) with a single coherent receiver, the procedure described in the following is considered. First the received data D, that include all the channel, are processed in order to receive ch2, which is encoded with a code rate

[25] The number of amplifiers traversed in the actual link depends on the loopback option chosen; actual numbers of amplifiers for the different options are: 20 for option 1, 22 for options 2 & 3, 21 for options 4 & 5. See MS2.2 for discussion of the loopback options.

of 31/40 (more powerful channel with less robust code). Then the retrieved data D2 (data of ch2) are subtracted from the received data D, thus obtaining digital data with the information regarding ch3 and ch4, D*≈D-D2. At his point D2 is processed and ch4 is received (R2=31/40). With the same procedure, D4 are subtracted from D* thus obtaining the digital data D**≈D*-D4≈D*-D2-D4≈D3. Finally D** are processed in order to correctly receive the central channel ch3 which is less powerful and encoded with a more robust code (R1=11/20) rate with respect to ch2 and ch4. Following this procedure, with a gross baud rate of 24 Gbaud and a frequency spacing of 9 GHz a spectral efficiency SE=7.06 bit/s/Hz is obtained, thus increasing the SE obtained transmitting 1Tb/s superchannel in 150 GHz. In Figure 4.10 two screenshot of the signal processing output are depicted. On the left the screenshot reports the detection of the left channel, the right channel and finally of the central channel. The screenshot on the right shows the BER result for the detection of the channels.

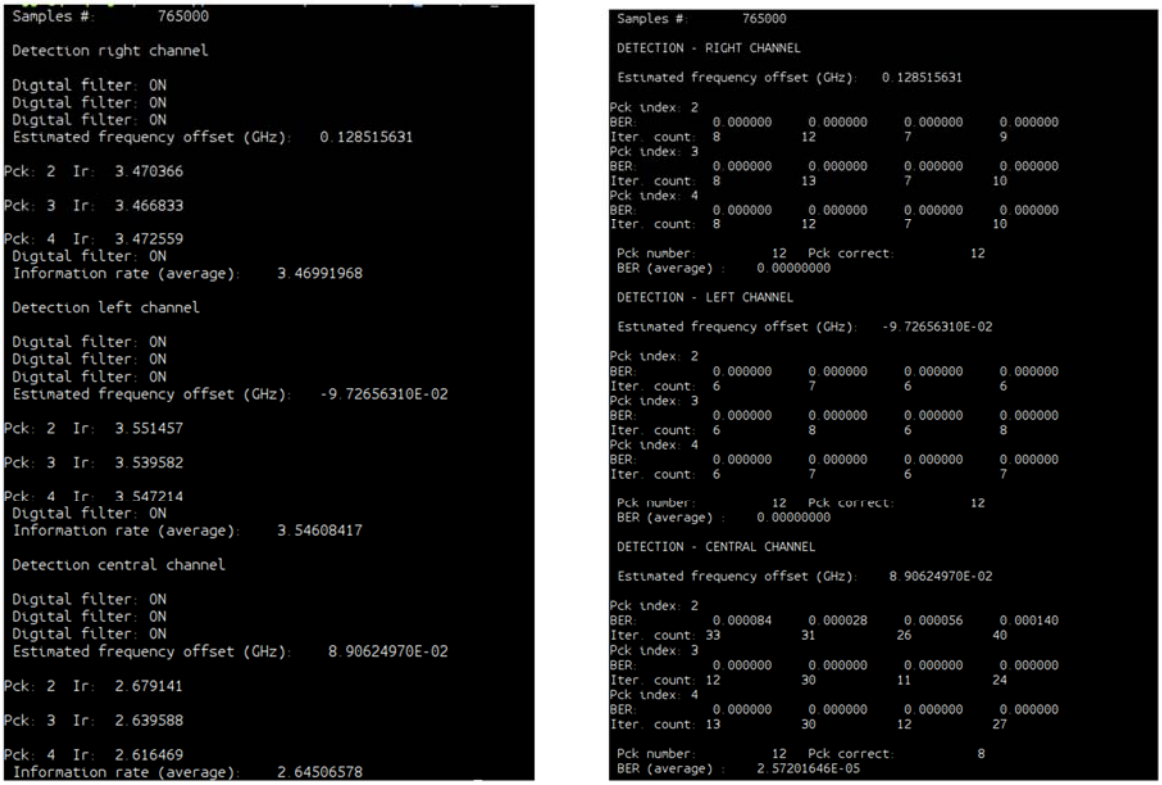

Figure 4.10 : screen shot of the multiuser processing output

4.2.4 Transmission Performance Measurements

4.2.4.1 *Back-to-Back*

Back-to-back measurements were taken with the transmitter and receiver described in section 2 (Figure 2.24), with a gross symbol rate of 96 GBd. System performance was investigated in terms of

required optical signal to noise ratio (OSNR), finding minimum OSNR values for error free[26] operation of about 20dB.

4.2.4.2 *After 7x Rounds of the Recirculating Loop with Dispersion Compensation Only*

Allowing a package to traverse the recirculating loop 7 times constitutes a good emulation Milan–Finkenstein fibre optic link with similar numbers of amplifiers and fibre spans traversed. The chromatic dispersion encountered per round of the recirculating loop has been estimated to be 1047ps/nm (assuming a fibre dispersion value of 6ps/nm/km as suggested by [6] and using fibre lengths of 65.3km and 2·54.6km as measured through OTDR). The lump dispersion compensation in the DSP is thus set to compensate for a total dispersion of 7329ps/nm when no DCM module is present.
With the DCM module present, the chromatic dispersion encountered per loop is estimated to be -313ps/nm. A typical dispersion of 17ps/nm/km of G.652 fibre is assumed and DCM for 80km is used, yielding a DCM dispersion of -1360ps/nm that – together with the estimated 1047ps/nm dispersion of the fibre spans – gives a residual dispersion of -313ps/nm per round of the loop. The lump dispersion compensation in the DSP is thus set to compensate for a total dispersion of -2191ps/nm in the presence of the DCM module.
With chromatic dispersion compensated, system performance will depend on OSNR and nonlinear impairments mainly. Measurements have been taken at different launch powers per channel.

Decoding results with only lump dispersion compensation in terms of post LDPC BER, clearly show a maximum launch power limit for error free[27] decoding in all traces. This limit is found to be about -2dB per channel.
The estimated minimum OSNR is thus roughly 24dB, suggesting a penalty in minimum OSNR compared to the back-to-back case.

4.3 Field Trail with Receiver Single User Approach- Linear Regime

4.3.1 Introduction

The task is aimed at real network testbed characterization and system performance evaluation in linear regime for different network power profile with a single user approach at the receiver. All the administrative and financial activities including logistics support, transportation, insurances, mobility of personnel and equipment in order to successfully setup the testbed for the measurements has been completed. The trial is in the process and here we report the experimental setup and initial link evaluation results obtained so far. The way forward is described .

[26] "Error free" refers to the case with BER = 10^{-7}, i.e. equal to the error floor of the LDPC code.
[27] "Error free" refers to the case with BER = 10^{-7}, i.e. equal to the error floor of the LDPC code.

4.3.2 Field Trial Setup

The overview of the scheme for the field trial is shown in the Fig. 4.11. The signal from the CNIT Tbps transmitter is coupled to Alcatel 1626LM node at Milan Mix site. The signal from Milan traverses all the way to the Finkenstien POP and is then loopback on the return path back to Milan Mix site.

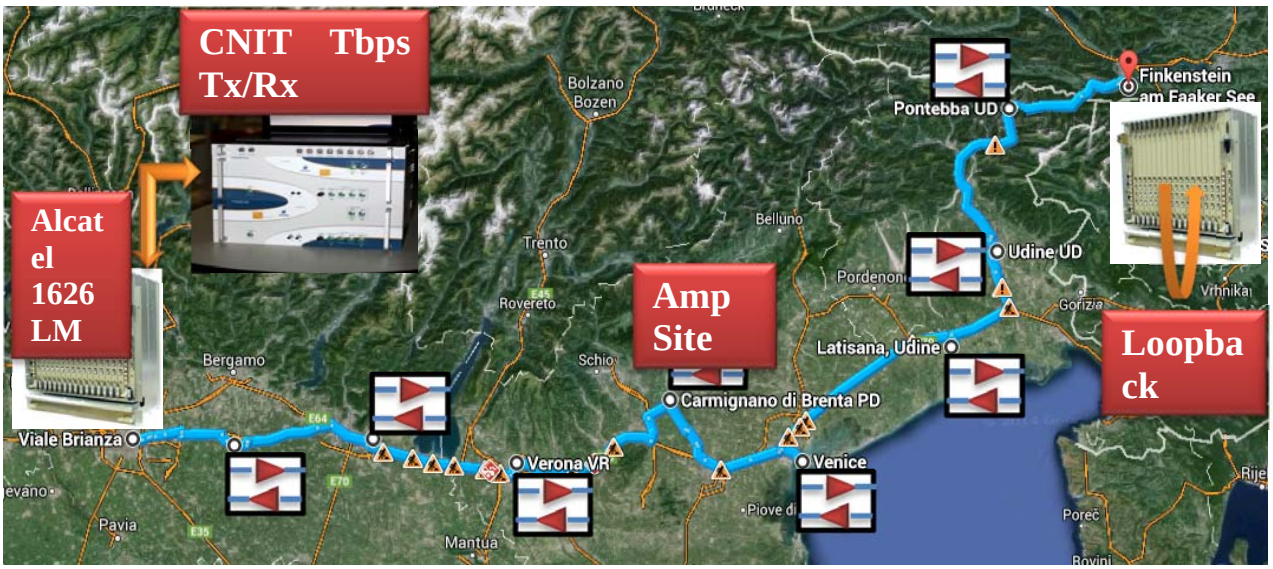

Figure 4.11 : The Field trial Setup

Figure 4.11 shows the detailed setup for both the physical and the management plane. The transmitter and the receiver are the same as already described in the previous sections. The distinctive feature of the setup is management control for almost all the devices in the setup. The connectivity for the management plane is shown with the orange dotted lines. Such a management setup provides the possibility to remotely control the parameters of both Alcatel 1626LM and Terabit setup. The MEMS based switches have been used in the setup to avoid the repetitive make and break of the connections and to monitor the transmitted and received signals on the OSA, oscilloscopes and power meter etc.

Two PM-QPSK transmitters (one for even and one for the odd channels) are fed by the four lasers each. The output of the transmitted fed to variable optical attenuators for the spectral flatness and channel power optimization for different profiles. The odd and even channels are coupled with the help of a 2x2 coupler. One branch of the coupler is connected to Alcatel 1626LM system to launch the signal on the link and the other is fed to the switch which is further connected to receiver setup. This arrangement is useful for interchanging between back to back and transmission link measurements. The signal coming from the Finkenstien is coupled to second port of the first switch. The two wavelength selective switches can be configured to match the transmitted profiles i.e., number of channels and channel spacing. The second WSS selects the single carrier for reception at the receiver and DSP to retrieve the transmitted data. The 10% of the power at the receiver is taped to monitor

the power into the receiver. The second switch is connected to optical spectrum analyser. We can monitor the spectrum of the transmitted signal for BTB measurements, spectrum of the signal launched on the fiber by 1626LM and signal received from Finkenstien. The switching is performed by the software control available in the CNIT numerical tool.

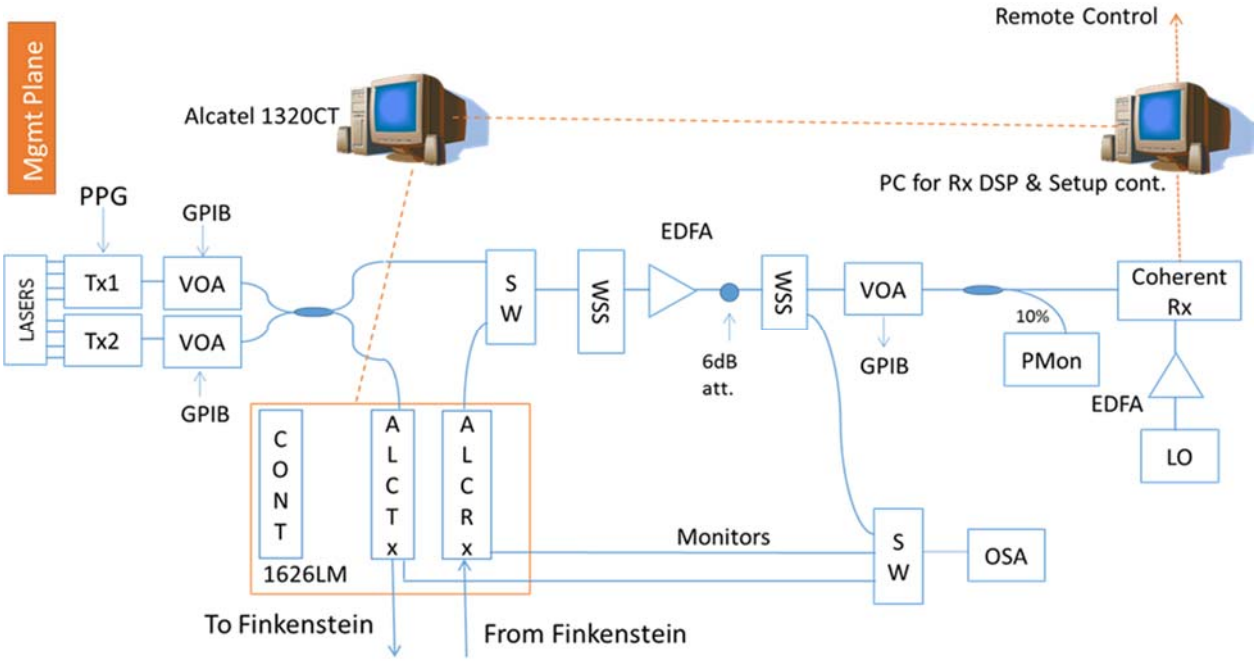

Figure 4.12 : The detailed physical and management plane setup for the field trial at Milan Mix site

4.3.3 Preliminary Results

The activity is in the progress and preliminary link evaluations have been carried out. In order to find the optimum power profiles the OSNR measurements for the single channel and 8 channel transmission were made. The spectra are obtained from the monitors at ALC Tx and ALC Rx. Fig. 4.13 (left) shows the 28Gbaud PM QPSK single channel spectrum at the transmitter and Fig. 3 (right) shows the received signal. The received signal OSNR was found to be 20dB. The recovered constellations at the receiver after post processing for X and Y polarization are shown in the Fig. 4.14. The BER was found to be 6E-3.

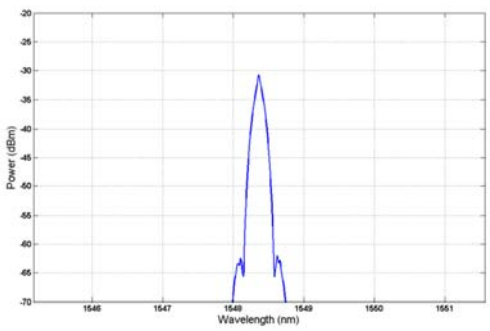

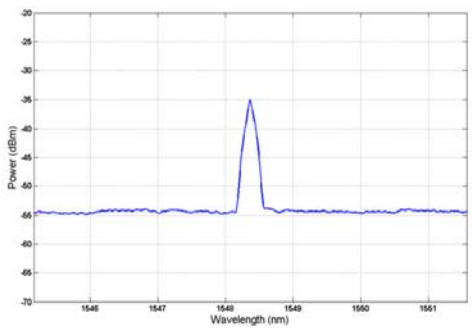

Figure 4.13 : PM QPSK 28GBaud single channel spectrum left) Transmitted signal from Milan (from monitor port) right) Received signal after loopback from Finkenstein (from monitor port).

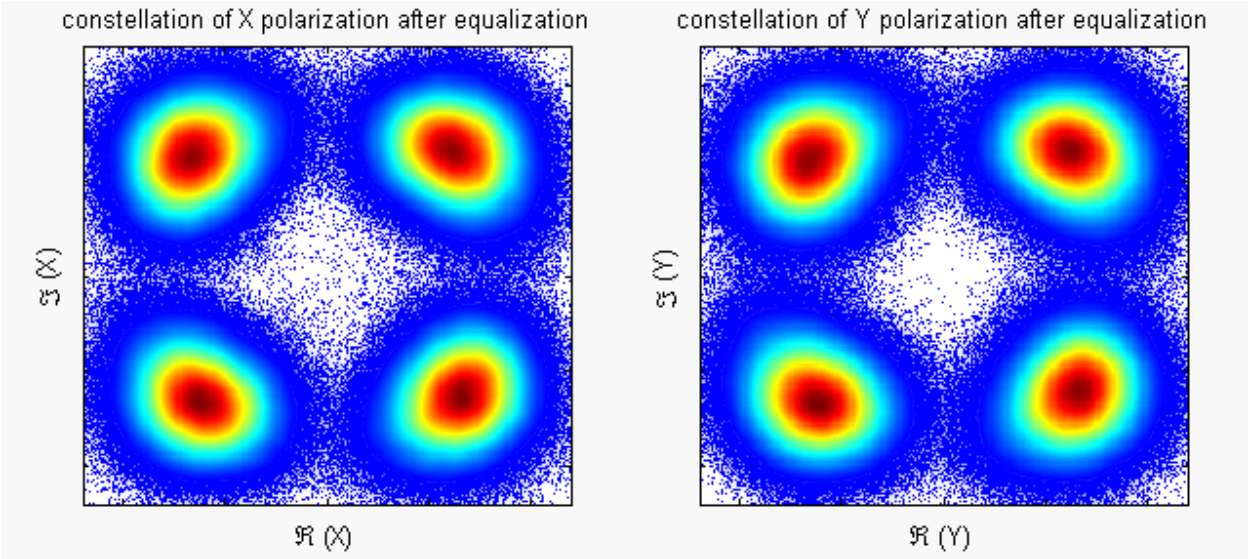

Figure 4.14 : Recovered constellation for single channel transmission 28GBaud, BER 6 E-3

Similarly, OSNR measurements were also made for an eight carrier superchannel following 50GHz for different baud rates. The spectrum of the received superchannel for 10Gbaud is shown in the Fig. 4.15. The OSNR was found to be 10-12dB.

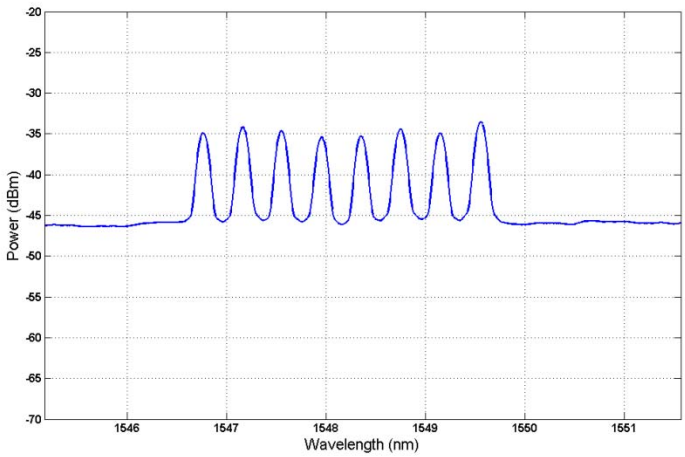

Figure 4.15 : Received signal spectrum for 8 carrier superchannel 10Gbaud, 50GHz spacing.

The optical spectra of transmitted and received signals for the eight carrier superchannel at 28Gbaud 50GHz spacing are depicted in the Fig. 4.16. The received signal OSNR was approximately 12dB for most of the carriers.

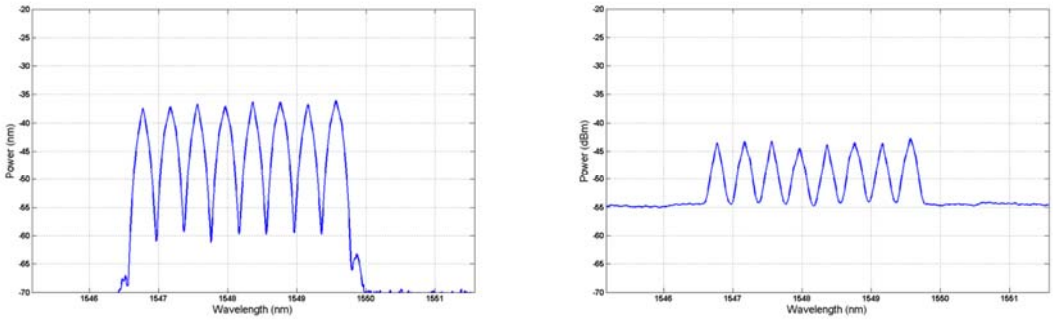

Figure 4.16 : The spectra for 8 carrier superchannel 28Gbaud 50GHz spacing left) Transmitted b) Received after loopback from Finkenstien.

4.3.4 The Way Forward

The OSNR measurements clearly indicate that there is a need for power optimization at the transmitter (both electrical and optical) and probably in the inline amplifiers. An optimum power profile in terms of OSNR will be then found while being in the linear regime. Moreover, the availability of spectral resources will be assessed. The performance for different carrier spacing and baud rate will also be evaluated and finally carriers will be packed as close as possible to achieve the maximum spectral efficiency while maintaining the performance.

4.4 Field Trial with Receiver Single User Approach – Nonlinear Regime MS 4.3.2

4.4.1 Introduction

The objective of the task is the Implementation of the novel electrical processing technique i.e. ESSFM for the nonlinear impairments mitigation and system performance evaluation for different network power profile with a single user approach at the receiver. The comparison between previous stochastic techniques such as SSFM and the new proposed ESSFM algorithm will also be carried out.

As explained in the MS 4.3.1. , the field trial activity is in the progress and output of linear regime would provide a useful input in terms of OSNR and an estimate of performance improvement which can be achieved using nonlinear impairment techniques such as SSFM and ESSFM.

4.4.2 System Setup and Approach

The system setup will be the same as described in MS 4.3.1. Initial investigations using emulated network in the lab have already been reported in the MS 3.2. Once identified a set of possible solution,

in order to find a trade-off between the OSNR at the receiver side and the nonlinear transmission impairments, different network power profile will be considered and performance on a single sub-channel will be evaluated. In particular a sub-channel with more adjacent channels will be considered, thus corresponding to the worst case in terms of nonlinear impairments. This way, an optimum value of power profile will be found. Once the power profile is chosen, the Tbps *superchannel* will be transmitted and the performance for each sub-channel will be evaluated. In particular, different baud-rate, spectral allocation and signal filtering will be considered following the outcomes from WP2, evaluating the system performance in term of bit error rate and obtained spectral efficiency.

In a second measurement a stochastic back propagation will be considered at the receiver electronic processing. The optimum network power profile will be chosen evaluating the performance in the worst case (sub-channels with more adjacent sub-channels). The objective is to demonstrate the possibility to increase the signal power with a consequent increase of the OSNR at the receiver network PoP without performance degradation due to nonlinear impairments, mitigated by the implemented algorithms. Different baud-rate, spectral shaping, sub-channels spacing, signal filtering and code rate will be considered, evaluating the system performance on each sub-channel, in terms of bit error rate and obtained spectral efficiency. In order to improve the overall performances given by more efficient nonlinear impairments mitigation, advanced novel electronic processing techniques ESSFM will be tried on real network. A comparison between the ESSFM and the stochastic back propagation in terms of performance and system complexity will be drawn.

4.5 Optimum power profile evaluation with nonlinear impairments mitigation

4.5.1 Introduction

The task is aimed at the evaluation of the optimum network power profile considering a multi user approach at the receiver. The idea, numerical simulations and preliminary experimental evaluations have already been reported in the MS 2.6 and MS 3.3.

4.5.2 The Approach

This task will be focused on the experimental demonstration of the Tbps transmission, considering a multi user scenario. Advanced novel processing techniques that allow to take into account the information carried by the adjacent sub-channels will be (implemented in MS2.6 and MS 3.3) tested on the real link. Different baud-rate, spectral allocation, signal filtering and code rates will be considered, evaluating the system performance on each sub-channel, in terms of bit error rate and obtained spectral efficiency. The objective is to demonstrate a high spectral efficiency 1 Tbps transmission with a tuning of the main parameter (i.e. baud rate, spectral shaping and sub-channels spacing), obtaining better performances due to the multi user approach and resultantly an optimum network power profile will be drawn.

5 Conclusions

The report presented the key achievements of the COFFEE project with the objective of increasing the spectral efficiency to enhance the overall capacity of already installed fiber. The CNIT terabit solution is based on the highly spectral efficient Time Frequency Packing technique.

The deliverables of system design work package provided the opportunities to understand the user requirements and issues of commercial optical core systems and link engineering. The complete characterization of Alcatel system components and subsystems helped to model the transmission channel between Milan and Finkenstein and to evaluate the candidate solutions for next generation terabit transmission. Resultantly, a complete system model including transmitter and coherent receiver was chalked out and incorporated into CNIT numerical simulation tool. The simulation results paved the way for optimizing the transmitter, receiver and link parameters for different baud rates and spectral spacing.

We also proposed and demonstrated innovative techniques for spectral efficiency (SE) enhancement. The techniques included channel shortening (CS), enhanced split step Fourier method (ESSFM) for nonlinear impairment mitigation and multiuser processing at the receiver. Channel shortening is a useful technique to improve the spectral efficiency without increasing the receiver complexity. We evaluated the achievable gain for five carrier superchannel, each carrier PM QPSK modulated and having 160Gbps bit rate, considering different receiver complexities. We demonstrated through simulations that the use of CS can increase the SE by 1 b/s/Hz for the same receiver complexity. The innovative ESSFM technique for nonlinear impairment mitigation was also demonstrated by emulating the network conditions in the lab using Alcatel 1626LM system. ESSFM reduces the computational complexity by four fold for the same accuracy compared to standard SSFM. It also implies that for the same complexity ESSFM can provide higher accuracy which means more power can injected on the link and longer distances or higher spectral efficiency can be achieved. The multiuser processing technique was demonstrated in the lab and was shown that it can reduce the penalty due to inter channel interference (ICI) and thus more tight binding of optical can be realized.

Considering findings of lab demonstrations, the field trial is in the progress and preliminary measurements have been reported. Different power profiles, data rates, channel spacing and code rate will be tested for both single user and multiuser receiver configurations. We will demonstrate the transmission of 1Tbps in 200GHz on Milan Finkenstein link. All efforts would be made to achieve the

SE beyond project deliverables by transmitting 1Tbps in 150GHz spectrum. We will submit a final version of the document within a month after completion of the field trial.

Such field trials provide a real picture for the network operators to devise the migration plans for the future technologies. For, example while planning for 100Gbps links , the link power margins should be kept for the 400Gbps and 1Tbps transmission in the future to avoid replacing the amplifiers or network shutdowns. The COFFEE project has been a wonderful experience for understanding concerns/priorities of networks users, exchanging the networks operations and research expertise and market exposure for the innovative technologies. After the field GEANT testbed will be optimized for the future trials of innovative technologies and can become a platform for the academia.

References

For Section 2.1.

[1] ITU-T G.655, “Characteristics of a Non-Zero Dispersion-Shifted Single-Mode Optical Fibre and Cable”, Nov. 2009

[2] Corning Inc., “Corning LEAF Optical Fiber”, Product Information, Dec 2012

[3] ITU-T G.652, “Characteristics of a Single-Mode Optical Fibre and Cable”, Nov. 2009

For Section 2.2.

[1] Alcatel, “Alcatel 1626LM Technical Handbook”, May 2005

[2] Alcatel, “Alcatel 1626LM Stand Alone Turn-On & Commissioning Handbook”, Mar. 2005

[3] Douglas M. Barney, “Characterisation of Erbium-Doped Fiber Amplifiers”, pp. 519-595 in Dennis Derickson (Ed.), “Fiber Optic Test and Measurement”, Prentice Hall, Oct. 1997

[4] ITU-T G.694.1, “Spectral Grids for WDM Applications: DWDM Frequency Grid”, Feb. 2012

[5] ITU-T G.707, “Network Node Interface for the Synchronous Digital Hierarchy”, Jan. 2007

[6] ANSI T1.105, “Synchronous Optical Network (SONET) - Basic Description including Multiplex Structure, Rates and Formats”, May 2001

[7] IEEE 802.3, “IEEE Standard for Ethernet”, Dec. 2012

[8] ITU-T G.709/Y.1331, “Interfaces for the Optical Transport Network”, Feb. 2012

[9] ITU-T G.Sup43, “Transport of IEEE 10GBASE-R in Optical Transport Networks”, Feb. 2011

For Section 2.4.

[1] D. M. Arnold, H.-A. Loeliger, P. O. Vontobel, A. Kavˇci´c, andW. Zeng, “Simulation-based computation of information rates for channels with

memory," IEEE Trans. Inform. Theory, vol. 52no. 8, pp. 3498–3508, Aug. 2006.

[2] G. Colavolpe and T. Foggi, "Time-frequency packing for high capacity coherent optical links,IEEE Trans. Commun., vol. 62, pp. 2986–2995, Aug 2014.

[3] G. Ungerboeck, "Adaptive maximum-likelihood receiver for carrier-modulated datatransmission systems," IEEE Trans. Commun., vol. 22, no. 5, pp. 624–636, May 1974.

[4] G. Colavolpe and A. Barbieri, "On MAP symbol detection for ISI channels using the Ungerboeckobservation model," IEEE Commun. Letters, pp. 720–722, August 2005.

[5] R. Bahl, J. Cocke, F. Jelinek, and R. Raviv, "Optimal decoding of linear codes for minimizingsymbol error rate," IEEE Trans. Inform. Theory, vol. 20, pp. 284–284, Mar. 1974.

[6] A. Modenini, F. Rusek, and G. Colavolpe, "Optimal transmit filters for ISI channels under channelshortening detection," IEEE Trans. Commun., 2013.

[7] S. ten Brink, G. Kramer, and A. Ashikhmin, "Design of low-density parity-checkmodulation and detection," IEEE Trans. Commun., vol. 52, pp. 670–678, Apr. 2004.

[8] T. Richardson, A. Shokrollahi, and R. Urbanke, "Design of capacity-approaching irregular lowdensityparity check codes," IEEE Trans. Inform. Theory, vol. 47, pp. 619–637, Feb. 2001.

[9] H. Xiao and A. H. Banihashemi, "Improved progressive-edge-growth (PEG) construction ofirregular LDPC codes," IEEE Commun. Letters, vol. 8, pp. 715–717, Dec. 2004.

[10] X. Hu, E. Eleftheriou, and D. M. Arnold, "Regular and irregular progressive edge-growth tannergraphs," IEEE Trans. Inform. Theory, vol. 51, pp. 386–398, Jan. 2005.

[11] "Digital video broadcasting (DVB); second generation framing structure, channel coding andmodulation systems for broadcasting, interactive services, news gathering and other broad-bandsatellite applications (DVB-S2)," Standard EN 302 307.

[12] G. Colavolpe, T. Foggi, E. Forestieri, and G. Prati, "Robust multilevel coherent optical systemswith linear processing at the receiver," J. Lightwave Technol., vol. 27, no. 13, pp. 2357–2369,Jul. 2009.

[13] F. Fresi, M. Secondini, G. Berrettini, G. Meloni, and L. Poti, "Impact of optical and electricalnarrowband spectral shaping in faster than Nyquist Tb superchannel," IEEE Photon. TechnoLett., vol. 25, no. 23, pp. 2301–2303, 2013.

[14] G. Colavolpe, T. Foggi, A. Modenini, and A. Piemontese, “Faster-than-Nyquist and beyond:how to improve spectral efficiency by accepting interference,” Opt. Express, vol. 19, pp. 26 60026 609, December 2011.

[15] A. Abrardo and G. Cincotti, “Design of AWG devices for all-optical time-frequency packing,”J. Lightwave Tech., vol. 32, no. 10, pp. 1951–1959, May 2014.

[16] U. Mengali and M. Morelli, “Data-aided frequency estimation for burst digital transmission,”IEEE Trans. Commun., vol. 45, no. 1, pp. 23–25, January 1997.

[17] G. Colavolpe, A. Barbieri, and G. Caire, “Algorithms for iterative decoding in the presence ofstrong phase noise,” IEEE J. Select. Areas Commun., vol. 23, no. 9, pp. 1748–1757, Sept 2005.

[18] J. Hagenauer, “The turbo principle: Tutorial introduction and state of the art,” in Proc. InternationalSymposium on Turbo Codes and Related Topics, 1997, pp. 1–11.

For Section 2.5. References

[1] G. Colavolpe and T. Foggi, “Time-frequency packing for high capacity coherent optical links,” IEEE Trans. Commun., vol. 62, no. 8, pp. 2986–2995, Aug. 2014.

[2] L. Potí, G. Meloni, G. Berrettini, F. Fresi, M. Secondini, T. Foggi, G. Colavolpe, E. Forestieri, A. D’Errico, F. Cavaliere, R. Sabella, and G. Prati, “Casting 1 Tb/s DP-QPSK communication into 200 GHz bandwidth,” in Proc. European Conf. on Optical Commun. (ECOC’12), September 19-23, 2012.

[3] D. M. Arnold, H.-A. Loeliger, P. O. Vontobel, A. Kavˇci´c, and W. Zeng, “Simulation-based computation of information rates for channels with memory,” IEEE Trans. Inform. Theory, vol. 52, no. 8, pp. 3498–3508, Aug. 2006.

References for 2.6

[1] H. L. Van Trees, “Detection, Estimation, and Modulation Theory—Part I,” New York: Wiley, 1968.

[2] ETSI EN 301 307 Digital Video Broadcasting (DVB); V1.1.2 (2006-06). Second generation framing structure, channel coding and modulation systems for Broadcasting, Interactive Services, News Gathering and other Broadband satellite applications. [Online]. Available: http://www.etsi.org.

[3] H. Xiao and A. H. Banihashemi, “Improved progressive-edge-growth (PEG) construction of irregular LDPC codes,” IEEE Commun. Letters, vol. 8, pp. 715–717, Dec. 2004.

[4] S. ten Brink, G. Kramer, and A. Ashikhmin, “Design of low-density parity-check codes for modulation and detection,” IEEE Trans. Commun., vol. 52, pp. 670–678, Apr. 2004.

References for 3.1

[1] F. Rusek and A. Prlja, “Optimal channel shortening for MIMO and ISI channels,” IEEE Trans. Wireless Commun., vol. 11, pp. 810–818, Feb. 2012.

[2] G. Ungerboeck, “Adaptive maximum likelihood receiver for carrier-modulated data-transmission systems,” IEEE Trans. Commun., vol. com-22, pp. 624–636, May 1974.

[3] L. R. Bahl, J. Cocke, F. Jelinek, and J. Raviv, “Optimal decoding of linear codes for minimizing symbol error rate,” IEEE Trans. Inform. Theory, vol. 20, pp. 284–287, Mar. 1974.

[4] G. Colavolpe and A. Barbieri, “On MAP symbol detection for ISI channels using the Ungerboeck observation model,” IEEE Commun. Letters, vol. 9, pp. 720–722, Aug. 2005.

[5] D. Fertonani, A. Barbieri, and G. Colavolpe, “Reduced-complexity BCJR algorithm for turbo equalization,” IEEE Trans. Commun., vol. 55, pp. 2279–2287, Dec. 2007.

[6] G. Colavolpe, G. Ferrari, and R. Raheli, “Reduced-state BCJR-type algorithms,” IEEE J. Select. Areas Commun., vol. 19, pp. 848–859, May 2001.

For Section 3.2.

[1] E. Ip and J. M. Kahn, “Compensation of dispersion and nonlinear impairments using digital backpropagation,” J. Lightwave Technol., vol. 26, no. 20, pp. 3416–3425, 2008.

[2] D. Marsella, M. Secondini, and E. Forestieri, “Maximum likelihood sequence detection for mitigating nonlinear effects,” J. Lightwave Technol., vol. 32, no. 5, pp. 908–916, 2014.

[3] T. R. Taha and M. J. Ablowitz, “Analytical and numerical aspects of certain nonlinear evolution equation, II, numerical, nonlinear Schroedinger equation,” J. Computat. Phys., vol. 5, pp. 203 – 230, 1984.

[4] E. Forestieri and M. Secondini, “Solving the nonlinear Schrödinger equation,” in Optical Communication Theory and Techniques, E. Forestieri, Ed. plus 0.5em minus 0.4emNew York: Springer, 2004, pp. 3–11.

[5] M. Secondini, E. Forestieri, and G. Prati, “Achievable information rate in nonlinear WDM fiber-optic systems with arbitrary modulation formats and

dispersion maps," J. Lightwave Technol., vol. 31, no. 23, pp. 3839–3852, 2013.

[6] O. V. Sinkin, R. Holzlöhner, J. Zweck, and C. R. Menyuk, "Optimization of the split-step Fourier method in modeling optical-fiber communications systems," J. Lightwave Technol., vol. 21, no. 1, pp. 61–68, Jan. 2003.

For Section 3.3.

[1] S. Verdú, "Multiuser Detection," Cambridge, UK: Cambridge University Press,1998.

[2] G. Colavolpe, D. Fertonani, and A. Piemontese, "SISO detection over linear channels with linear complexity in the number of interferers," IEEEJ. of Sel. Topics in Signal Proc., vol. 5, pp. 1475-1485, Dec. 2011.

[3] A. Barbieri, D. Fertonani and G. Colavolpe, "Time-Frequency Packing for linear modulation: spectral efficiency and practical detection schemes,"IEEE Trans. on Commun., vol. 57, no. 10, pp. 2951-2959, Oct. 2009.

[4] G. Colavolpe and T. Foggi, "Time-Frequency Packing for High-Capacity Coherent Optical Links," IEEE Trans. On Commun., vol. 62, no. 8, pp. 2986-2995.

[5] S. ten Brink, G. Kramer and A. Ashikhmin, "Design of low-density parity-check codes for modulation and detection," IEEE Trans. On Commun., pp. 670-678, 2004.

[6] H. Xiao and A. H. Banihashemi, "Improved progressive-edge-growth (PEG) construction of irregular LDPC codes," IEEE Commun. Letters, pp. 715-717, 2004.

For Section 4.1

[1] Potì, L. et al., "Casting 1Tb/s DP-QPSK Communication into 200GHz Bandwidth", P4.19 in Proc. ECOC12, Sep. 2012

[2] Colavolpe, G. et al., "Faster-than-Nyquist and beyond: how to improve spectral efficiency by accepting interference", pp. 26600–26609 in Opt. Express vol. 19, Dec. 2011

[3] Bahl, R. et al., "Optimal Decoding of Linear Codes for Minimizing Symbol Error Rate", pp. 284-287 in IEEE Trans. Inform. Theory vol. 20, Mar. 1974

[4] Gallager, R. G., "Low-Density Parity-Check Codes", pp. 21-28 in IRE Transactions on Information Theory vol. 8, Jan. 1962

[5] Hagenauer, J., "The Turbo Principle: Tutorial Introduction and State of the Art", pp. 1-11 in Proceedings of the 1st International Symposium on Turbo Codes, Brest, 1997

[6] Corning Inc., "Corning LEAF Optical Fiber", Product Information, Jun 2014

[7] Agrawal, G. P., "Fiber-Optic Communications Systems", 3rd Edition, 978-0-471-21571-4, John Wiley & Sons, New York, Jun. 2002

[8] Drapela, T. J., "Effective Area and Nonlinear Coefficient Measurements of Single-Mode Fibers: Recent Interlaboratory Comparisons", pp. 293-297 in Proc. SPIE vol. 4087, Dec. 2000.

For Section 4.2

[1] Potì, L. et al., "Casting 1Tb/s DP-QPSK Communication into 200GHz Bandwidth", P4.19 in Proc. ECOC12, Sep. 2012

[2] Colavolpe, G. et al., "Faster-than-Nyquist and beyond: how to improve spectral efficiency by accepting interference", pp. 26600–26609 in Opt. Express vol. 19, Dec. 2011

[3] Bahl, R. et al., "Optimal Decoding of Linear Codes for Minimizing Symbol Error Rate", pp. 284-287 in IEEE Trans. Inform. Theory vol. 20, Mar. 1974

[4] Gallager, R. G., "Low-Density Parity-Check Codes", pp. 21-28 in IRE Transactions on Information Theory vol. 8, Jan. 1962

[5] Hagenauer, J., "The Turbo Principle: Tutorial Introduction and State of the Art", pp. 1-11 in Proceedings of the 1st International Symposium on Turbo Codes, Brest, 1997

[6] Corning Inc., "Corning LEAF Optical Fiber", Product Information, Jun 2014.

Glossary

APSD	Automatic power shutdown
AWGN	Additive White Gaussian Noise
AOM	Acousto-optic modulators
BER	Bit Error Rate
DCM	Dispersion compensation modules
DGD	Differential group delay
DSP	Digital Signal Processing
EDFA	Erbium Doped Fiber Amplifier
FEC	Forward Error Correction
FFE	Feed Forward Equalizer
GFF	Gain-flattening filter
GVD	Group Velocity Dispersion
ICI	Interchannel Interference
ISI	Intersymbol Interference
LDPC	Low Density Parity Check
LDT	Link Description Table
LO	Local Oscillator
MAP	Maximum a Posteriori
NZDSF	Non-Zero Dispersion Shifted FIber
OFDM	Orthogonal Frequency Division Multiplexing
OSA	Optical Spectrum Analyzer
OSNR	Optical Signal-to-Noise Ratio
PMD	Polarization Mode DIspersion
QPSK	Quadrature Phase Shifting Keying
SFM	Self-Phase Modulation
SMF	Single Mode Fiber
SNR	Signal-to-Noise Ratio
TFP	Time-Frequency Packing
WDM	Wavelength Division Multiplexing
XFM	Cross-Phase Modulation